Piezoresistive Sensors

Z. Kozioł,

Orel State Technical University, 29 Naugorskoye Shosse, Orel, 302020, Russia.

November 13, 2009

Abstract

This is abstract - to be written.

Contents

1 Introduction

1.1 Modeling with COMSOL Multiphysics

COMSOL Multiphysics is a multiphysics modelling software based on the finite element method (FEM)

1.2 Properties of Titanium Alloys

1.2.1 Chemical Composition and Structure of Titanium Alloys

The Titanium alloy used for membrane is BT9. You can find properties of this alloy on:

Характеристика материала ВТ9 From: Марочник стали и сплавов (www.splav.kharkov.com) Классификация : Титановый деформируемый сплав Применение: детали, работающие при температуре до 500°C; класс по структуре $\alpha + \beta$

кристаллическую структуру можно представить себе как физически однородное тело, в котором атомы располагаются в периодическом порядке. Подобное расположение атомов определяет физические свойства металлов. Металлы кристаллизуются по большей части в кубической объемно-центрированной или гранецентрированной и в гексагональной плотно упакованной решетках.

до температуры около 882°C титан имеет плотно упакованную гексагональную структуру, известную под названием a-модификации. Температура полиморфного a « b -превращения составляет 882°C. высокотемпературную модификацию b -титана с кубической объемно-центрированной решеткой.

Химический состав материала ВТ9
Примечание: Ti - основа; процентное содержание Ti дано приблизительно

Fe - up to 0.25
C - up to 0.1
Si - 0.2-0.35
Mo -2.8-3
N - up to 0.05
Ti - 86.785 - 90.4

Al - 5.8-7
Zr - 0.8-2
O - up to 0.15
H - up tp 0.015
Other - 0.3

1.2.2 The Tensile Strength of Titanium Alloys

Mechanical properties at 20°C: sв 1050-1300 MPa (Предел кратковременной прочности; Tensile strength) d5 8-16y 25-45E 118 MPa (Модуль упругости первого рода)

При повышении температуры до 250°C прочность титана снижается почти в 2 раза. Однако жаропрочные Ti-сплавы по удельной прочности в интервале температур 300–600°C не имеют себе равных; при температурах выше 600°C сплавы титана уступают сплавам на основе железа и никеля.

Механические свойства прутков из титановых сплавов (ГОСТ 26492–85) (ВТ9):
В скобках приведены данные для прутков повышенного качества.

Предел прочности sв, МПа 980 (1030–1230)
Относительное удлинение d 7(9)
Относительное сужение y 16(28)
Ударная вязкость KCU,Дж/см2 25(30)

The tensile strength of titanium and its alloys at ambient temperature ranges from 240 MPa for the softest grade of commercially pure titanium to more than 1400 MPa for very high strength alloys. Proof strengths vary from around 170 to 1100 MPa according to grade and condition.

As a figure shows, tensile strength will gon down nearly linearly with temperature for most of alloys that have large tensile strength, with a slope of around 1000 MPa/1000 degrees. Hence, if alloy had a tensile strength of 1000 MPa at 0 degreess, it will go to around 500 MPa at 500 degrees.

0.2% Proof stress goes down slower, about 2 times, with a slope of the order of 500 MPa/1000 degrees

Typical elongation values for titanium and its alloys do not change much with temperature, for alloys of interest, and temperatures below 500 degrees.

1.2.3 Thermal expansion coefficient of Titanium and its alloys.

$T(°K)$	200	293	500	800	1100
α_{Ti}	7.4	8.6	9.9	11.1	11.7

For the purpose of numerical modeling, it is desirable to have a simple approximation of $\alpha(T)$. A good approximation is obtained with the following function:

$$\alpha(T) = \alpha_0 + \beta \cdot (T - T_0)^{\gamma}\,, \tag{1.1}$$

where $\alpha_0 = 6.91$, $\beta = 0.35$, $T_0 = 236.4$, and $\gamma = 0.39$.

1.3 Solder Пср72

Solder is Пср72. Some properties you can find on pages: Серебро 72%, Медь Остально

Silver-Copper Eutectic Alloy (72Ag-28Cu), Cold Drawn then Annealed at 250° C:
Tensile Strength, Ultimate 345 MPa
Elongation at Break 9.00

Silver-Copper Eutectic Alloy (72Ag-28Cu), Cold Drawn then Annealed at 350° C:
Tensile Strength, Ultimate 355 MPa
Elongation at Break 11.00

Silver-Copper Eutectic Alloy (72Ag-28Cu), Cold Drawn then Annealed at 550° C
Tensile Strength, Ultimate 460 MPa
Elongation at Break 22.00

Silver-Copper Eutectic Alloy (72Ag-28Cu), Cold Drawn then Annealed at 700° C
Tensile Strength, Ultimate 540 MPa
Elongation at Break 28.00

Silver-Copper Eutectic Alloy (72Ag-28Cu), 10Tensile Strength, Ultimate 415 MPa
Elongation at Break 7.00

Silver-Copper Eutectic Alloy (72Ag-28Cu), 20Tensile Strength, Ultimate 450 MPa
Elongation at Break 5.00

Silver-Copper Eutectic Alloy (72Ag-28Cu), 30Tensile Strength, Ultimate 475 MPa
Elongation at Break 5.00

Silver-Copper Eutectic Alloy (72Ag-28Cu), 50Tensile Strength, Ultimate 520 MPa
Elongation at Break 5.00

Silver-Copper Eutectic Alloy (72Ag-28Cu), 70Tensile Strength, Ultimate 590 MPa
Elongation at Break 4.00

Copper Young modulus 17E6 PSI
Silver Young modulus 83 GPa

Толщина слоя припоя ПСр 72, $0.04 \pm 0.01 mm$
Температура плавления 779°C

1.3.1 Coefficient of Thermal Expansion of Solder Пср72

There is no known to us data on thermal expansion coefficient of alloy Пср72. However, assuming that it is that as of combination of thermal expansion coefficients of Silver (α_{Ag})

and Copper (α_{Cu}) should give us a sufficiently good approximation. The table shows these coefficients ([2]), and a computed value $\alpha = 0.72 \cdot \alpha_{Ag} + 0.28 \cdot \alpha_{Cu}$ for several temperatures (in units of $10^{-6}/K$).

$T(°K)$	200	293	500	800	1100
α_{Ag}	17.8	18.9	20.6.5	23.7	27.1
α_{Cu}	15.2	16.5	18.3	20.3	23.7
α	17.07	18.2	20.0	22.75	26.15

We find that the following approximation for $\alpha(T)$ is good for the temperature range from $200K$ to $1100K$:

$$\alpha(T) = \alpha_a + \alpha_b \cdot T \tag{1.2}$$

where T is in Kelvin degrees, $\alpha_a = 15.13 \cdot 10^{-6}/K$, and $\alpha_b = 0.01 \cdot 10^{-6}/K^2$.

1.4 Sapphire Mechanical Properties

Sapphire (Al_2O_3) has a rhombohedral type structure and is a highly anisotropic material, with properties that are largely dependent on crystallographic orientation.

Tensile Strength: 400 MPa at 20 °C, 275 MPa at 500 °C, 355 MPa at 1000 °C

Young's Modulus, E 435 GPa // c at 25 °C and 386 GPa // c at 1000 °C Poisson's Ratio 0.28-0.33

A trigonal crystal is known to have six independent elastic constants, as shown in the following equation:

$$\begin{bmatrix} \sigma_{11} \\ \sigma_{22} \\ \sigma_{33} \\ \sigma_{23} \\ \sigma_{13} \\ \sigma_{12} \end{bmatrix} = \begin{bmatrix} C_{11} & C_{12} & C_{13} & C_{14} & 0 & 0 \\ C_{12} & C_{11} & C_{13} & -C_{14} & 0 & 0 \\ C_{13} & C_{13} & C_{33} & 0 & 0 & 0 \\ C_{14} & -C_{14} & 0 & C_{44} & 0 & 0 \\ 0 & 0 & 0 & 0 & C_{44} & C_{14} \\ 0 & 0 & 0 & 0 & C_{14} & \frac{1}{2}(C_{11} - C_{12}) \end{bmatrix} \begin{bmatrix} \varepsilon_{11} \\ \varepsilon_{22} \\ \varepsilon_{33} \\ \gamma_{23} \\ \gamma_{13} \\ \gamma_{12} \end{bmatrix} \tag{1.3}$$

where engineering notation is used: $\gamma_{12} = 2\varepsilon_{12}$, $\gamma_{13} = 2\varepsilon_{13}$, and $\gamma_{23} = 2\varepsilon_{23}$.

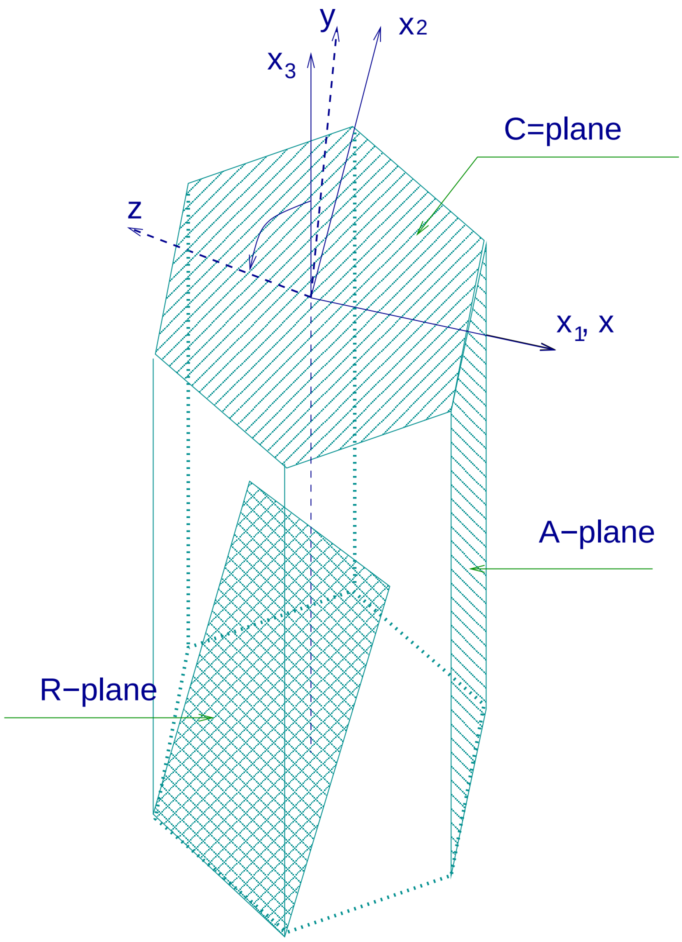

Figure 1: Crystallographic structure of sapphire, Al_2O_3. Lattice parameters (at 20° C) are $a = 4.758\mathring{A}$ and $c = 12.991\mathring{A}$. $R-$plane coordinate system results by rotation of coordinate system (x_1, x_2, x_3) by an angle θ along the x_1 axis. After simple calculations, we find that the angle θ is equal to 57.11°.

Wachtman et. al. (1960) give the following values: $(C_{11}, C_{33}, C_{44}, C_{12}, C_{13}, C_{14}) = (496.8, 498.1, 147.4, 163.6, 110.9, -23.5)$ GPa, where x_1 and x_3 axes are perpendicular to $a-$ and $c-$ planes of the crystal, as shown in Figure 1.

We however need stiffness tensor parameters for a rotated coordinate system, as shown in Figure 1, where two Cartesian coordinates (x, y) are within the $R-$plane and the third one (z) is perpendicular to that plane.

Transforming vectors is trivialy simple.

For a general rotation transformation, when rotation occurs along each of axes, we have the following transformation matrix $\mathbf{R}$ for vectors:

$$\mathbf{R} = \begin{bmatrix} cos\alpha \cdot cos\beta + sin\alpha \cdot sin\theta \cdot sin\beta & sin\alpha \cdot sin\theta & -cos\alpha \cdot sin\beta + sin\alpha \cdot sin\theta \cdot cos\beta \\ -sin\alpha \cdot cos\beta + cos\alpha \cdot sin\theta \cdot sin\beta & cos\alpha \cdot cos\theta & sin\alpha \cdot sin\beta + cos\alpha \cdot sin\theta \cdot cos\beta \\ cos\theta \cdot sin\beta & -sin\theta & cos\theta \cdot cos\beta \end{bmatrix} \tag{1.4}$$

In particular, in case that interests us, when rotation is along x_1 axes only, as in Figure 1, we have the following transformation matrix for vectors:

$$\mathbf{R} = \begin{bmatrix} 1 & 0 & 0 \\ 0 & cos\theta & sin\theta \\ 0 & -sin\theta & cos\theta \end{bmatrix} \tag{1.5}$$

Transforming tensors under rotation is somewhat more complex.

In new (x, y, z) coordinates (refer to Figure 1), stiffness tensor $\mathbf{C}$, defined by (1.3), will have the form: $\mathbf{C'} = \mathbf{Q}^{-\mathbf{T}}\mathbf{C}\mathbf{Q}^{-1}$, where $\mathbf{Q}$ is rotation matrix [9, 5].

An ij element of transformation matrix $\mathbf{Q}$, $\mathbf{Q}_{ij} = q_{ij}$, is computed as a product of two products of unit vectors before and after transformation, each of them with proper indexes.

These indexes depend on indexes of transformed σ_{ij} (ij in this example), and on indexes of strain tensor ε_{km} on which σ_{ij} acts on.

Schematicaly: if $\sigma_{ij} \to \varepsilon_{km}$, than parameter of matrix $\mathbf{Q}$ at the proper place will be equal to $\hat{x}_i\hat{x}_k \cdot \hat{x}_j\hat{x}_m \equiv a_{ik} \cdot a_{jm}$ (refer to Equation (1.3) for available indexes).

Hence, we have for $\mathbf{Q}$:

$$\mathbf{Q} = \begin{bmatrix} a_{11}^2 & a_{12}^2 & a_{13}^2 & 2a_{12}a_{13} & 2a_{11}a_{13} & 2a_{12}a_{11} \\ a_{21}^2 & a_{22}^2 & a_{23}^2 & 2a_{22}a_{23} & 2a_{21}a_{23} & 2a_{21}a_{22} \\ a_{31}^2 & a_{32}^2 & a_{33}^2 & 2a_{32}a_{33} & 2a_{31}a_{33} & 2a_{31}a_{32} \\ a_{21}a_{31} & a_{22}a_{32} & a_{23}a_{33} & a_{22}a_{33} + a_{23}a_{32} & a_{21}a_{33} + a_{23}a_{31} & a_{21}a_{32} + a_{32}a_{31} \\ a_{11}a_{31} & a_{12}a_{32} & a_{13}a_{33} & a_{12}a_{33} + a_{13}a_{32} & a_{11}a_{33} + a_{13}a_{31} & a_{11}a_{32} + a_{12}a_{31} \\ a_{11}a_{21} & a_{12}a_{22} & a_{13}a_{23} & a_{12}a_{23} + a_{13}a_{22} & a_{11}a_{23} + a_{13}a_{21} & a_{11}a_{22} + a_{12}a_{21} \end{bmatrix} \tag{1.6}$$

Let us notice now that products of unit vectors are given by matrix $\mathbf{R}$, (1.4).

Hence, we have:

$$\mathbf{Q} = \begin{bmatrix} 1 & 0 & 0 & 0 & 0 & 0 \\ 0 & C^2 & S^2 & 2CS & 0 & 0 \\ 0 & S^2 & C^2 & -2CS & 0 & 0 \\ 0 & -CS & CS & C^2 - S^2 & 0 & 0 \\ 0 & 0 & 0 & 0 & C & -S \\ 0 & 0 & 0 & 0 & S & C \end{bmatrix} \tag{1.7}$$

where C stands for $cos\theta$ and S for $sin\theta$.

The inverse transformation is obtained by changing sign of $sin\theta$.

Now, we may compute $\mathbf{C'} = \mathbf{Q}^{-\mathbf{T}}\mathbf{C}\mathbf{Q}^{-1}$, obtaining the following parameters of transformed matrix (not listed items are equal to 0) [1]:

$$\begin{aligned}
c'_{11} &= C_{11} \\
c'_{12} &= cos^2\theta \cdot C_{12} + sin^2\theta \cdot C_{13} + 0.5 \cdot sin(2\theta) \cdot C_{14} \\
c'_{13} &= sin^2\theta \cdot C_{12} + cos^2\theta \cdot C_{13} - 0.5 \cdot sin(2\theta) \cdot C_{14} \\
c'_{14} &= -sin(2\theta) \cdot C_{12} + sin(2\theta) \cdot C_{13} + cos(2\theta) \cdot C_{14} \\
c'_{21} &= c'_{12} \\
c'_{22} &= cos^2\theta \cdot C_{11} + 2 \cdot sin^2\theta \cdot cos^2\theta \cdot C_{13} - 0.5 \cdot sin(2\theta) \cdot sin^2\theta \cdot C_{14} + sin^4\theta \cdot C_{33} \\
&\quad + cos^2\theta \cdot sin^2\theta \cdot C_{44} \\
c'_{23} &= sin^2\theta \cdot cos^2\theta \cdot C_{11} + (cos^4\theta + sin^4\theta) \cdot C_{13} \\
&\quad + 0.5 \cdot sin(2\theta) \cdot cos(2\theta) \cdot C_{14} + sin^2\theta \cdot cos^2\theta \cdot C_{33} - cos^2\theta \cdot sin^2\theta \cdot C_{44} \\
c'_{24} &= -0.5 \cdot sin(2\theta) \cdot cos^2\theta \cdot C_{11} + 0.5 \cdot sin(2\theta) \cdot cos(2\theta) \cdot C_{13} + (2cos^2\theta \cdot sin^2\theta - cos^4\theta) \cdot C_{14} \\
&\quad + 0.5 \cdot sin(2\theta) \cdot sin^2\theta \cdot C_{33} + 0.5 \cdot sin(2\theta) \cdot cos(2\theta) \cdot C_{44} \\
c'_{31} &= c'_{13} \\
c'_{32} &= c'_{23} \\
c'_{33} &= sin^4\theta \cdot C_{11} + 2cos^2\theta \cdot sin^2\theta \cdot C_{13} + sin(2\theta) \cdot sin^2\theta \cdot C_{14} + cos^4\theta \cdot C_{33} + cos^2\theta \cdot sin^2\theta \cdot C_{44} \\
c'_{34} &= -sin(2\theta) \cdot sin^2\theta \cdot C_{11} + 0.5 \cdot sin(2\theta) \cdot sin^2\theta \cdot C_{13} - sin(2\theta) \cdot cos^2\theta \cdot C_{13} - sin^2\theta \cdot (3cos^2\theta - sin^2\theta) \cdot C_{14} \\
&\quad + sin(2\theta) \cdot cos^2\theta \cdot C_{33} - 0.5 \cdot cos(2\theta) \cdot sin(2\theta) \cdot C_{44} \\
c'_{41} &= c'_{14} \\
c'_{42} &= c'_{24} \\
c'_{43} &= c'_{34} \\
c'_{44} &= 2cos^2\theta \cdot sin^2\theta \cdot C_{11} - 4cos^2\theta \cdot sin^2\theta \cdot C_{13} + 3 \cdot cos\theta \cdot sin\theta \cdot cos(2\theta) \cdot C_{14} + 2cos^2\theta \cdot sin^2\theta \cdot C_{33} + cos(2\theta)^2 \cdot C_{44} \\
c'_{55} &= cos^2\theta \cdot C_{44} - sin^2\theta \cdot 0.5(C_{11} - C_{12}) \\
c'_{56} &= 0.5 \cdot sin(2\theta) \cdot C_{44} + cos(2\theta) \cdot C_{14} - 0.5 \cdot sin(2\theta) \cdot 0.5(C_{11} - C_{12}) \\
c'_{65} &= c'_{56} \\
c'_{66} &= sin^2\theta \cdot C_{44} + sin(2\theta) \cdot C_{14} + cos^2\theta \cdot 0.5(C_{11} - C_{12})
\end{aligned} \tag{1.8}$$

[1] Matrix manipulation has actually been done by custom designed, simple Perl script that can perform symbolic manipulation on matrices, generating as an ouput a text as well, that can be used either for subsequent computation or in *LaTeX*.

Please note that above, indexes in c_{ij} denote $ij-$ element in transformed $\mathbf{C'}$ matrix, not new value of stiffness parameters (though one may coincide with the other one).

Numerically, for angle $\theta = 57.11^{\circ}$:

$$\mathbf{C'} = \begin{bmatrix} 496.8 & 115.72 & 158.78 & -38.42 & 0 & 0 \\ 115.72 & 478.47 & 245.39 & -29.496 & 0 & 0 \\ 158.78 & 245.39 & 351.97 & 20.62 & 0 & 0 \\ -38.42 & -29.496 & -20.62 & 359.49 & 0 & 0 \\ 0 & 0 & 0 & 0 & -74.01 & 0.886 \\ 0 & 0 & 0 & 0 & 0.886 & 131.63 \end{bmatrix} MPa \tag{1.9}$$

These results may be used for input into Comsol when considering fully anisotropic situation.

However, using FEM in Comsol is much more efficient in terms of CPU time, and much more accurate, when geometricaly symmetric problems are studied, possibly in reduced dimentions (2D rather than 3D). Mechanical properties of sapphire are actually fully symmetric in z-plane (it is orthotropic material with transverse symmetry). Moreover, since stiffness parameter C_{33} is nearly identical with $C_{11} = C_{12}$, we do not expect huge differences in mechanical properties between z-plane and planes perpendicular to it.

Engeeneers by convention are used to engeneering parameters in their calculations. The engineering constants are related to the components of the stiffness tensor by (for orthotropic body):

$$\begin{aligned}
E_1 = & \left(c_{11}c_{22}c_{33} + 2c_{23}c_{12}c_{13} - c_{11}c_{23}^2 - c_{22}c_{13}^2 - c_{33}c_{12}^2\right) / \left(c_{22}c_{33} - c_{23}^2\right) \\
E_2 = & \left(c_{11}c_{22}c_{33} + 2c_{23}c_{12}c_{13} - c_{11}c_{23}^2 - c_{22}c_{13}^2 - c_{33}c_{12}^2\right) / \left(c_{11}c_{33} - c_{13}^2\right) \\
E_3 = & \left(c_{11}c_{22}c_{33} + 2c_{23}c_{12}c_{13} - c_{11}c_{23}^2 - c_{22}c_{13}^2 - c_{33}c_{12}^2\right) / \left(c_{11}c_{22} - c_{12}^2\right) \\
\nu_{21} = & \left(c_{12}c_{33} - c_{13}c_{23}\right) / \left(c_{11}c_{33} - c_{13}^2\right) \\
\nu_{12} = & \left(c_{12}c_{33} - c_{13}c_{23}\right) / \left(c_{22}c_{33} - c_{23}^2\right) \\
\nu_{31} = & \left(c_{13}c_{22} - c_{12}c_{23}\right) / \left(c_{11}c_{22} - c_{12}^2\right) \\
\nu_{13} = & \left(c_{22}c_{13} - c_{12}c_{23}\right) / \left(c_{22}c_{33} - c_{23}^2\right) \\
\nu_{23} = & \left(c_{11}c_{23} - c_{12}c_{13}\right) / \left(c_{11}c_{33} - c_{13}^2\right) \\
\nu_{32} = & \left(c_{11}c_{23} - c_{12}c_{13}\right) / \left(c_{11}c_{22} - c_{12}^2\right) \\
G_{23} = & \; c_{44} \\
G_{13} = & \; c_{55} \\
G_{12} = & \; c_{66}
\end{aligned} \tag{1.10}$$

Figure 2 shows angle dependence for $E_1(\theta)$, $E_2(\theta)$, $E_3(\theta)$, where θ is angle between $z-$ and x_3- axes for rotation along $x-$ axes, computed with Equations (1.10).

For $R-$plane, in MPa:

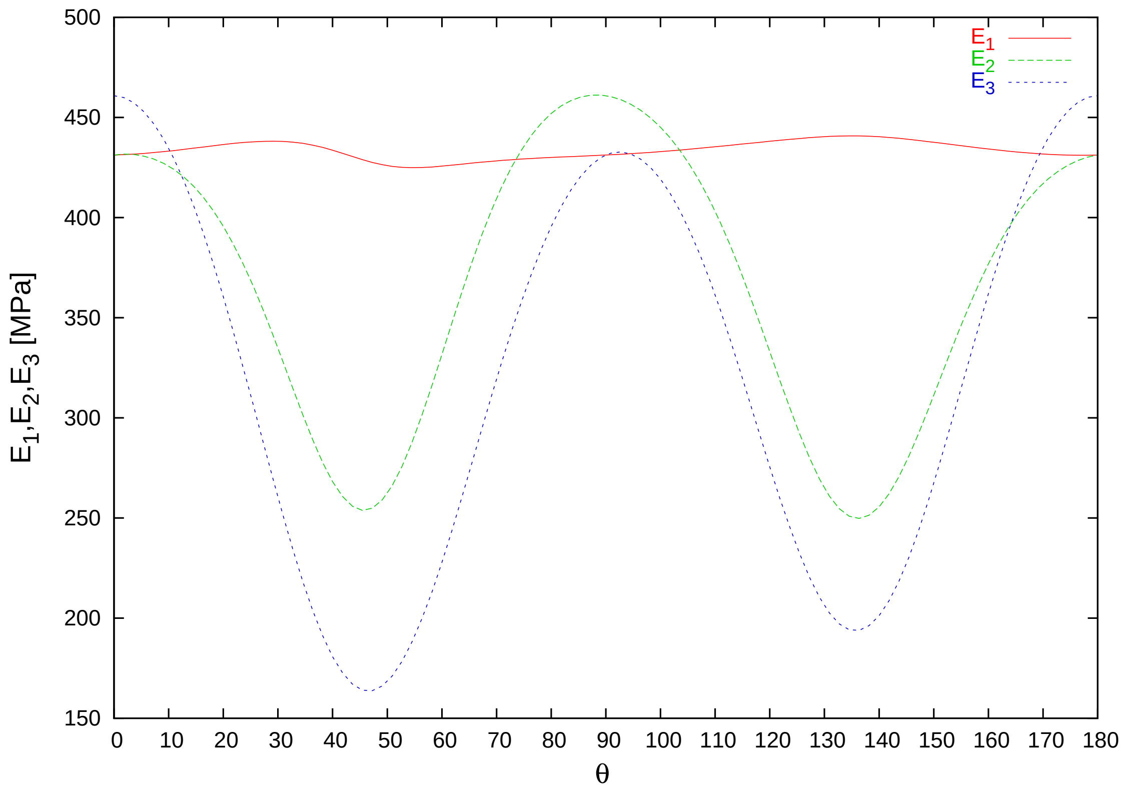

Figure 2: Angle dapendence for $E_1(\theta)$, $E_2(\theta)$, $E_3(\theta)$, where θ is angle between $z-$ and x_3- axes for rotation along $x-$ axes, computed with Equations (1.10)

$$
\begin{aligned}
E_1 &= 468.66 \\
E_2 &= 338.82 \\
E_3 &= 226.04 \\
\nu_{21} &= 0.012 \\
\nu_{12} &= 0.016 \\
\nu_{31} &= 0.212 \\
\nu_{13} &= 0.440 \\
\nu_{23} &= 0.692 \\
\nu_{32} &= 0.462 \\
G_{23} &= 359.49 \\
G_{13} &= -74.01 \\
G_{12} &= 131.63
\end{aligned}
\tag{1.11}
$$

For completeness, we provide also a complianse matrix $\mathbf{S}'$ that may be obtained from (1.4) for orthotropic material, with E_i, ν_{jk}, and G_{lm} defined by Equations (1.10):

$$\mathbf{C'} = \begin{bmatrix} 1/E_x & -\nu_{yx}/E_y & -\nu_{zx}/E_z & 0 & 0 & 0 \\ -\nu_{xy}/E_x & 1/E_y & -\nu_{zy}/E_z & 0 & 0 & 0 \\ -\nu_{xz}/E_x & -\nu_{yz}/E_y & 1/E_z & 0 & 0 & 0 \\ 0 & 0 & 0 & 1/2G_{yz} & 0 & 0 \\ 0 & 0 & 0 & 0 & 1/2G_{zx} & 0 \\ 0 & 0 & 0 & 0 & 0 & 1/2G_{xy} \end{bmatrix} \tag{1.12}$$

Because of symmetry of compliance matrix, the following conditions must be satisfied: $\nu_{yx}/E_y = \nu_{xy}/E_x$, $\nu_{zx}/E_z = \nu_{xz}/E_x$, $\nu_{zy}/E_z = \nu_{yz}/E_y$. These conditions may be used as an additional criterion for checking of consistency of calculations.

1.5 Thermal Expansion Coefficient of Sapphire

$T(^\circ K)$	200	293	500	800	1100
$\alpha_{sapph}^{\parallel c}$	4.1	4.8	7.9	8.9	9.8
$\alpha_{sapph}^{\perp c}$	3.0	6.6	7.4	8.3	9.1

For sapphire along $R-$direction [3] (National Institute of Standards and Technology Reference Data):

$T(^\circ K)$	293	300	350	400	450	500	550	600	650	700	750	800	900	1000	11
α_r	5.38	5.48	6.12	6.61	7.0	7.32	7.59	7.82	8.02	8.20	8.37	8.52	8.79	9.05	9.

A good approximation on thermal expansion coefficient along $R-$direction, $\alpha_R(T)$, is obtained with Equation (1.2.3), with parameters $\alpha_0 = -27.9$, $\beta = 26.46$, $T_0 = 195.1$, and $\gamma = 0.05$.

The Thermal Expansion Coefficient along $r-$direction is however a combination of values along $c-$axis and these perpendicular to $c-$axis:

$$\alpha_r = cos^2(\theta) \cdot \alpha_{\parallel} + sin^2(\theta) \cdot \alpha_{\perp} \tag{1.13}$$

There are some inconsistences between values of $\alpha_{\parallel}$, $\alpha_{\perp}$ found in literature. We will assume that Reference [3] provides accurate data. We will take temperature-dependent anisotropy deduced from the data published in CRC Handbook ([1]), instead of the values of $\alpha_{\parallel}$ and $\alpha_{\perp}$ from there and based on these two sets of data and Equation (1.13), we compute parameters $\alpha_{\parallel}$ and $\alpha_{\perp}$.

Anisotropy $a(T) = \alpha_{\parallel}/\alpha_{\perp}$ above $200K$ is sufficientely well approximated by function:

$$a(T) = \delta + \zeta/T^{\kappa} \tag{1.14}$$

where $\delta = 1.09$, $\zeta = 8.74$, $\kappa = 0.88$, and temperature T is in Kelvins.

Therefore:

$$\alpha_{\perp} = \frac{\alpha_R(T)}{a(T) \cdot cos^2(\theta) + sin^2(\theta)} \tag{1.15}$$

$$\alpha_{\parallel} = \alpha_{\perp} \cdot a(T) \tag{1.16}$$

1.6 *Effective* Thermal Expansion Coefficient

When computing residual strains and stress by using Comsol Multiphisics, one enters initial and final temperature of materials and coefficients of thermal expansion. However, thermal expansion coefficients depend on temperature, and there is no way to enter that variation into parameters governing strain equations. Alternatively, we should compute rather an effective thermal expansion coefficient, α_{eff}, for a given temperature range from T_1 to T_2:

$$\frac{\Delta L}{L} = \alpha_{eff} \cdot (T_2 - T_1) = \int_{T_1}^{T_2} \alpha(T) \cdot dT \tag{1.17}$$

For solder, we use Equation (1.3.1) for integration in (1.17), obtaining:

$$\alpha_{eff} = \alpha_a + \alpha_b \cdot (T_2 - T_1)/2 \tag{1.18}$$

For Titanium, and for sapphire expansion in r-direction, we use Equation (1.2.3) with their corresponding parameters, as discussed already:

$$\alpha_{eff} = \alpha_0 + \frac{\beta}{(\gamma + 1) \cdot (T_2 - T_1)} \cdot \left[(T_2 - T_0)^{\gamma+1} - (T_1 - T_0)^{\gamma+1} \right] \tag{1.19}$$

Once we have α_{eff} for expansion in $r-$direction for sapphire, we compute anisotropy ratio from Equations (1.15) and (1.16), followed by computing of expansion coefficients along the $c-$axis and within $c-$plane.

The following are computed results when T_1 is assumed $300K$ and T_2 is $972K$ (melting point of solder):

Solder: $\alpha_{eff} = 18.49 \cdot 10^{-6}/K$
Titanium: $\alpha_{eff} = 10.41 \cdot 10^{-6}/K$
Sapphire, along r-direction: $\alpha_{eff}^{R} = 7.77 \cdot 10^{-6}/K$

Sapphire anisotropy $a(T)$ at $972K$ = 1.1105
Sapphire, along r-direction, at $972K$: $\alpha^R = 9.006 \cdot 10^{-6}/K$
Sapphire, within c-plane, at $972K$: $\alpha^{\perp} = 8.722$
Sapphire, along c-plane, at $972K$: $\alpha^{\parallel} = 9.686$

Sapphire anisotropy $a(T)$ at $300K$ = 1.1478
Sapphire, along r-direction, at $300K$: $\alpha^R = 5.491 \cdot 10^{-6}/K$
Sapphire, within c-plane, at $300K$: $\alpha^{\perp} = 5.261 \cdot 10^{-6}/K$
Sapphire, along c-plane, at $300K$: $\alpha^{\|} = 6.039$

Knowing however values of anisotropy parameters at T_1 and T_2 is not sufficient to determine effective thermal expantion coefficients in $c \parallel$ and $c \perp$ directions. These must be computed from integrals of equations (1.15) and (1.16):

$$\alpha^{\perp}_{eff} = \frac{1}{T_2 - T_1} \cdot \int_{T_1}^{T_2} \frac{\alpha_R(T)}{(\delta + \zeta/T^{\kappa}) \cdot cos^2(\theta) + sin^2(\theta)} dT \tag{1.20}$$

$$\alpha^{\|}_{eff} = \frac{1}{T_2 - T_1} \cdot \int_{T_1}^{T_2} \alpha_{\perp} \cdot \left(\delta + \zeta/T^{\kappa}\right) dT \tag{1.21}$$

Numerical integration gives us: Sapphire, within c-plane: $\alpha^{\perp}_{eff} = 7.503 \cdot 10^{-6}/K$
Sapphire, along c-direction: $\alpha^{\|}_{eff} = 8.414 \cdot 10^{-6}/K$

There is one more step to perform before we may use the obtained anisotropic parameters for input into Comsole Multiphysics calculations. Sapphire plate is oriented with $r-$direction perpendicular to its surface and the surface of Titanium plate, after rotation along $x-$axes of the crystal (as Figure 1 shows). Therefore, the thermal expansion tensor will have xx component $\alpha_{xx} = \alpha^{\perp}_{eff}$, zz component $\alpha_{zz} = \alpha^{R}_{eff}$, and yy component given by: $\alpha_{yy} = \alpha^{\perp}_{eff} \cdot cos^2(\theta) + \alpha^{\|}_{eff} \cdot sin^2(\theta)$, which has a value of $8.145 \cdot 10^{-6}/K$:

$$\alpha_{\mathbf{eff}} = \begin{bmatrix} 7.503 & 0 & 0 \\ 0 & 8.145 & 0 \\ 0 & 0 & 7.77 \end{bmatrix} 10^{-6}/K \tag{1.22}$$

Толщина слоя сапфировой подложки ЭЧП, 80-110 мкм (for sensor up to 1.6 MPa) 140-200 мкм (for sensor for higher pressures) than 1.6 MPa)

1.7 Silicon Mechanical Properties

Diamont structure with fcc Bravais lattice.

For ideally pure silicon, lattice parameters at $22.500\ ^{\circ}\ C$: $a = 543.102pm$

Linear thermal expansion coefficient, $\alpha(T)$:

$\alpha(T) = (3.725)$

Кремниевые тензорезисторы ориентированы вдоль направлений <110> плоскости кремния.

At room temperature:

$C_{11} = 1656.4 MPa$
$C_{12} = 639.4 MPa$
$C_{44} = 795.1 MPa$

1.8 Thermal Expansion Coefficient of Silicon

1.9 Диапазон параметров и характеристики моделируемого объекта

Элемент полупроводниковый чувствительный (ЭПЧ) микроэлектронного одномембранного тензопреобразователя (ТП) серии МД (ВМИУ.408854.039, ТУ4212-163-00227459-98) и РТ (ВМИУ.408854.074, ТУ4212-281-00227459-2008), выпускаемых ЗАО «ОРЛЭКС», изготавливается из КНС (кремний на сапфире) структуры методом фотолитографии после насыщения кремния бором до величины удельного поверхностного сопротивления 4,0-5,5 Ом/кв и представляет из себя тензочувствительную схему в виде моста Уитстона, в исполнении «Замкнутый мост» или «Разомкнутый мост», сформированную в виде мезаструктуры из гетероэпитаксиального кремния с кристаллографической ориентацией (001) на сапфировой подложке с плоскостью кристаллографической ориентации (012) (r-плоскость) с толщиной от 80 до 200 мкм.

Кремниевые тензорезисторы ориентированы вдоль направлений $<110>$ плоскости кремния, одна пара из которых ориентирована параллельно радиусу мембраны, а другая — перпендикулярно. ЭПЧ располагается на поверхности титановой аксиально-симметричной мембраны из сплава ВТ9, со слоем припоя ПСр72 толщиной 0,04±0,01 мм между ними, образуя чувствительный элемент (ЧЭ) ТП.

Сапфировая подложка КНС-структуры, титановая мембрана и слой припоя между ними образуют трёхслойную (сапфир-припой-титан) мембрану, являющуюся упругим элементом (УЭ) ТП и, соответственно, механической частью ЧЭ ТП.

Максимальное рабочее давление моделируемых ТП лежит в диапазоне от 1,6 МПа до 150 МПа и определяется соответствующим ТУ.

Диапазон рабочих температур определён ТУ и может лежать в диапазоне от -50°C (ТП серии МД) до +200°C (ТП серии РТ-3XX-XXX).

Диаметр титановой мембраны от 2,5 до 5,8 мм, толщина от 0,11 до 1,8 мм. У мембраны, предназначенной для измерения малых давлений, может быть жесткий центр (ТП МД10-1,6-V имеет жесткий центр диаметром 2,8 мм и толщиной 1 мм).

1.10 A few definitions

SI units are used in this article.

Young's modulus E is the slope of the stress-strain curve in uniaxial tension. It has dimensions of stress (N/m^2). You can think of E as a measure of the stiffness of the solid.

The larger the value of E, the stiffer the solid. For a stable material, $E > 0$.

$$E = \frac{stress}{strain} = \frac{\sigma}{\varepsilon} = \frac{F/A_0}{\Delta L/L_0} \tag{1.23}$$

Poisson's ratio ν is the ratio of lateral to longitudinal strain in uniaxial tensile stress. It is dimensionless and typically ranges from 0.2-0.49, and is around 0.3 for most metals. For a stable material, $-1 < \nu < 0.5$. It is a measure of the compressibility of the solid. If $\nu = 0.5$, the solid is incompressible its volume remains constant, no matter how it is deformed. If $\nu = 0$, then stretching a specimen causes no lateral contraction.

Elastic limit. Greatest stress that can be applied to a material without causing permanent deformation. For metals and other materials that have a significant straight line portion in their stress-strain diagram, elastic limit is approximately equal to proportional limit. For materials that do not exhibit a significant proportional limit, elastic limit is an arbitrary approximation (apparent elastic limit).

Yield strength. Indication of maximum stress that can be developed in a material without causing plastic deformation. It is the stress at which a material exhibits a specified permanent deformation and is a practical approximation of elastic limit.

Proportional limit is the limit behind which the relation between stress and strain is no longer linear. Since, strictly, that relation is never linear (it could be only up to certain accuracy), the *proportional limit* parameter is seldom used by engineers: it depands on definition of linearity and interpretation of experimental results.

The *Elastic limit* is significantly higher usually than the not so well defined *proportional limit*.

The *tensile strength* of a material is the maximum amount of tensile stress that it can be subjected to before it breaks.

2 Classical Thin Plate Equation

2.1 Theory limitations

Thin plate theory limitation: the contradicting assumptions of zero transverse normal stress and the corresponding strain. The *Classical Thin Plate Theory* does not account for radial strain component. It is assumed that there is no plate deformation in radial direction when deriving plate equations. The only deformation considered is the one in z-direction. However, deformation in r-direction can be computed from the deformation in z-direction obtained.

The theory assumes also that all displacements are small.

Regardless of the above mentioned limitations, the theory describes resonably well a broad range of practical problems and is extremely usuful in testing validity of numerical results.

2.2 General displacement-strain relation

We assume that the material is an isotropic, linear elastic solid, with Young's modulus E and Poisson's ratio ν. We need to solve for the displacement field u_i, the strain field ε_{ij}, and the stress field σ_{ij}.

$$\varepsilon_{ij} = \frac{1}{2}\left(\frac{\partial u_i}{\partial x_j} + \frac{\partial u_j}{\partial x_i}\right) \tag{2.1}$$

While in cylindrical polar coordinates:

$$\begin{aligned}
\varepsilon_{rr} &= \tfrac{\partial u}{\partial r} \\
\varepsilon_{\theta\theta} &= \tfrac{1}{r}\tfrac{\partial \nu}{\partial \theta} + \tfrac{u}{r} \\
\varepsilon_{zz} &= \tfrac{\partial w}{\partial z} \\
\varepsilon_{r\theta} &= \tfrac{1}{2}\left(\tfrac{\partial \nu}{\partial r} + \tfrac{1}{r}\tfrac{\partial u}{\partial \theta} - \tfrac{\nu}{r}\right) \\
\varepsilon_{\theta z} &= \tfrac{1}{2}\left(\tfrac{1}{r}\tfrac{\partial w}{\partial \theta} + \tfrac{\partial \nu}{\partial z}\right) \\
\varepsilon_{zr} &= \tfrac{1}{2}\left(\tfrac{\partial u}{\partial z} + \tfrac{\partial w}{\partial r}\right)
\end{aligned} \tag{2.2}$$

2.3 Stress-strain relation

$$\sigma_{ij} = \frac{E}{1+\nu}\left(\varepsilon_{ij} + \frac{\nu}{1-2\nu}\varepsilon_{kk}\delta_{ij}\right) \tag{2.3}$$

or:

$$\begin{aligned}
\sigma_{xx} &= \tfrac{E}{(1+\nu)(1-2\nu)}\left[(1-\nu)\varepsilon_{xx} + \nu(\varepsilon_{yy} + \varepsilon_{zz})\right] \\
\sigma_{yy} &= \tfrac{E}{(1+\nu)(1-2\nu)}\left[(1-\nu)\varepsilon_{yy} + \nu(\varepsilon_{zz} + \varepsilon_{zz})\right] \\
\sigma_{zz} &= \tfrac{E}{(1+\nu)(1-2\nu)}\left[(1-\nu)\varepsilon_{zz} + \nu(\varepsilon_{xx} + \varepsilon_{yy})\right] \\
\sigma_{xy} &= \tfrac{E}{(1+\nu)}\varepsilon_{xy} \\
\sigma_{yz} &= \tfrac{E}{(1+\nu)}\varepsilon_{yz} \\
\sigma_{zx} &= \tfrac{E}{(1+\nu)}\varepsilon_{zx}
\end{aligned} \tag{2.4}$$

In cylindrical polar coordinates, the relations are identical, with appropriate replacement of σ_{ij} by σ_{kl}, etc.

2.4 Equations of Local Equilibrium

Equilibrium Equation in static case, has the form (for each $j-$direction):

$$\frac{\partial \sigma_{ij}}{\partial x_i} + b_j = 0 \tag{2.5}$$

where summation is done over $i-$indexes, and b_j is the volume density of internal body forces. b_j could be caused, for instance, by external electromagnetic interaction with the material. In our case, when result of external hydrostatic pressure on a plate is studied, exerted in $z-$direction, body force density in that direction is p/h, where p is value of pressure and h is plate thickness.

In cylindrical polar coordinates, a general form of the above set of equations will have the form:

$$\begin{aligned}
\frac{\partial \sigma_{rr}}{\partial r} + \frac{1}{r}\frac{\partial \sigma_{r\theta}}{\partial \theta} + \frac{\partial \sigma_{rz}}{\partial z} + \frac{\sigma_{rr}-\sigma_{\theta\theta}}{r} + b_r &= 0 \\
\frac{\partial \sigma_{r\theta}}{\partial r} + \frac{1}{r}\frac{\partial \sigma_{\theta\theta}}{\partial \theta} + \frac{\partial \sigma_{\theta z}}{\partial z} + \frac{2\sigma_{r\theta}}{r} + b_\theta &= 0 \\
\frac{\partial \sigma_{rz}}{\partial r} + \frac{1}{r}\frac{\partial \sigma_{\theta z}}{\partial \theta} + \frac{\partial \sigma_{zz}}{\partial z} + \frac{\sigma_{rz}}{r} + b_z &= 0
\end{aligned} \tag{2.6}$$

2.5 Equations of Global Equilibrium

In general, body force density components b_i could be functions of coordinates. In other words, the above equations represent conditions of *local* equilibrium.

To add conditions of *global* equilibrium, it is convenient to consider integrated moments of forces and share, and note that these all must be in equilibrium as well (equal to 0 in our case).

$$
\begin{aligned}
M_x &= \textstyle\int_{-h/2}^{h/2} z\sigma_{xx} dz \\
M_y &= \textstyle\int_{-h/2}^{h/2} z\sigma_{yy} dz \\
M_{xy} &= \textstyle\int_{-h/2}^{h/2} z\sigma_{xy} dz \\
Q_{xz} &= \textstyle\int_{-h/2}^{h/2} \sigma_{xz} dz \\
Q_{yz} &= \textstyle\int_{-h/2}^{h/2} \sigma_{yz} dz
\end{aligned} \tag{2.7}
$$

In equilibrium:

$$
\begin{aligned}
Q_{yz} &= \frac{\partial M_{xy}}{\partial x} + \frac{\partial M_y}{\partial y} \\
Q_{xz} &= \frac{\partial M_{xy}}{\partial y} + \frac{\partial M_x}{\partial x} \\
\frac{\partial Q_{xz}}{\partial x} + \frac{\partial Q_{yz}}{\partial y} &= -p_z
\end{aligned} \tag{2.8}
$$

We combine the above equations, to elliminate Q_{xz} and Q_{yz}:

$$
\frac{\partial^2 M_x}{\partial x^2} + 2\frac{\partial^2 M_{xy}}{\partial x \partial y} + \frac{\partial^2 M_y}{\partial y^2} = -p_z \tag{2.9}
$$

Now, we can write the above in the form of integrals:

$$
\int_{-h/2}^{h/2} \left(\frac{\partial^2 \sigma_{xx}}{\partial x^2} + 2\frac{\partial^2 \sigma_{xy}}{\partial x \partial y} + \frac{\partial^2 \sigma_{yy}}{\partial y^2} \right) dz = -p_z \tag{2.10}
$$

At this point, we substitute stress by strain, to finally get:

$$
\int_{-h/2}^{h/2} \frac{Ez^2}{1-\nu^2} dz \left(\frac{\partial^4 w}{\partial x^4} + 2\frac{\partial^4 w}{\partial x^2 \partial y^2} + \frac{\partial^4 w}{\partial y^4} \right) = -p_z \tag{2.11}
$$

And, for convenience, we introduce the bending (flexual rigidity) parameter D:

$$
D = \int_{-h/2}^{h/2} \frac{Ez^2}{1-\nu^2} dz = \frac{Eh^3}{12\left(1-\nu^2\right)} \tag{2.12}
$$

With that definition, we can write the *Classical Plate Equation* in the form:

$$
\nabla^4 w = \frac{p}{D} \tag{2.13}
$$

where

$$\nabla^4 = \left(\frac{\partial^4}{\partial x^4} + 2\frac{\partial^4}{\partial x^2 \partial y^2} + \frac{\partial^4}{\partial y^4} \right) \tag{2.14}$$

Let us note that p and D have been assumed constant accross plate, when deriving Eq. (2.13). In a more rigurous form (and a more general one), when D is a function of coordinates, the integration in Eq. (2.12) should be done in Eq. (2.9), and that will result in the following form of plate equation:

$$\nabla^2 D(x, y, z) \nabla^2 w(x, y, z) = p_z(x, y) \tag{2.15}$$

In cylindrical polar coordinates, the final result is the same, with the change of Laplace operator ∇^2, and change of bi-harmonic operator ∇^4, where ∇^2 is given there by:

$$\nabla^2 = \frac{\partial^2}{\partial r^2} + \frac{1}{r}\frac{\partial}{\partial r} + \frac{1}{r^2}\frac{\partial^2}{\partial \theta^2} + \frac{\partial^2}{\partial z^2} \tag{2.16}$$

Equation (2.13) (with D independent of coordinates) leads us finally to the following equation on $w(r)$:

$$\begin{aligned} &D\left(\frac{d^4 w}{dr^4} + \frac{2}{r}\frac{d^3 w}{dr^3} - \frac{1}{r^2}\frac{d^2 w}{dr^2} + \frac{1}{r^3}\frac{dw}{dr} \right) \\ &= D\frac{1}{r}\frac{d}{dr}\left(r\frac{d}{dr}\left(\frac{1}{r}\frac{d}{dr}\left(r\frac{dw}{dr} \right) \right) \right) = p \end{aligned} \tag{2.17}$$

After repeated integration, we receive a general solution:

$$w = \frac{1}{64D} pr^4 + C_1 r^2 ln(r) + C_2 ln(r) + C_3 r^2 + C_4, \tag{2.18}$$

where parameters C_1, C_2, C_3 and C_4 are integration constants, to be determined from boundary conditions.

The displacement w at $r = 0$ must be finite, and therefore C_1 and C_2 must be equal to 0. Without these conditions, the curvature at $r = 0$ would be infinite also.

Hence, we arrive to a simpler solution:

$$w = \frac{1}{64D} pr^4 + C_3 r^2 + C_4 \tag{2.19}$$

3 Clamped plate

Assume that the plate is fixed at $r = R$. Hence, $w(r = R) = 0$, and we have:

$$\frac{1}{64D}pR^4 + C_3R^2 + C_4 = 0; \tag{3.1}$$

But we must also have dw/dr equal 0 at $r = R$, otherwise an infinite share would result at support boundary:

$$\frac{1}{64D}4pR^3 + 2C_3R = 0; \tag{3.2}$$

Hence, we have:

$$C_3 = -\frac{1}{64D}2pR^2; C_4 = \frac{1}{64D}pR^4 \tag{3.3}$$

Hence:

$$w = \frac{p}{64D}\left(r^2 - R^2\right)^2 \tag{3.4}$$

3.1 $u(r)$ - radial displacement

The *Classical Thin Plate Theory* does not account for radial strain component, as already explained. However, deformation in r-direction, $u(r)$, can be computed from $w(r)$, the obtained deformation in z-direction. This is the domain of Timoshenko and Woinowsky-Krieger theory [4]. After basic analysis of deformation's geometry, one obtains [4]:

$$u(r) = \frac{h}{2}\frac{dw}{dr} \tag{3.5}$$

Hence, by using (3.4), we obtain:

$$u(r) = 2\frac{h}{R}\cdot\frac{p}{64D}\cdot\frac{r}{R}\cdot\left(\left(\frac{r}{R}\right)^2 - 1\right)\cdot R^4 \tag{3.6}$$

3.2 Strain $\varepsilon_{zr}(r)$

In the *Classical Thin Plate Theory*, radial and $z-$deformations u and w do not depend on z. Also, they do not depand on polar angle θ, in case of cylindrical symmetry that interests us. Therefore, in equations (2.2) $\partial w/\partial\theta$, $\partial u/\partial\theta$, and $\partial\nu/\partial\theta$ must be equal to 0, $\partial w/\partial z$, $\partial u/\partial z$, $\partial\nu/\partial z$ must be 0.

Now, here, we take however into account that we are able to compute (r), and, with the above mentioned conditions, we modify the equations (2.2) on strain tensor into the following set:

$$
\begin{aligned}
\varepsilon_{rr} &= \frac{du}{dlr} \\
\varepsilon_{\theta\theta} &= \frac{u}{r} \\
\varepsilon_{zr} &= \frac{1}{2}\frac{dw}{dr}
\end{aligned} \tag{3.7}
$$

Hence, we have:

$$\varepsilon_{zr}(r) = \frac{p}{32D}\left(\frac{r}{R}\right)\cdot\left(\left(\frac{r}{R}\right)^2 - 1\right)\cdot R^3 \tag{3.8}$$

With $\varepsilon_{zr} = 0$ at $r = 0$ and $r = R$, the function has a minimum (maximum of absolute value) at $r/R = 1/\sqrt{3} \approx 0.577$, with value there of $-2/(3\sqrt{3})\cdot pR^3/32D$.

Some care is needed here, however. In a real case of plate of finite thickness, w and u do depand on z. This will have influance on ε_{zr} tensor component, and also on ε_{zz}, as discussed later.

ε_{zr} tensor component should be equal to 0, or it should be close to 0. Why I do not see that?

3.3 $\varepsilon_{rr}(r)$ - radial component of strain tensor

According to equations (3.7), radial component of strain tensor in cylindrical-polar coordinates, ε_{rr}, is equal to du/dr:

$$\varepsilon_{rr}(r) = \frac{h}{R}\cdot\frac{2p}{64D}\cdot\left(3\left(\frac{r}{R}\right)^2 - 1\right)\cdot R^3 \tag{3.9}$$

At $r = 0$, $\varepsilon_{rr}(r)$ has value of $-(h/R)\cdot(p/32D)\cdot R^3$ and twice as much with opposite sign at $r = R$. $\varepsilon_{rr}(r)$ passes through zero at $r/R = 1/\sqrt{3} \approx 0.577$.

It is interesting to compare maximum absolute values of ε_{rr} and ε_{zr}: $\varepsilon_{rr}/\varepsilon_{zr} = 3\sqrt{3}\cdot(h/R)$, i.e. at h/R larger than about 0.2, we expect to observe a bigger amplitude of $\varepsilon_{rr}(r)$ than that of $\varepsilon_{zr}(r)$, regardless of pressure applied. Thin plate theory is obviously not valid any more at such a high ratio of h/R, however, it's qualitative results are likely to remain valid within reasonable accuracy, up to certain extend of parameters.

4 Clamped plate with core of different thickness

4.1 $z-$ displacement $w(r)$

Assume that the plate central core thickness is different, that it is h_a, while it's radius is R_a. The external ring has thickness h_b and radius R_b. We still expect that the equation (2.19) describes the problem. Now, however, a different set of boundary conditions must be used, and parameter D will also be different for both parts of plate:

$$
\begin{aligned}
D_a &= E h_a^3 / \left(12\left(1-\nu^2\right)\right) \\
D_b &= E h_b^3 / \left(12\left(1-\nu^2\right)\right)
\end{aligned} \tag{4.1}
$$

Two boundary conditions will have the form, as before:

$$
\begin{aligned}
\frac{p}{64 D_b} R_b^4 + C_{b3} R_b^2 + C_{b4} &= 0 \\
\frac{4p}{64 D_b} R_b^3 + 2 C_{b3} R_b &= 0
\end{aligned} \tag{4.2}
$$

And we have two additional boundary conditions at $r = R_a$, one that imposes that $w(r)$ is the same for both functions, and another that $dw(r)/dr$ is the same for both functions, e.i.:

$$
\begin{aligned}
\frac{p}{64 D_a} R_a^4 + C_{a3} R_a^2 + C_{a4} &= \frac{p}{64 D_b} R_a^4 + C_{b3} R_a^2 + C_{b4} \\
\frac{4p}{64 D_a} R_a^3 + 2 C_{a3} R_a &= \frac{4p}{64 D_b} R_a^3 + 2 C_{b3} R_a
\end{aligned} \tag{4.3}
$$

Hence, we have four equations and four unknown boundary parameters: C_{a3}, C_{a4}, C_{b3}, and C_{b4}. This looks not bad, so far...

Solving the above set of equations gives us the following values:

$$
\begin{aligned}
C_{b3} &= -\frac{2p}{64 D_b} R_b^2 \\
C_{b4} &= \frac{p}{64 D_b} R_b^4 \\
C_{a3} &= -\frac{2p}{64 D_a}\left[\frac{D_a}{D_b}\left(\frac{R_b}{R_a}\right)^2 + 1 - \frac{D_a}{D_b}\right] R_a^2 \\
C_{a4} &= \frac{p}{64 D_a}\left[\frac{D_a}{D_b}\left(\frac{R_b}{R_a}\right)^4 + 1 - \frac{D_a}{D_b}\right] R_a^4
\end{aligned} \tag{4.4}
$$

We are not surprized that constants C_{b3} and C_{b4} have exactly the same value as these derived from eq. (3.3); the solution for $R_b \leq r \leq R_a$ does not depend on the solution for $r < R_a$.

Let us write the solution for $r < a$ in its full form:

$$
w = \frac{p}{64 D_a}\left\{ r^4 - 2\left[\frac{D_a}{D_b}\left(\frac{R_b}{R_a}\right)^2 + 1 - \frac{D_a}{D_b}\right] R_a^2 r^2 + \left[\frac{D_a}{D_b}\left(\frac{R_b}{R_a}\right)^4 + 1 - \frac{D_a}{D_b}\right] R_a^4 \right\} \tag{4.5}
$$

Intuition tells us that it should be possible to write the above formula in a similar form as eq. (3.4), with change of some parameters. If eq. (4.5) was valid at $r > R_a$, its minimum would occur at $r = r_0$, where r_0 is given by:

$$r_0^2 = \left[\frac{D_a}{D_b}\left(\frac{R_b}{R_a}\right)^2 + 1 - \frac{D_a}{D_b}\right] R_a^2 \tag{4.6}$$

The value of w_0, i.e. of $w(r = r_0)$, would be:

$$w_0 = \frac{1}{64D_a} p r_0^4 + C_{3a} r_0^2 + C_{4a} \tag{4.7}$$

After same basic algebra one finds that (4.5) can be written indeed in the form:

$$w = \frac{1}{64D_a} p \left(r^2 - r_0^2\right)^2 + w_0 \tag{4.8}$$

We see that the solution for plate with core, for $r > R_a$, is identical to the solution for plate without core. This is another simple observation that helps us to understand better properties of possible solutions of Classical Plate Equation.

4.2 $r-$ displacement $u(r)$

When deriving equations for $w(r)$, we assumed that a boundary conditions at $r = R_a$ is that $dw(r)/dr$ is the same for both functions, i.e. that radial strain must be a continuous fonction of r.

For external ring, we have already expression on $u(r)$ as given by (4.9). We rewrite it in the form (which is valid for $r > R_a$):

$$u_b(r) = \frac{2h_b}{R_b} \cdot \frac{p}{64D_b} \cdot \frac{r}{R_b} \cdot \left(\left(\frac{r}{R_b}\right)^2 - 1\right) \cdot R_b^3 \tag{4.9}$$

For internal core, the equation is identical, with replacement of a few parameters (and the equation is valid for $r < R_a$):

$$u_a(r) = \frac{2h_a}{R_a} \cdot \frac{p}{64D_a} \cdot \frac{r}{r_0} \cdot \left(\left(\frac{r}{r_0}\right)^2 - 1\right) \cdot r_0^3 \tag{4.10}$$

4.3 $\varepsilon_{rr}(r)$ - radial component of strain tensor

The radial component of strain tensor is given by (3.9) for $r > R_a$, where R_a is core size. While for $r < R_a$ a modified version of that equation will hold:

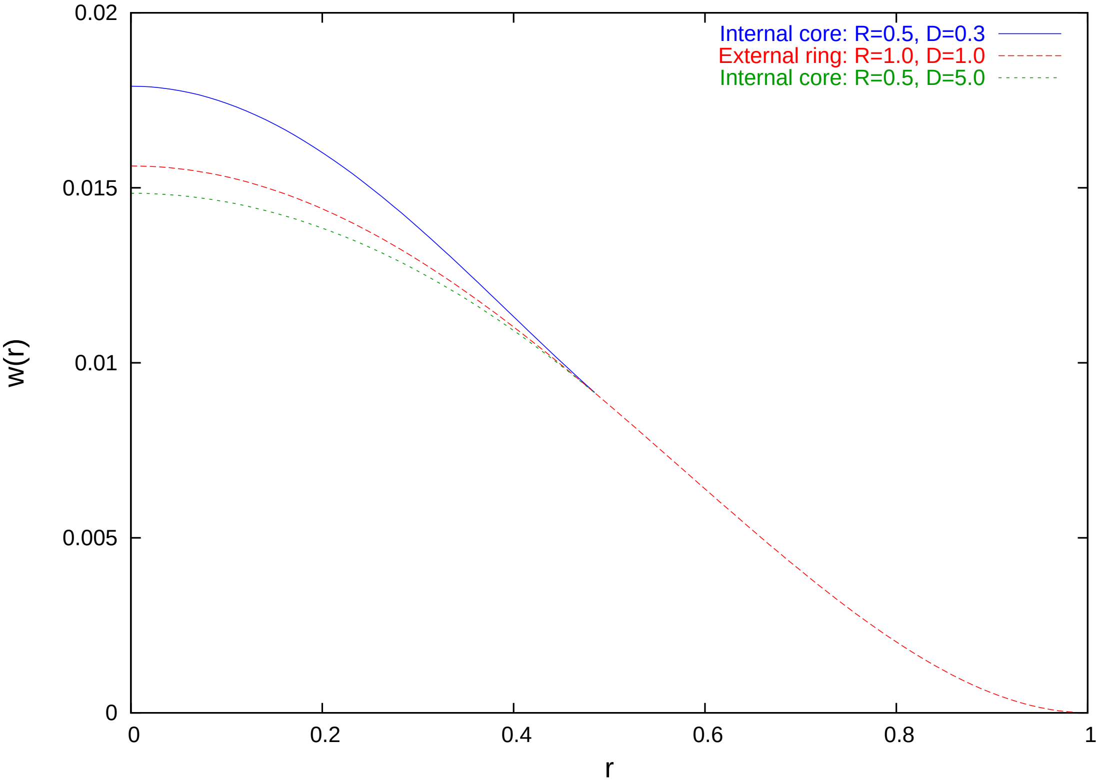

Figure 3: $z-$ displacement $w(r)$ computed by using equations (3.4) and (4.5). Dimensionless units are assumed, with pressure $p = 1$, radius of the external ring and internal core equal 0.5 and 1, respectively, and different values of parameter D, as shown in the figure. All three curves meet at $r = 0.5$ with the same values and slope.

$$\varepsilon_{rr}(r) = \frac{h_a}{r_0} \cdot \frac{2p}{64D_a} \cdot \left(3\left(\frac{r}{r_0}\right)^2 - 1\right) \cdot r_0^3 \tag{4.11}$$

where r_0 is given by equation (4.6).

5 Circular Plates of Variable Thickness

The method illustrated in previous section can be extended to calculations for any circular plate of variable thickness, loaded symmetrically with respect to the center. The stresses and deflections can be found as follows: The plate is divided into an arbitrary number of concentric rings, each of which is assumed to have a uniform thickness equal to its mean thickness. The problem becomes to determine boundary conditions that the slope of each ring at its inner circumference is equal to the slope of the next inner ring at its outer circumference.

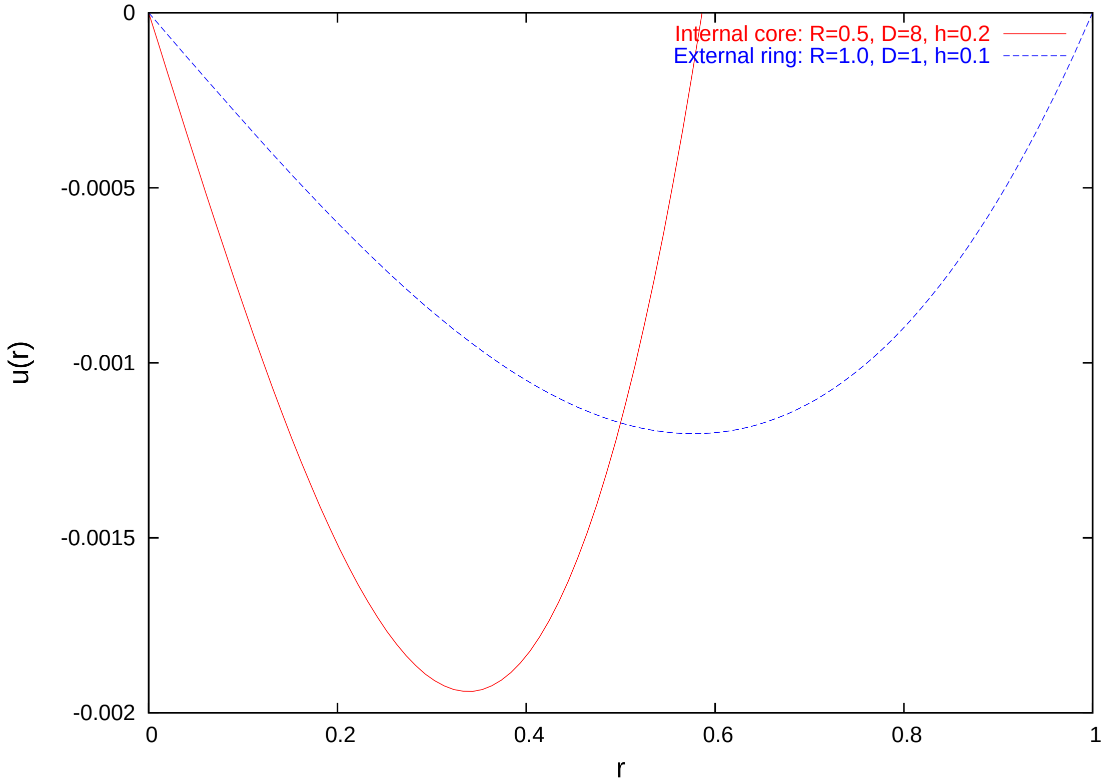

Figure 4: $r-$ displacement $u(r)$ computed by using equations (4.9) and (4.10). Dimensionless units are assumed, with pressure $p = 1$, radius of the external ring and internal core equal 0.5 and 1, respectively, and different values of parameter D, as shown in the figure. The curve for case with internal core of radius $R = 0.5$ is computed also for $r > 0.5$ but in reality the valid solution for r greater than core radius is given by equation (4.9) for coreless plate. Both curves intersect at $r = R_a$, assuring continuity of $u(r)$ on the boundary of internal core and external ring.

6 Multilayer problem

Let us go back to the equation on global equilibrium of forces, (2.11), and on D, (2.12). That last formula is valid also when Young's Modulus E and/or Poisson's ratio ν change accross the plate thickness, i.e. when both are functions of z. Just remember only that (2.11) is used to derive global equilibrium of force moments, and therefore the integration there must be done between $-h/2$ and $h/2$, where h is the thickness of all layers combined: In case of a set of discrete layers, $h = \Sigma_i h_i$.

For simplicity, let us consider a situation of two layers, of thickenss h_1 and h_2, where $h_1 > h_2$, and corresponding Young's and Poisson's parameters are, respectively, E_1, ν_1, and E_2, ν_2.

We ought now to define D for equation (2.13) in the following manner, different than that given by (2.12):

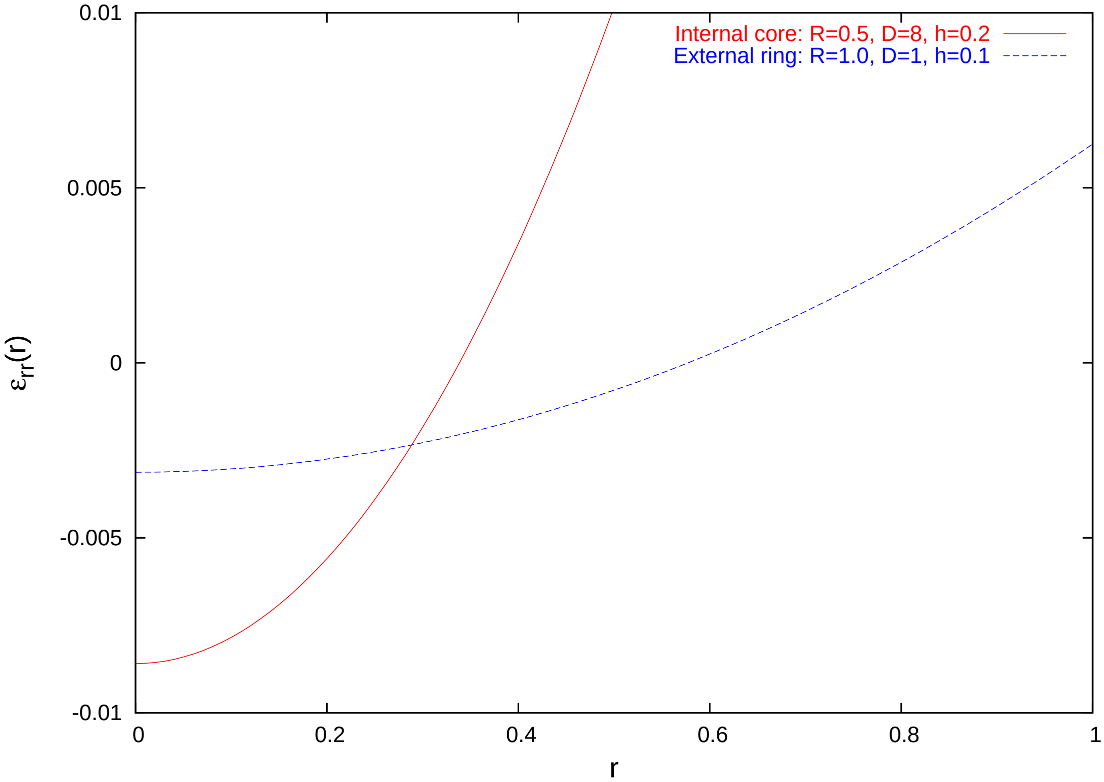

Figure 5: The strain tensor component, ε_{rr}, as a function of r computed by using equations (3.9) and (4.11). Dimensionless units are assumed, with the same parameters as in Fig. 4.

$$D = \int_{-h/2}^{h_1 - h/2} \frac{E_1 z^2}{1-\nu_1^2} dz + \int_{h_1-h/2}^{h/2} \frac{E_2 z^2}{1-\nu_2^2} dz \tag{6.1}$$

Defining $s_i = E_i/(1-\nu_i^2)$, we get:

$$D = (s_1/3) \cdot z^3|_{-h/2}^{h_1-h/2} + (s_2/3) \cdot z^3|_{h_1-h/2}^{h/2} \tag{6.2}$$

7 Anisotropy

7.1 Isotropic Elliptical Plate

Intuition tells us that solutions to *Classical Plate Equation* (2.13) for an anisotropic material (two sets of properties, like Young's modulus and Poison's ratio, in two principal directions, x and y) should be identical to these for isotropic plate, with some change of parameters, and that these solutions should envolve elliptical geometry.

Consider first an elliptical solution to Eq. (2.13) in Cartesian coordinates, with ∇^4 defined by Eq. (2.14). We find that the following solution is valid:

$$w = w_0 \cdot \left(\left(\frac{x}{a}\right)^2 + \left(\frac{y}{b}\right)^2 - 1 \right)^2 \tag{7.1}$$

with w_0 given by:

$$w_0 = \frac{p}{D\left(24/a^4 + 24/b^4 + 16/a^2b^2\right)} \tag{7.2}$$

7.2 Anisotropic Circular Plate

The case is toooo complex...!!!

8 Comsol solutions

8.1 Comparing Analytical Thin Plate Solution and Comsol Computed Results

In this subsection, we are testing how good is Analytical Thin Plate Solution depanding on plate thickness.

We use here the following parameters of an isotropic material (these are for Titanium; values for E and ν in Comsol are incorrect for Titanium): $E = 106 GPa$ and $\nu = 0.34$

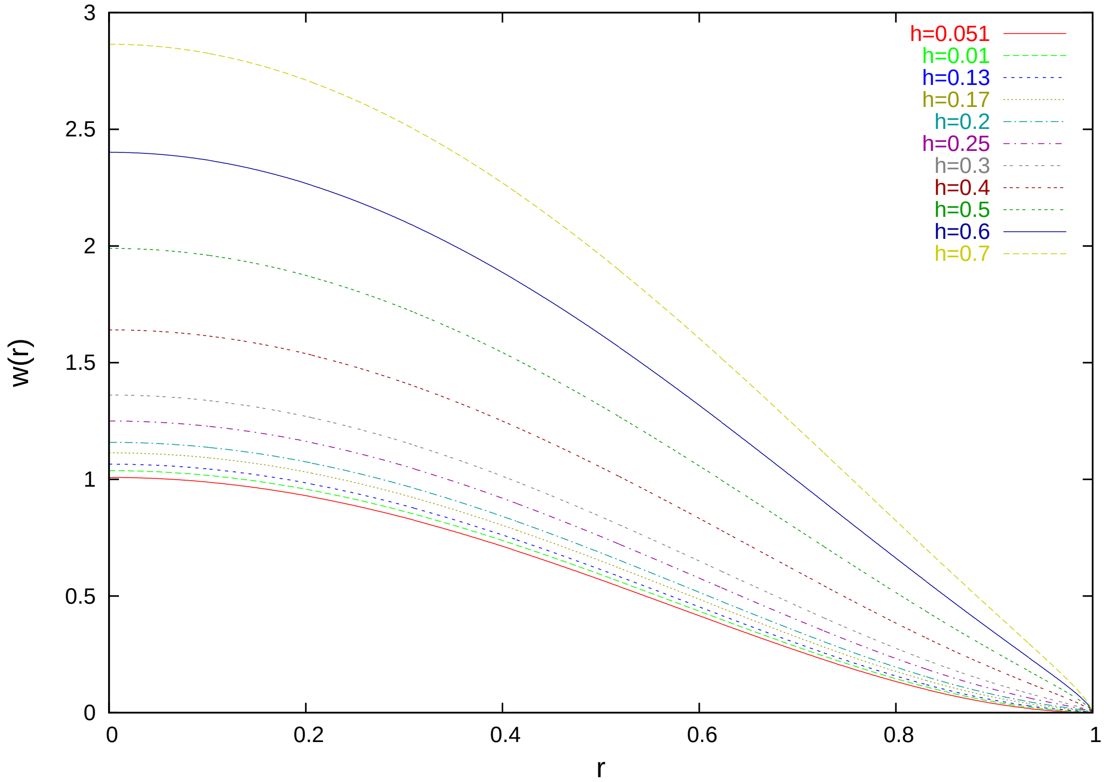

Figure 6: FEM computed $z-$ displacement $w(r)$ for a plate fixed at the edges, for a range of thickness h values. Equations (3.4) and (2.12) were used to normalize $w(r)$ with computed values of $w(r = 0)$. In order to avoid large deformations, low pressure was assumed.

As Figures 6 and 7 show, a nearly perfect agreement is observed between analytical results for thin-plate and simulation by Comsol software, when the plate thickeness is less than about 0.1, e.i. less than about 10% of plate radius. For larger thickenesses, starting at around $h = 0.1$, thin-plate analytical solution deteriorates significantly from the results of computer simulation. We observe that the analiticaly computet values of $w(r)$ and $u(r)$ become much lower that the computer-modelled one.

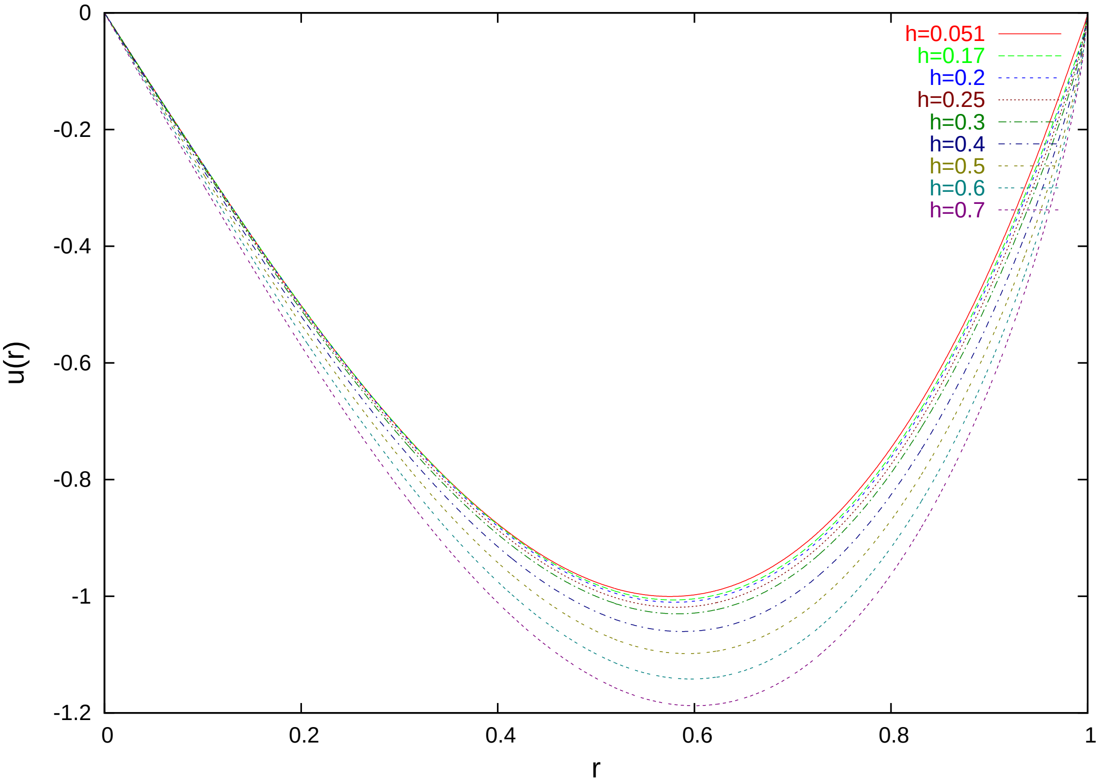

Figure 7: FEM computed $r-$ displacement $u(r)$ for a late fixed at the edges, for a range of thickness h values. Equations (3.4) and (2.12) were used to normalize $u(r)$ with computed values of $u(r = 1/\sqrt{3})$, where maximum of absolute value is found according to thin plate theory. In order to avoid large deformations, low pressure was assumed.

8.2 Multilayers

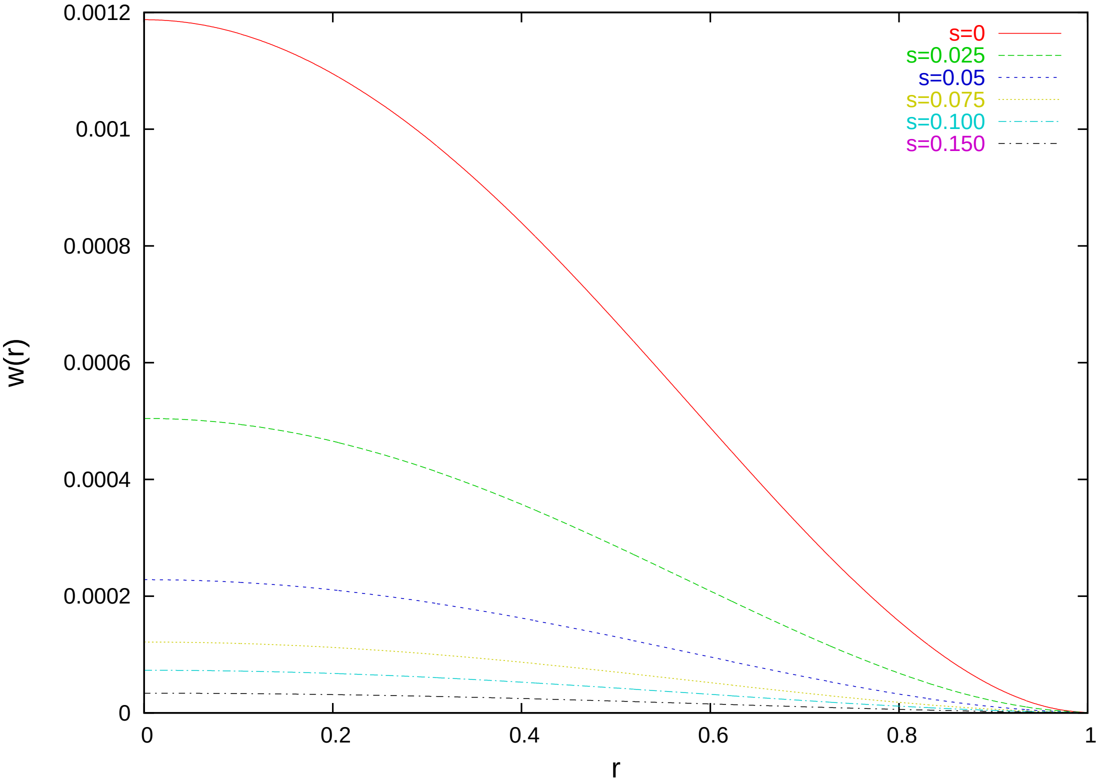

Figure 8: $z-$displacement $w(r)$ computed by FEM method for a two-layer plate with fixed external boundary. Results shown are at the upper surface of the upper layer. The lower layer is of thickness $h = 0.51$, and the upper layer has several values of thickness s ranging from 0.025 to 0.150, as shown in the figure. The Young modulus is $E = 10693.2\ Pa$ and half of that value, for lower and upper layers, respectively, and Poisson ratio $\nu = 0.33$, the same for both layers, has been assumed. With pressure as low as $0.01\ Pa$, a linear response is assured.

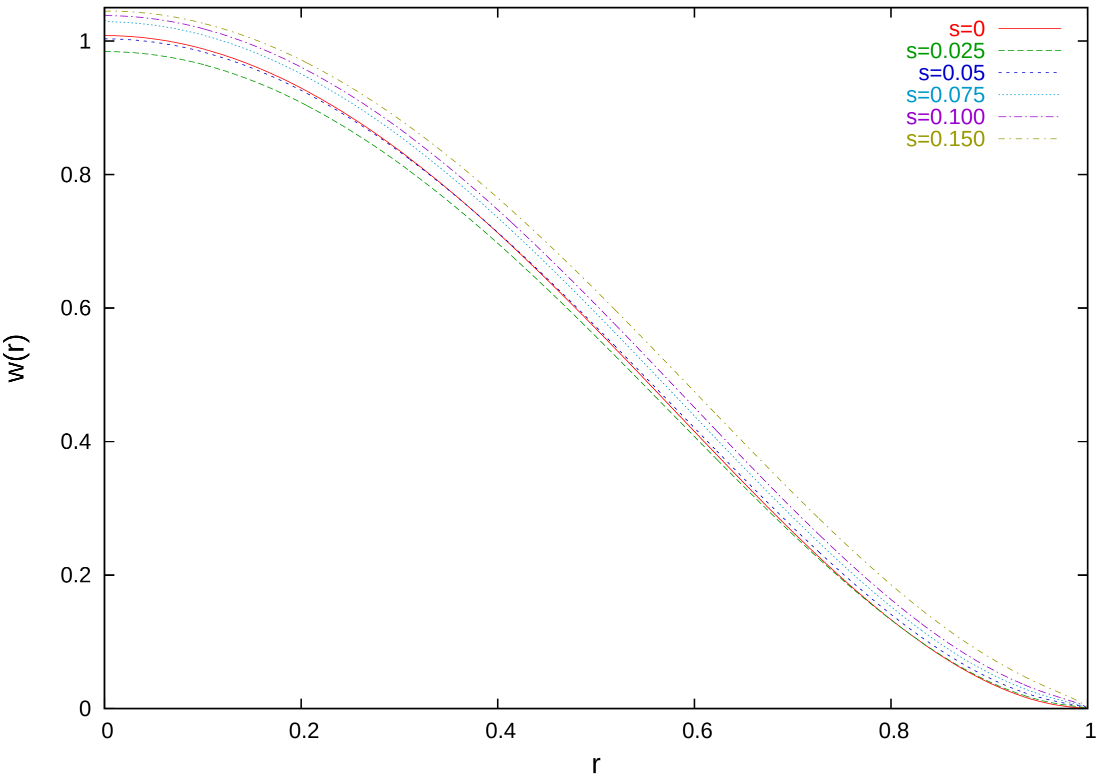

Figure 9: $z-$displacement $w(r)$ normalized by $w(r = 0)$, where $w(r = 0)$ is computed by using thin plate theory and equation (6.2) for a two-layer case. Data used are exactly the same as in Figure 8.

8.3 The role of external boundary

The role of external plate boundary and boundary conditions has been modeled with FEM on geometry as shown in Figure 10.

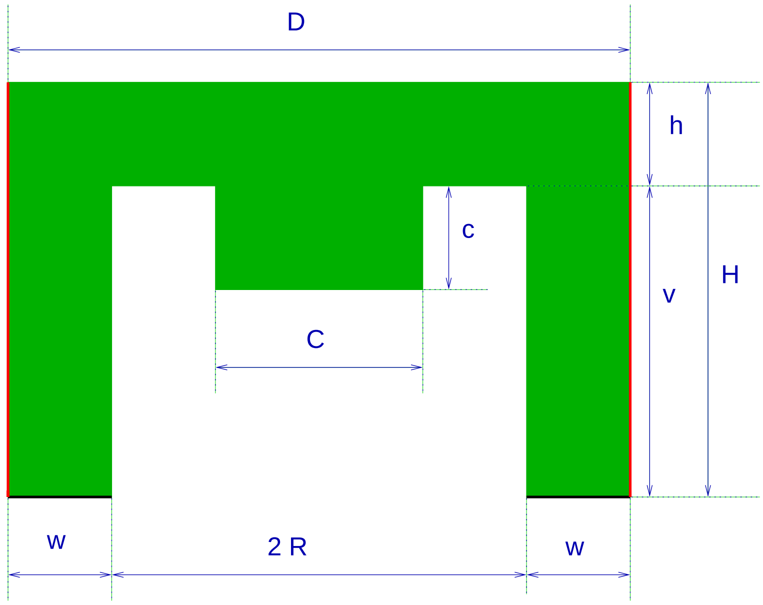

Figure 10: An axially symmetric plate model of diameter $2R$, joined to a supporting tube of diameter D made of the same material. The tube walls have thickness w (with $2R+2w=D$). The plate itself has thickness h (with $h+v=H$). The plate may have an inner core of diameter C and thickness c; The parameter c value may be equal to 0. The studied element is assumed to be fixed at the bottom (black thick lines). The outer surface of supporting tube (red thick lines) is assumed either as free or fixed, as described in the text.

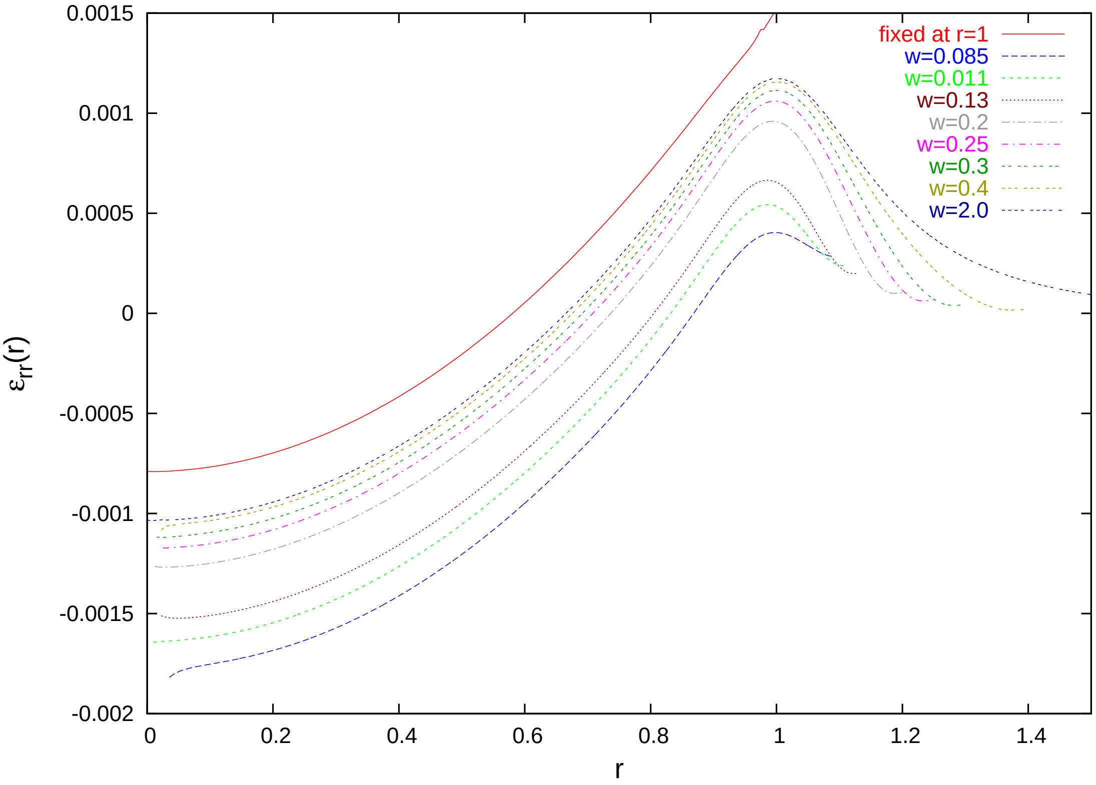

Figure 11: The role of wall thickness (w) is studied in case of external wall set to be free, when no internal core is present ($c = 0$). The strain tensor component, ε_{rr}, as a function of r computed by FEM is drawn. The most upper curve is for reference and has been computed with edges fixed at $r = 1$. Other curves, counting from bottom, are in increasing order of w. Plate thickness is $h = 0.2$. Refer to Figure 10 for explanation of parameters used.

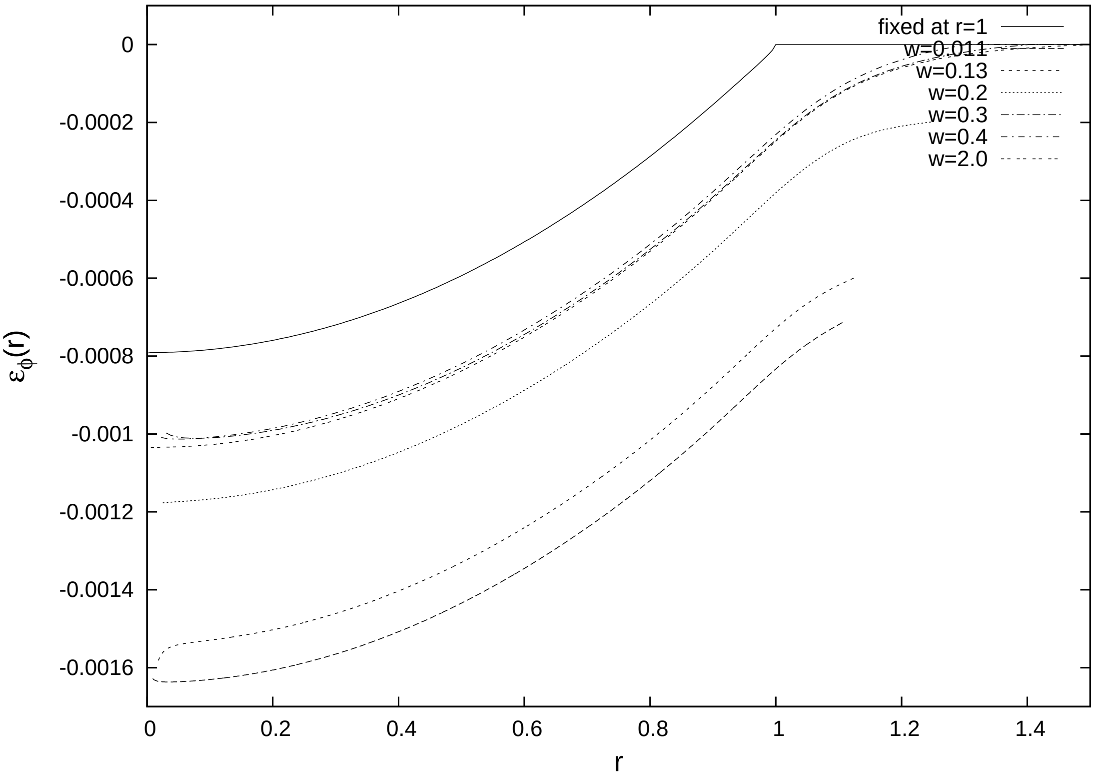

Figure 12: The role of wall thickness (w) is studied in case of external wall set to be free, when no internal core is present ($c = 0$). The strain tensor component, ε_ϕ, as a function of r computed by FEM is drawn. The most upper curve is for reference and has been computed with edges fixed at $r = 1$. Other curves, counting from bottom, are in increasing order of w. Plate thickness is $h = 0.2$. Refer to Figure 10 for explanation of parameters used.

8.4 The role of internal core

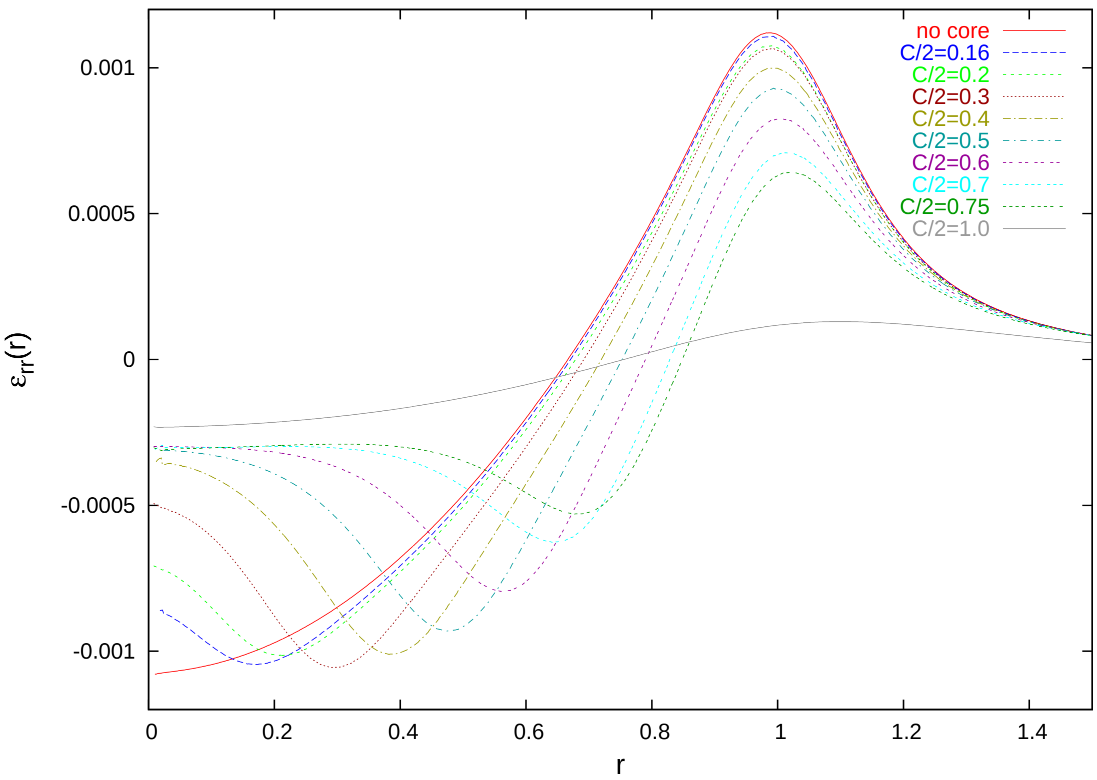

Figure 13: The role of internal core diameter C on the strain tensor component, ε_{rr}. Plate thickness is $h = 0.2$. The most upper curve, when there is no core inside, is drawn for reference. The curve that crosses each other has the diameter $C/2 = 1$, that is the diameter of plate. It represents the ultimate shape of all curves for $\varepsilon_{rr}(r)$ when core size tends to the maximum possible value. Plate thickness h is 0.2. Refer to Figure 10 for explanation of parameters used.

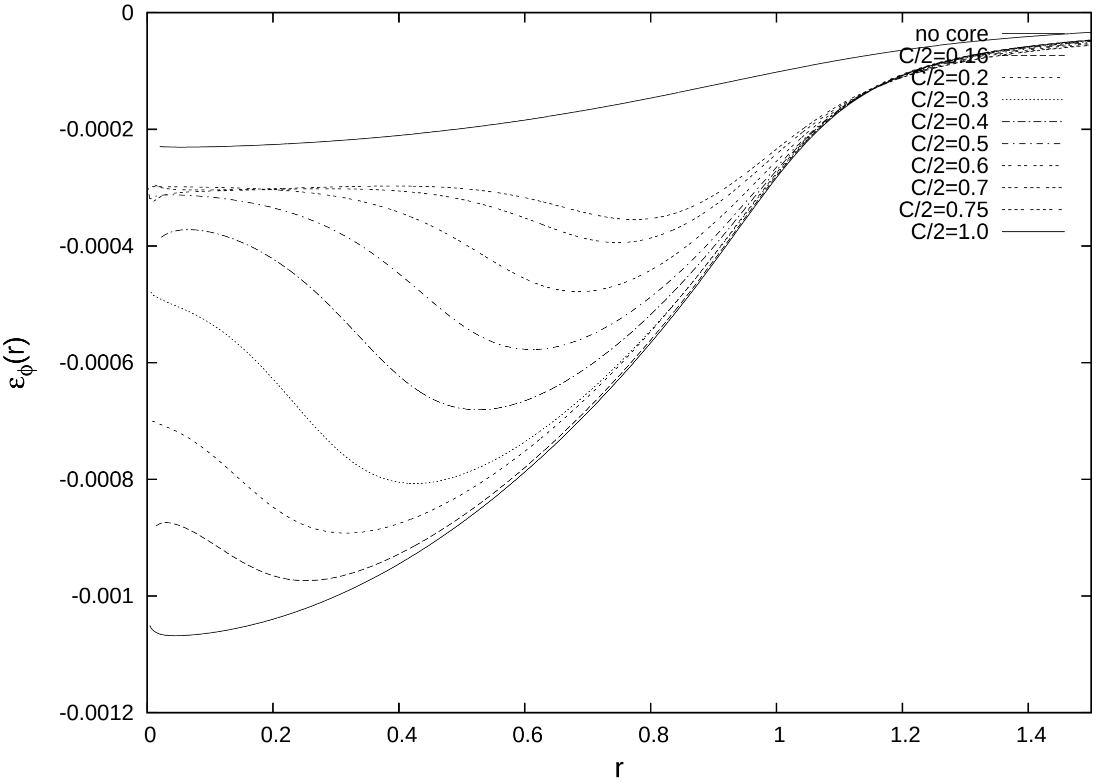

Figure 14: The role of internal core diameter C on the strain tensor component, ε_ϕ. Plate thickness is $h = 0.2$. The most upper curve, when there is no core inside, is drawn for reference. Plate thickness h is 0.2. Refer to Figure 10 for explanation of parameters used.

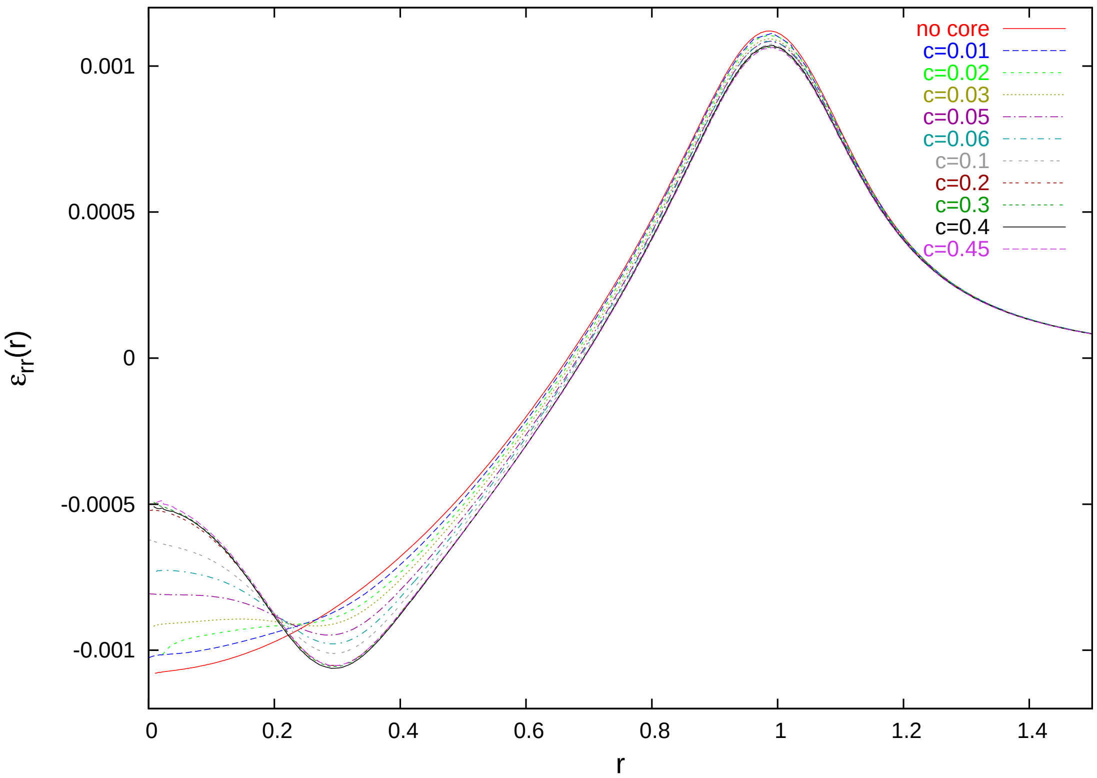

Figure 15: Studying $\varepsilon_{rr}(r)$ on core hight c. The core radius is 0.3, and the plate thickness is $h = 0.2$. The most upper curve, when there is no core inside, is drawn for reference. Refer to Figure 10 for explanation of parameters used.

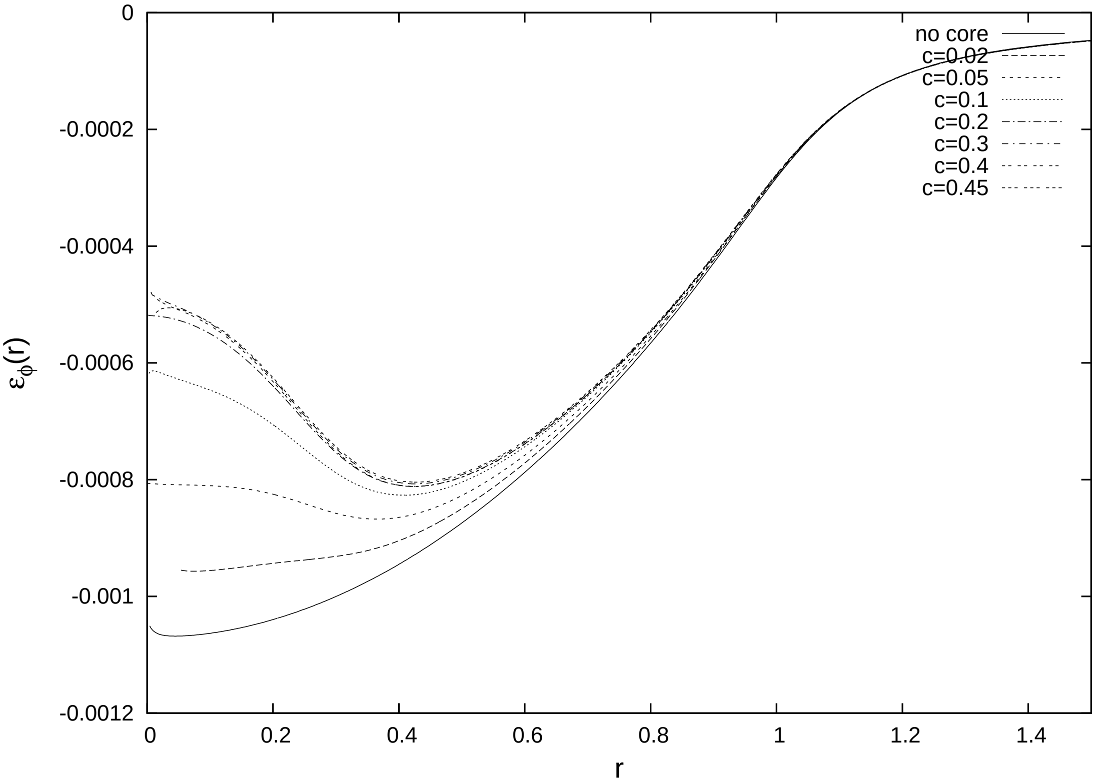

Figure 16: Studying $\varepsilon_\phi(r)$ on core hight c. The core radius is 0.3, and the plate thickness is $h = 0.2$. The most upper curve, when there is no core inside, is drawn for reference. Refer to Figure 10 for explanation of parameters used.

8.5 Shaping $\varepsilon_{rr}(r)$ of the internal core

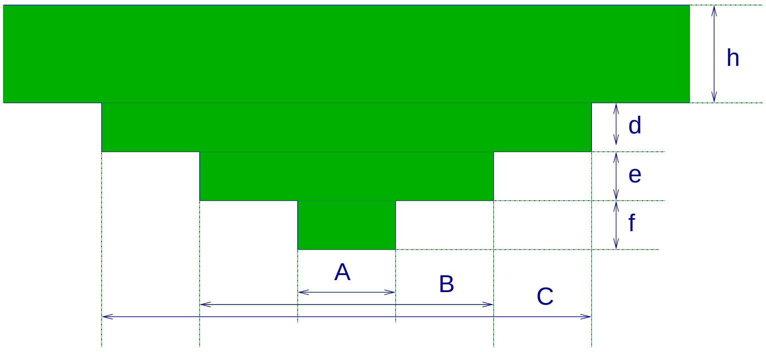

Figure 17: Diameters $A = 0.2$, $B = 0.4$, and $C = 0.6$. Thicknesses are d, e and f. Plate thickness is h

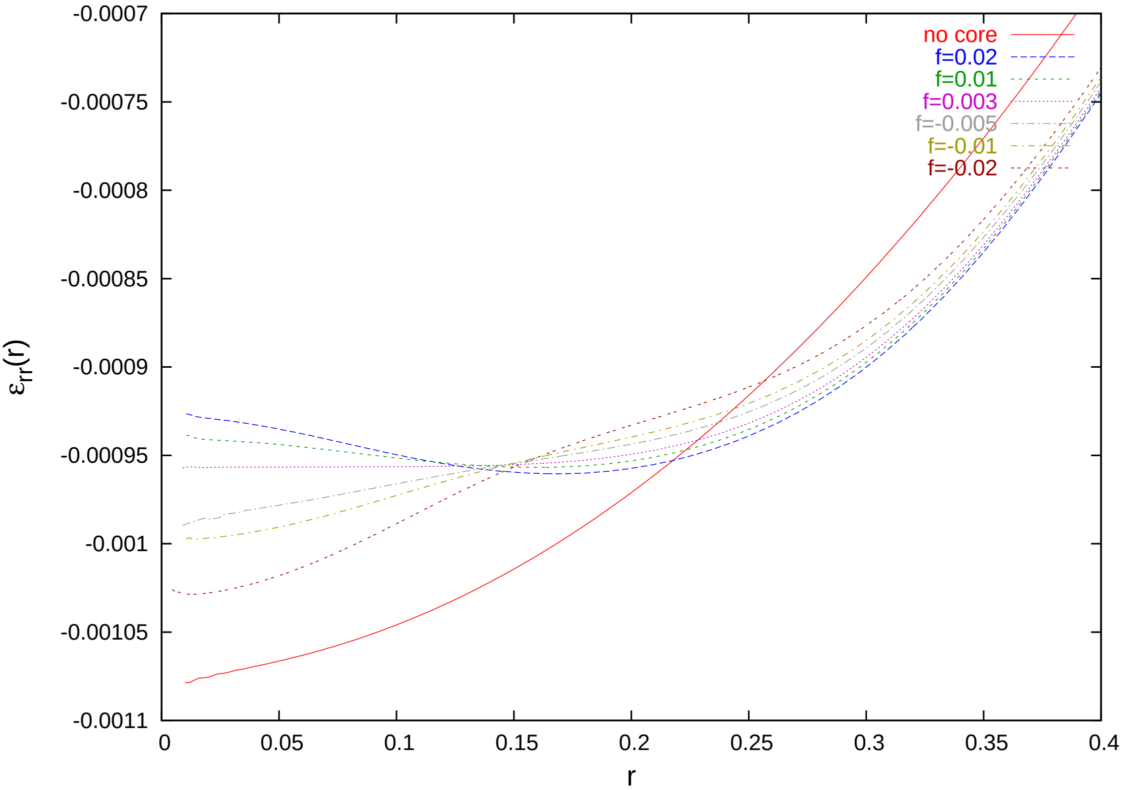

Figure 18: The strain tensor component, $\varepsilon_{rr}(r)$, is drawn near the plate center, where the internal core playes crucial role in $\varepsilon_{rr}(r)$ dependance. Parameters used are as these described in Figure 17: Diameters $A = 0.2$, $B = 0.4$, and $C = 0.6$. Thicknesses d and e are both equal to 0.01, while f is as shown in the figure. Plate thickness h is 0.2. The curve, when there is no core inside, is drawn for reference. For $f = 0.003$, within accuracy of calculations, a perfectly independent on r (for r less than about 0.15) strain tensor is observed.

8.6 Position of Maximum in $\varepsilon_{rr}(r)$.

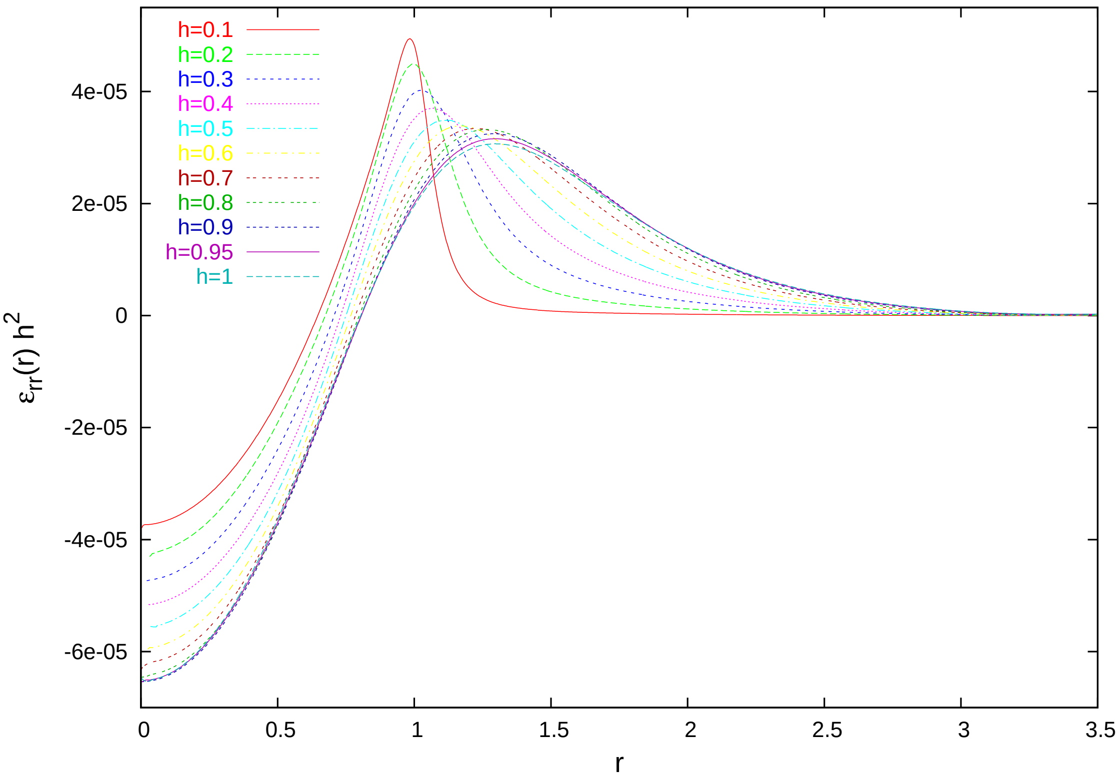

Figure 19: The strain tensor component $\varepsilon_{rr}(r)$, normalized by plate thickness h, for several values of plate thickness, when $p = 1Pa$, $E = 10693Pa$, and wall thickness $w = 2.5$. The strain tensor component is shown at the upper plate surface. The geometry and meaning of parameters is the same as in Figure 10 (there is no core in this case, i.e. $c = 0$, and $H = 1$ was assumed). $\varepsilon_{rr}(r)$ scales as $1/h^2$ in classical thin plate theory, therefore, all the data are scaled in this figure by multiplying $\varepsilon_{rr}(r)$ by h^2, in order to have an easier comparison between different curves (the absolute magnitude of $\varepsilon_{rr}(r)$ varies for around 100 times between $h = 0.1$ and $h = 1$).

Of important interest to us is the position of maxima in $\varepsilon_{rr}(r)$.

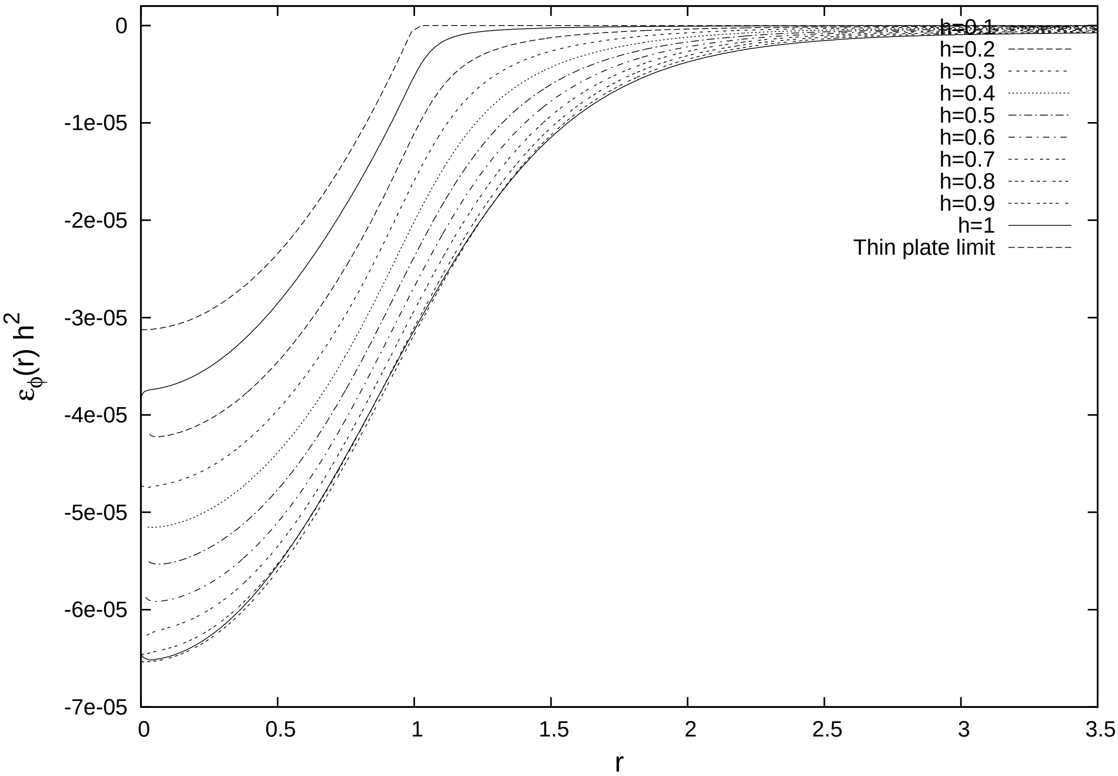

Figure 20: The strain tensor component $\varepsilon_{\phi}(r)$, normalized by plate thickness h, for several values of plate thickness, when $p = 1Pa$, $E = 10693Pa$, and wall thickness $w = 2.5$. The strain tensor component is shown at the upper plate surface. The geometry and meaning of parameters is the same as in Figure 10 (there is no core in this case, i.e. $c = 0$, and $H = 1$ was assumed). $\varepsilon_{\phi}(r)$ scales as $1/h^2$ in classical thin plate theory, therefore, all the data are scaled in this figure by multiplying $\varepsilon_{\phi}(r)$ by h^2, in order to have an easier comparison between different curves (the absolute magnitude of $\varepsilon_{\phi}(r)$ varies for around 100 times between $h = 0.1$ and $h = 1$). Thin plate limit is drawn also for comparison: $\varepsilon_{\phi}(r) = u/r = 2h \cdot \frac{p}{64D} \cdot \left(r^2 - 1\right)$

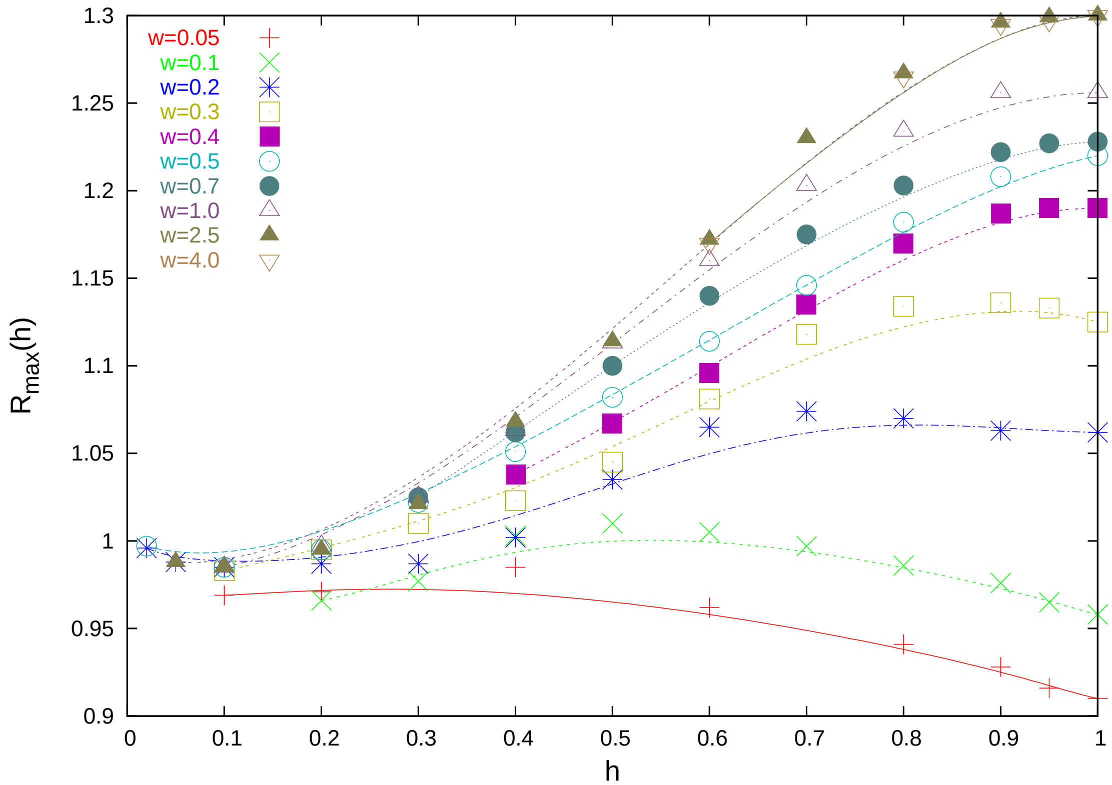

Figure 21: The position of maxima in $\varepsilon_{rr}(r)$, $R_{max}(h)$, for various wall thickness (parameter w in Figure 10). Calculations were performed for exactly the same conditions as these in Figure 19. The lines are only to guide eyes, though we expect that there exists a simple mathematical formula that would fit well the data for every value of w, and that such a formula would scale in a simple manner with w. In case of wall thickness $w = 2.5$ and $w = 4.5$ the results coincide well together, representing a limit of flow on $\varepsilon_{rr} - r$ plane. The set of results shown allows to estimate position of maximum for any combination of parameters (w, h), and, in more general, for any cell of similar shape as long as the ratio R/H remains equal to 1.

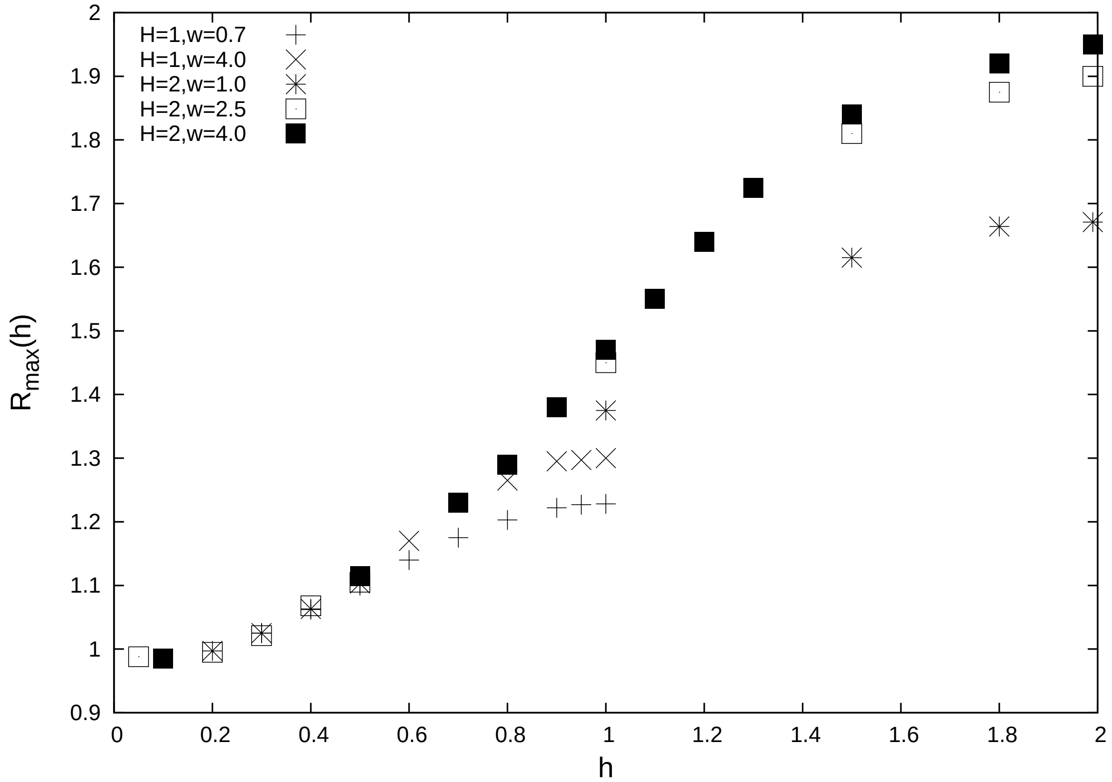

H=1,w=0.7
H=1,w=4.0
H=2,w=1.0
H=2,w=2.5
H=2,w=4.0
$R_{max}(h)$
h
0
0.2
0.4
0.6
0.8
1
1.2
1.4
1.6
1.8
2
0.9
1
1.1
1.2
1.3
1.4
1.5
1.6
1.7
1.8
1.9
2

Figure 22:

8.7 The role of boundary conditions on external surface of the wall.

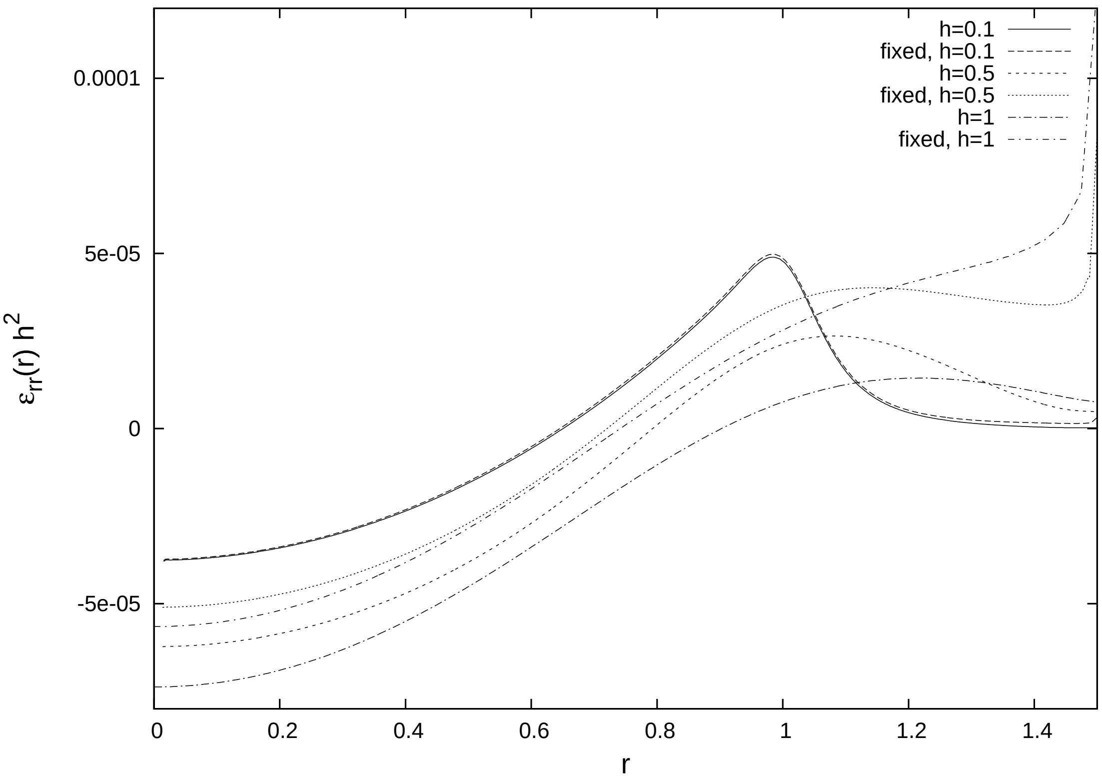

Figure 23: The external surface of the wall is fixed and $\varepsilon_{rr}(r)$ is compared with corresponding $\varepsilon_{rr}(r)$ dependence when that surface is free.

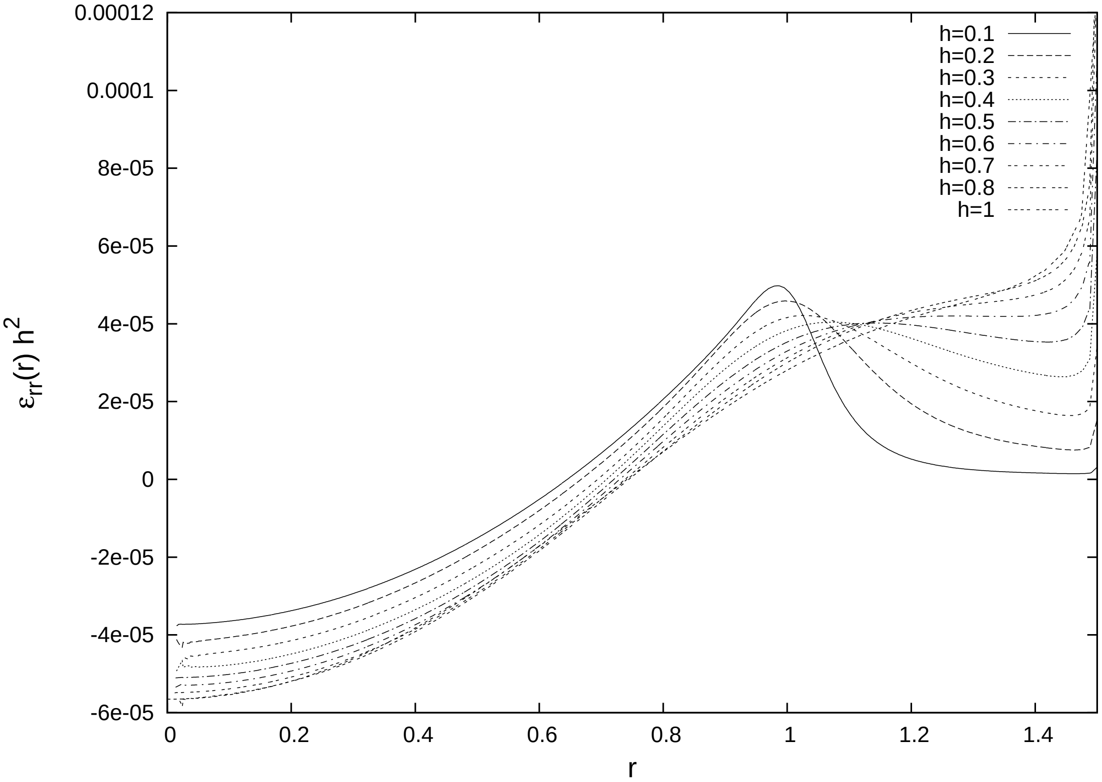

Figure 24: The external surface of the wall is fixed.

8.8 "Real" sensors - $\varepsilon_{rr}(r)$, $\varepsilon_\phi(r)$, and the role of external boundary conditions.

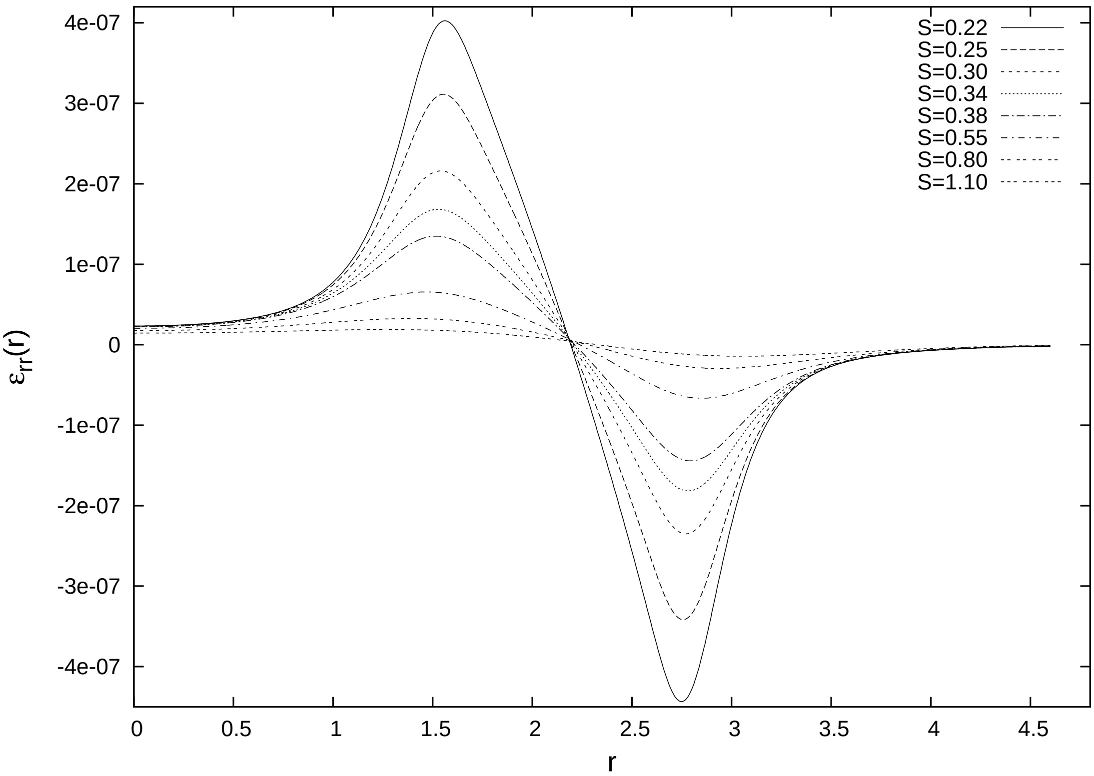

Figure 25: The strain tensor component $\varepsilon_{rr}(r)$, for several values of plate thickness S (in mm, as, shown in the figure, when $p = 1Pa$, $E = 10693Pa$, for a "real" membrane.

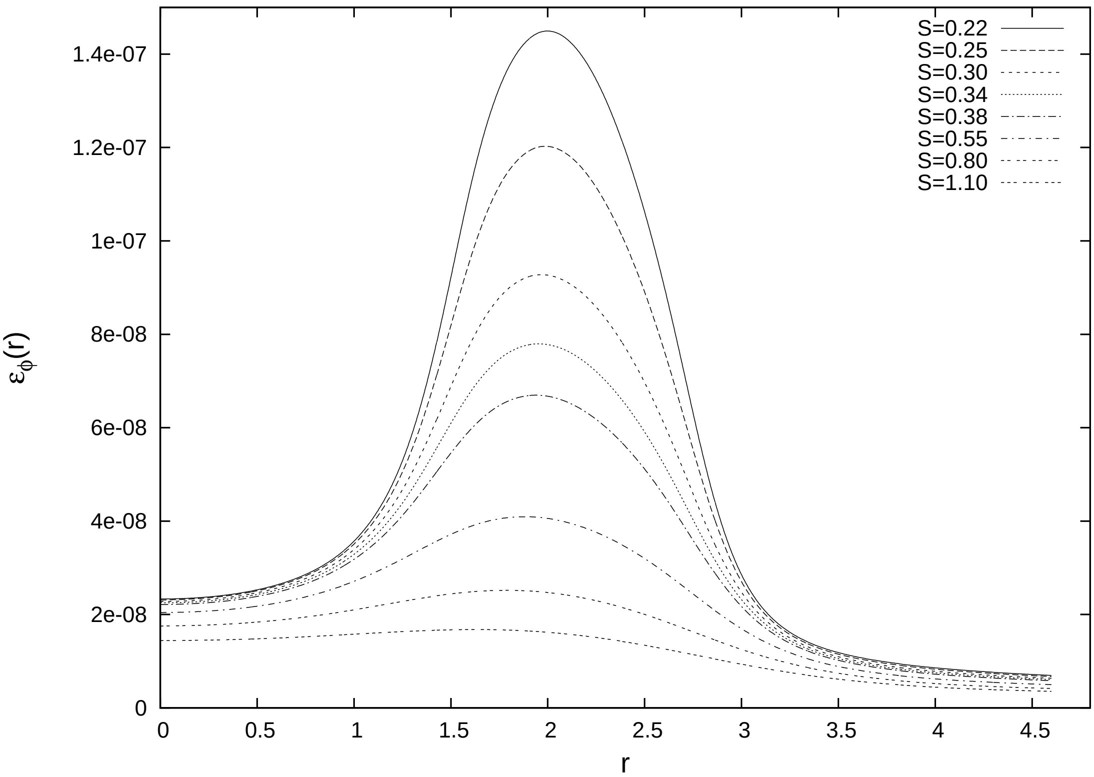

Figure 26: The strain tensor component $\varepsilon_\phi(r)$, for several values of plate thickness S (in mm, as, shown in the figure, when $p = 1Pa$, $E = 10693Pa$, for a "real" membrane.

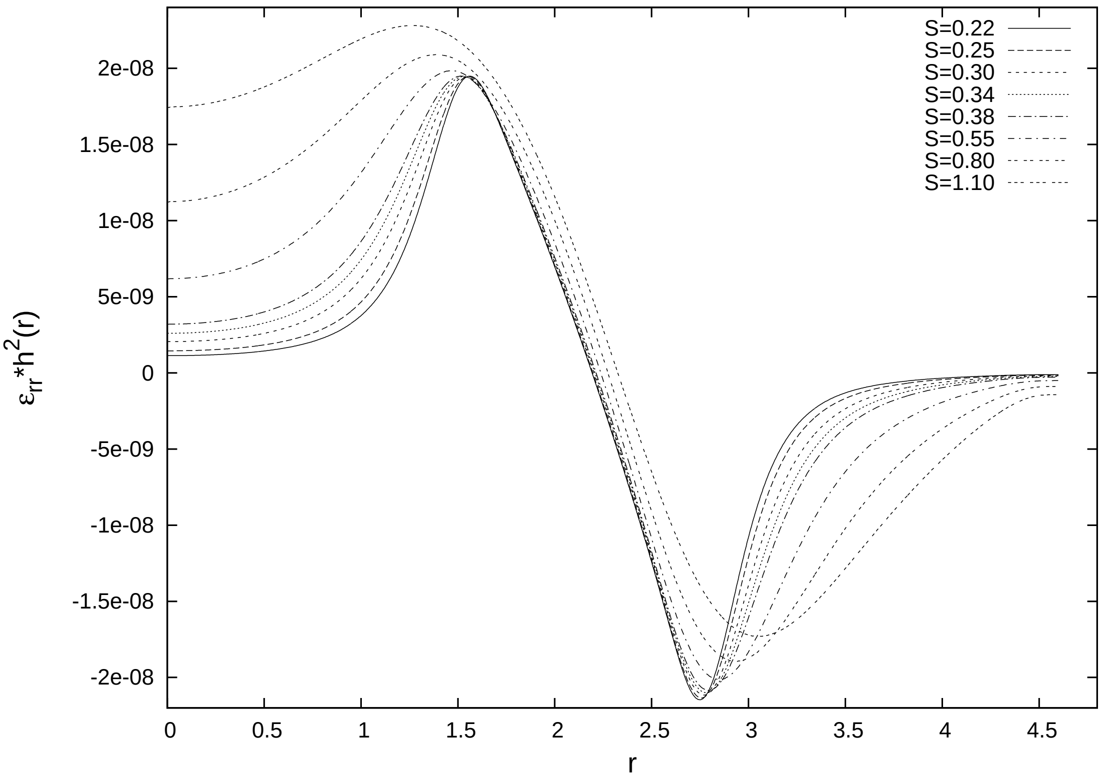

Figure 27: The strain tensor component $\varepsilon_{rr}(r) \cdot S^2$, for several values of plate thickness S (in mm, as, shown in the figure, when $p = 1Pa$, $E = 10693Pa$, for a "real" membrane.

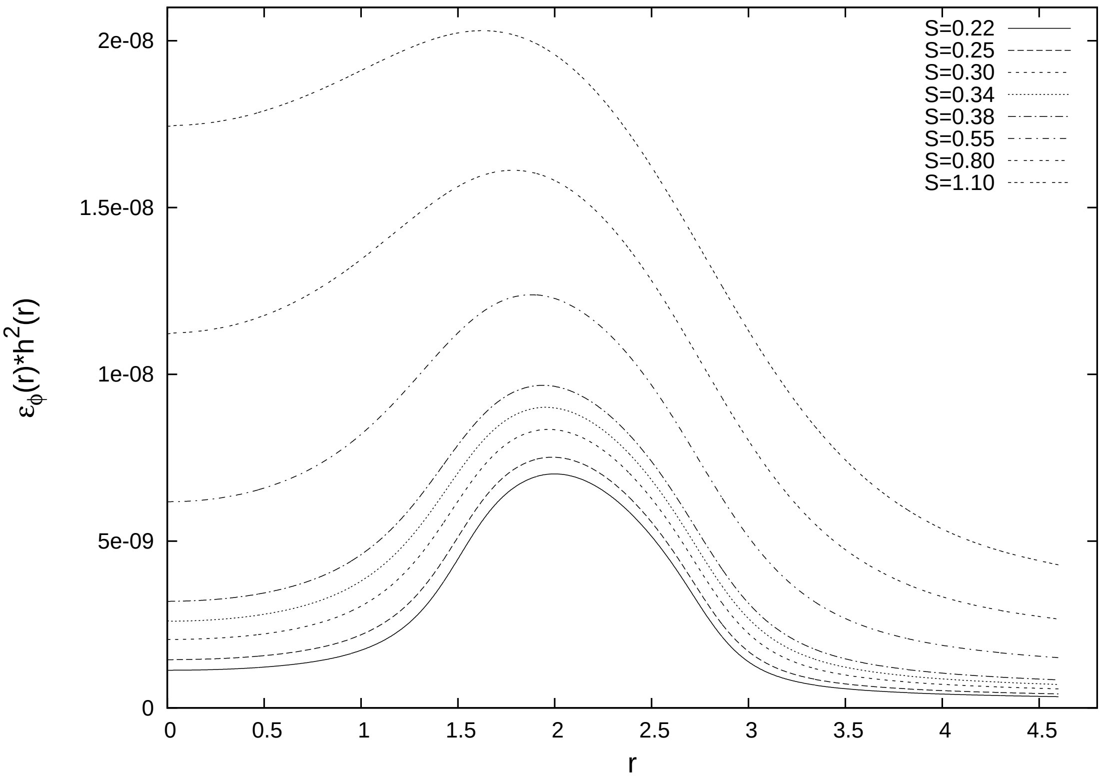

Figure 28: The strain tensor component $\varepsilon_{\phi}(r) \cdot S^2$, for several values of plate thickness S (in mm, as, shown in the figure, when $p = 1Pa$, $E = 10693Pa$, for a "real" membrane.

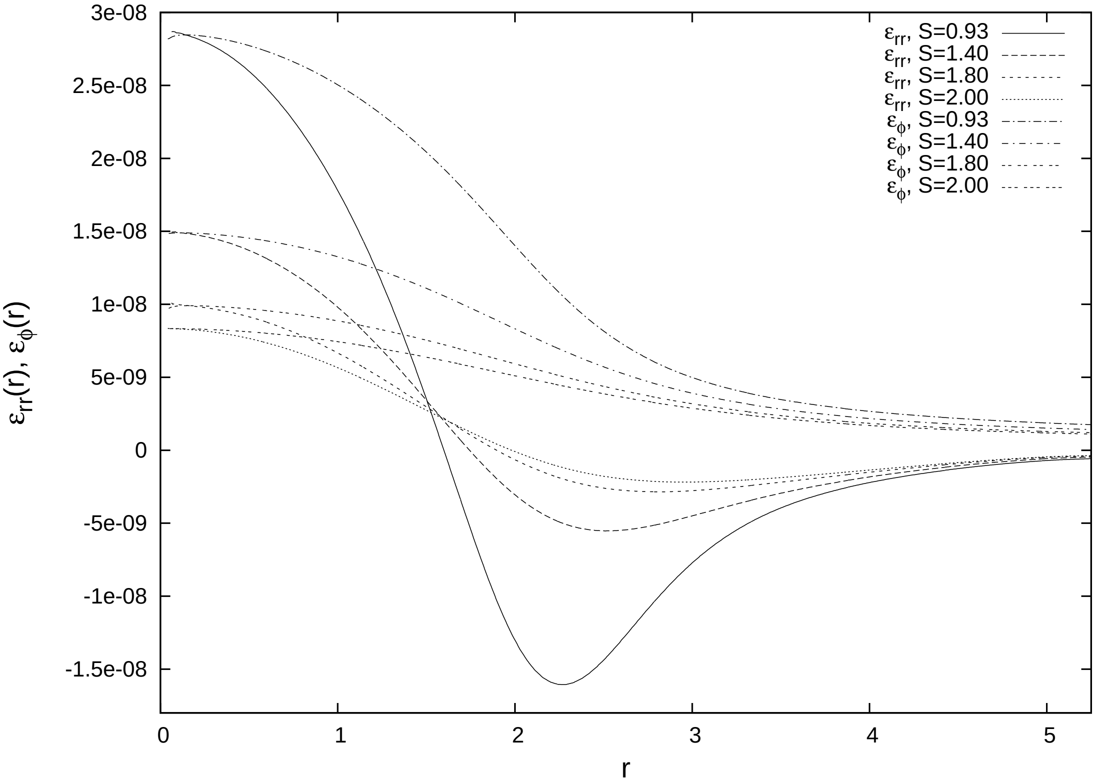

Figure 29: The strain tensor component $\varepsilon_{rr}(r)$, for several values of plate thickness S (in mm, as, shown in the figure, when $p = 1Pa$, $E = 10693Pa$, for a "real" membrane.

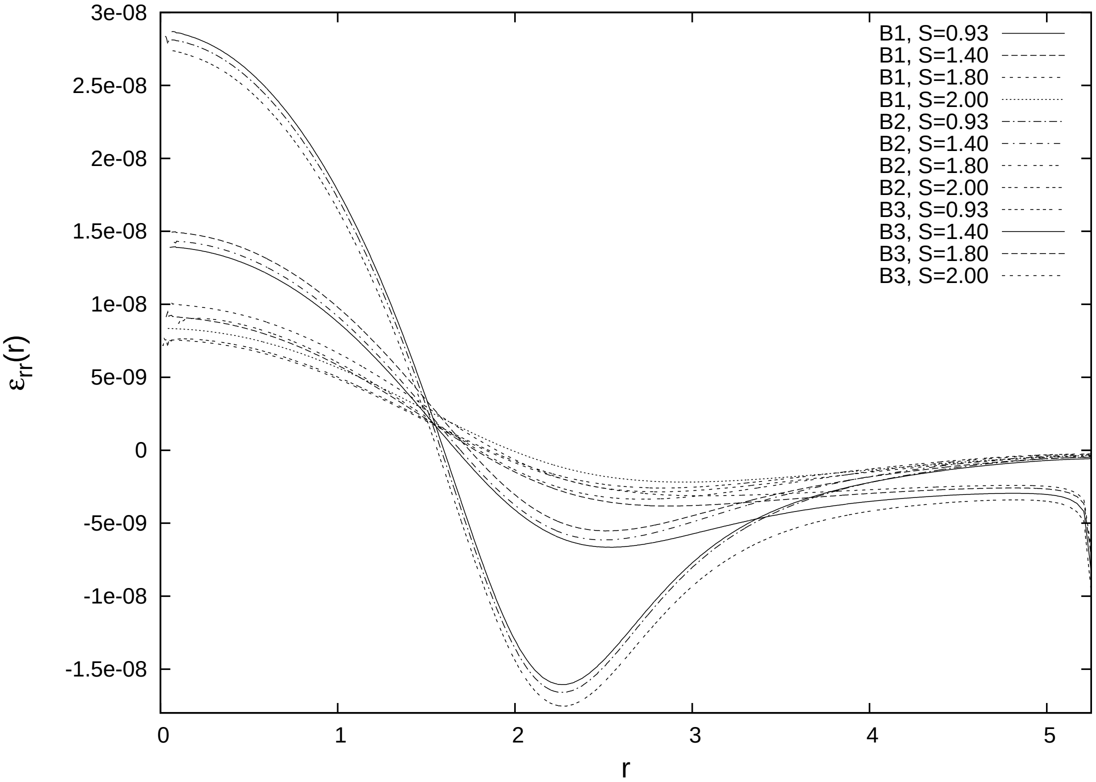

Figure 30: The strain tensor component $\varepsilon_{\phi}(r)$, for several values of plate thickness S (in mm, as, shown in the figure, when $p = 1Pa$, $E = 10693Pa$, for a "real" membrane.

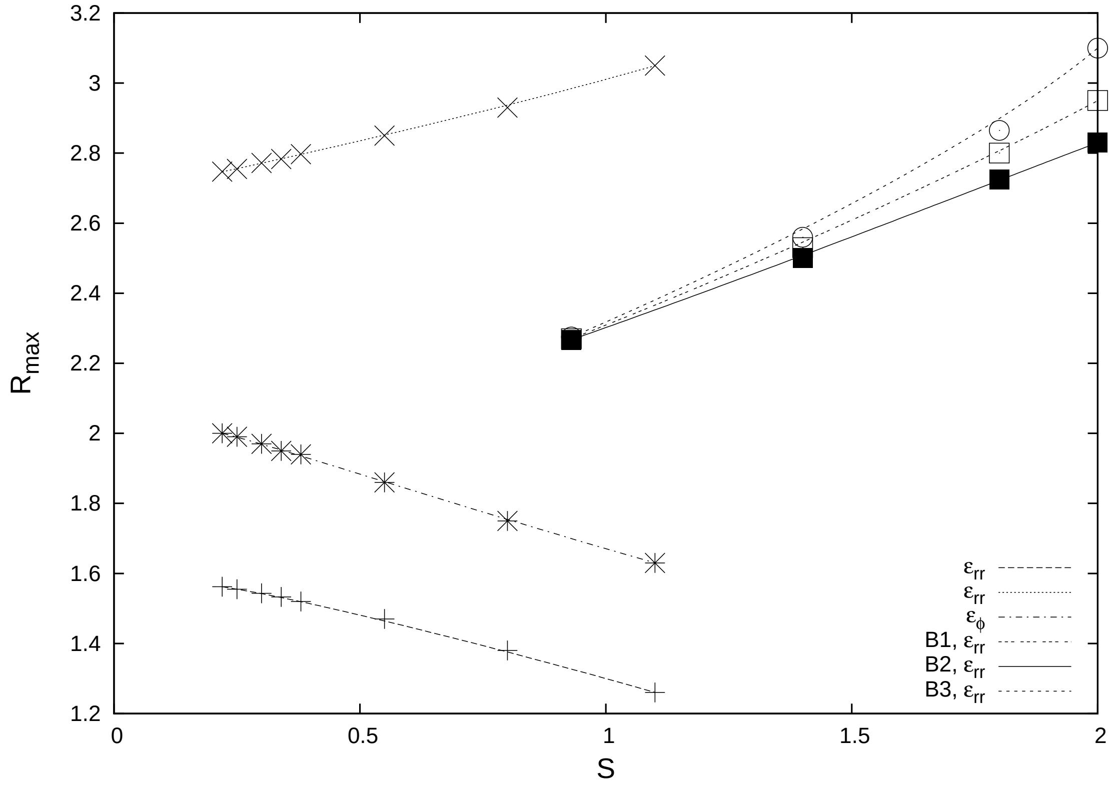

Figure 31: The position of maxima in $\varepsilon_{rr}(r)$ and $\varepsilon_{\phi}(r)$, $R_{max}(h)$ ....

8.9 Testing the range of linear pressure dependance

The titanium alloys may have a tensile elastic limit strength of 950 MPa or more, and an $elastic\ deformation\ capability$ of 1.6% or more.

Yield strength for grade-2 Titanium is "only" $275MPa$. Alloys of Titanium may have about 4 times higher yield strength. From another source: the elastic limit is of the order of 500 MPa for some Ti-Ni alloys. The not so well defined $proportional\ limit$ is however significantly lower than the $elastic\ limit$.

We can safely assume that any calculations based on linear strain-stress dependence must be error-prone for pressures larger than around 100 MPa. Unless we know very well mechanical properties of Ti-alloys used.

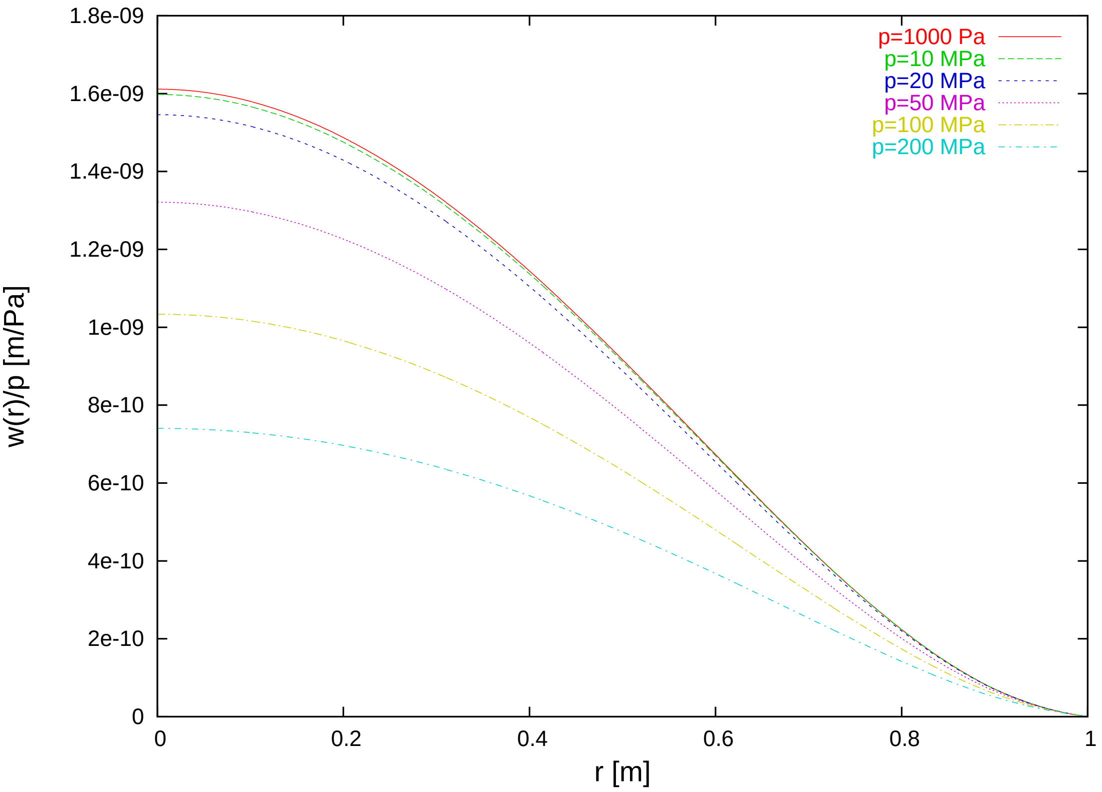

Figure 32: $w(r)$ normalized by pressure (in Pa), for several values of pressure applied, $1000\ Pa$, $10\ MPa$, $20\ MPa$, $50\ MPa$, $100\ MPa$, and $200\ MPa$, for curves from top to bottom, as described in the Figure. If linear theory was valid, $w(r)/p$ would be independant of pressure applied and all curves would coincide perfectely. A merely noticable departure from linearity is visible already at pressures around $10\ MPa$, and at higher pressures, the nonlinear contribution increases dramatically. Plate thickness is $h = 0.1$.

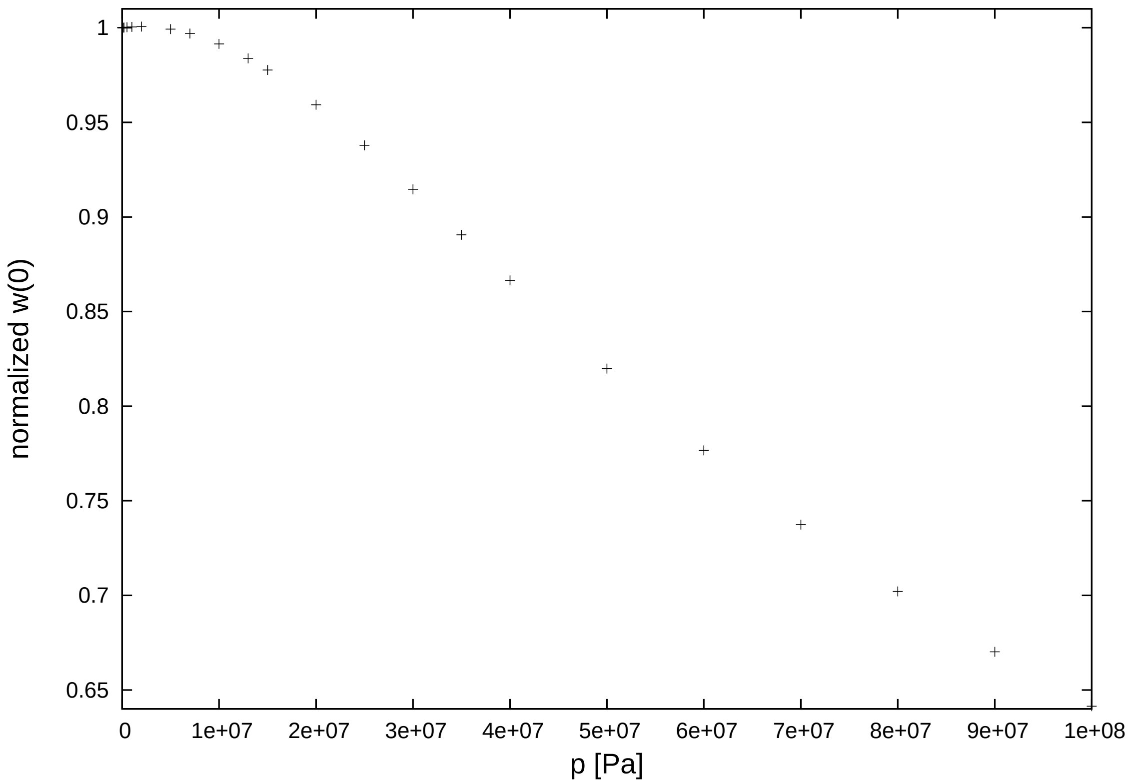

Figure 33: $w(0)$ as a function of pressure, normalized by pressure in such a way that $w(0) = 1$ is obtained at pressure of $1000\ Pa$, e.i., the normalization is of the form $w(0)/p[Pa]/w(at\ r = 0\ for\ 1000\ Pa) * 1000$. We see that a systematic, significant departure from linear theory starts at pressures around $10 - 20\ MPa$, which corresponds to deflaction at the center of the order $1.0\% - 4.0\%$, At higher pressures, the nonlinear contribution increases nearly linearly with pressure applied. We do not expect that calculated results remain valid for pressures of around 100 MPa or above - at these pressure ranges the material properties become too close to the elastic and linear-response limit of Titanium. Plate thickness is $h = 0.1$.

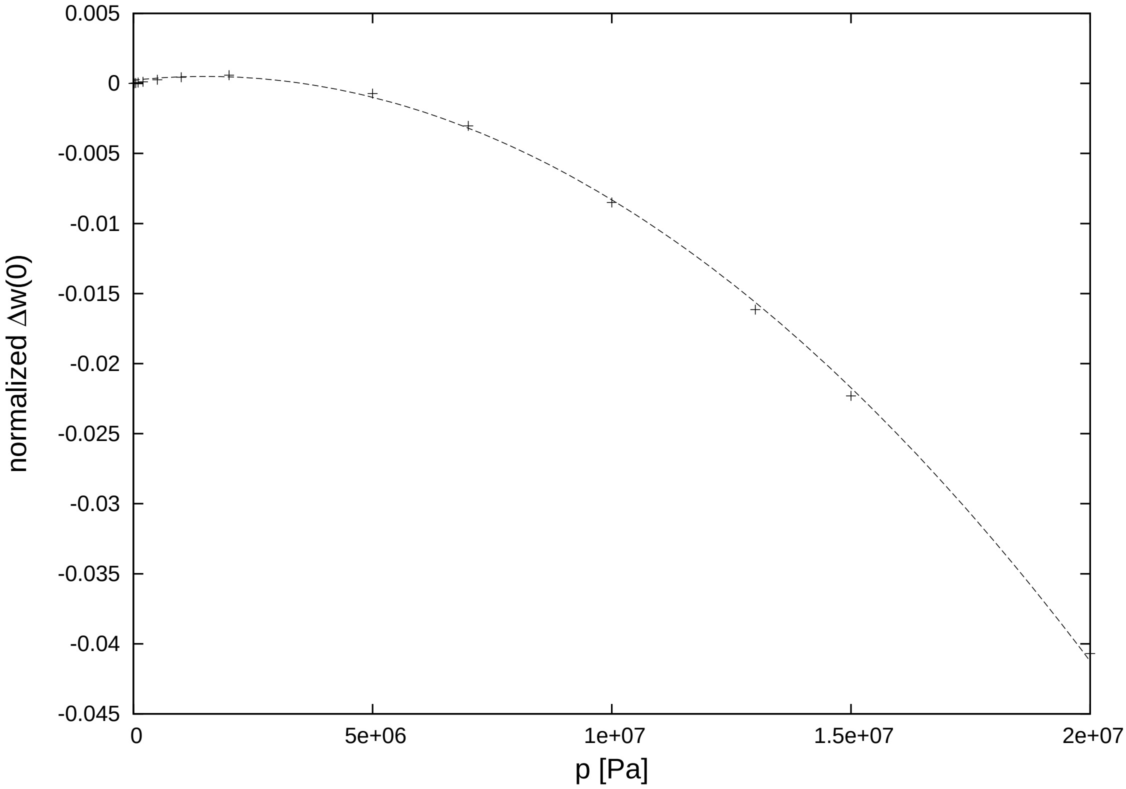

Figure 34: A difference between normalized $w(0)$ at near-zero-pressure (strictly, at pressure of $1000\ Pa$), and actual normalized $w(0)$ as a function of pressure. The normalization is of the form $w(0)/p[Pa]/w(at\ r = 0\ for\ 1000\ Pa) * 1000$. While at higher pressures, as shown in Figure 33, the nonlinear contribution increases nearly linearly with pressure applied, at these relatively low pressures shown, the nonlinear contribution changes nearly as a square of pressure applied. The solid curve in the Figure is the best fit to the data and is described by: $0.0005 - 1.22 \cdot 10^{-16}(p - 1500000)^2$. Plate thickness is $h = 0.1$.

8.10 Maximal Stress

Material brakes (passes through elastic response limit) after certain critical stress value, which is called *yield stress*, and which is characteristic for every material. *Yield stress* (called also *tensile strength*) value is known for commonly used materials, and in particular, in case of metals and many of metal alloys. For titanium alloy used as the membrane material here, *tensile strength* exceeds $1000\ MPa$ at room temperature. However, it does not exceeds much that value and with increasing temperature *tensile strength* may drop significantly. Therefore, a value of $1000\ MPa$ should be considered as an ultimate, and not even a safe value. A real device may be not able to sustain stresses even as high as that.

One of the used criterions of computing when material brakes is based on so called von Mises criterion, which takes into account that material becomes plastic at even lower stresses, if additional stresses are applied in other directions.

A physical interpretation of von Mises criterion suggests that yielding begins when the elastic energy of distortion reaches a critical value.

Von-Mises stress is shown in Figure 35 for a model of geometry close to the real one. Refer to Figure 10 for explanation of parameters used. Units are in millimeters: $D = 9.2$, $h = 0.51$, $C = 2.8$, $R = 2.9$, $c = 1.49$, $H = 4.0$.

We plot here von-Mises stress at the surface, and at the plate center and the bottom of plate ($z = 0$ corresponds to the upper surface, while $z = -0.51$ to the plate bottom).

Pressure applied is $1MPa$, and material parameters are these as used for Titanium: $E = 106MPa$ and $\nu = 0.34$.

The graphs are normalized by applied pressure (which is $1MPa$ in this case). The reason for that is to show how much stresses inside of the material can be larger than the applied pressure, e.i. in other words, the stresses shown are in units of the applied pressure.

Huge peaks near the core and plate boundaries are probably due to inaccuray in calculations. Nevertheless, as these data show, one should expect stresses inside of the material larger at least 10 or 20 times of the applied pressure.

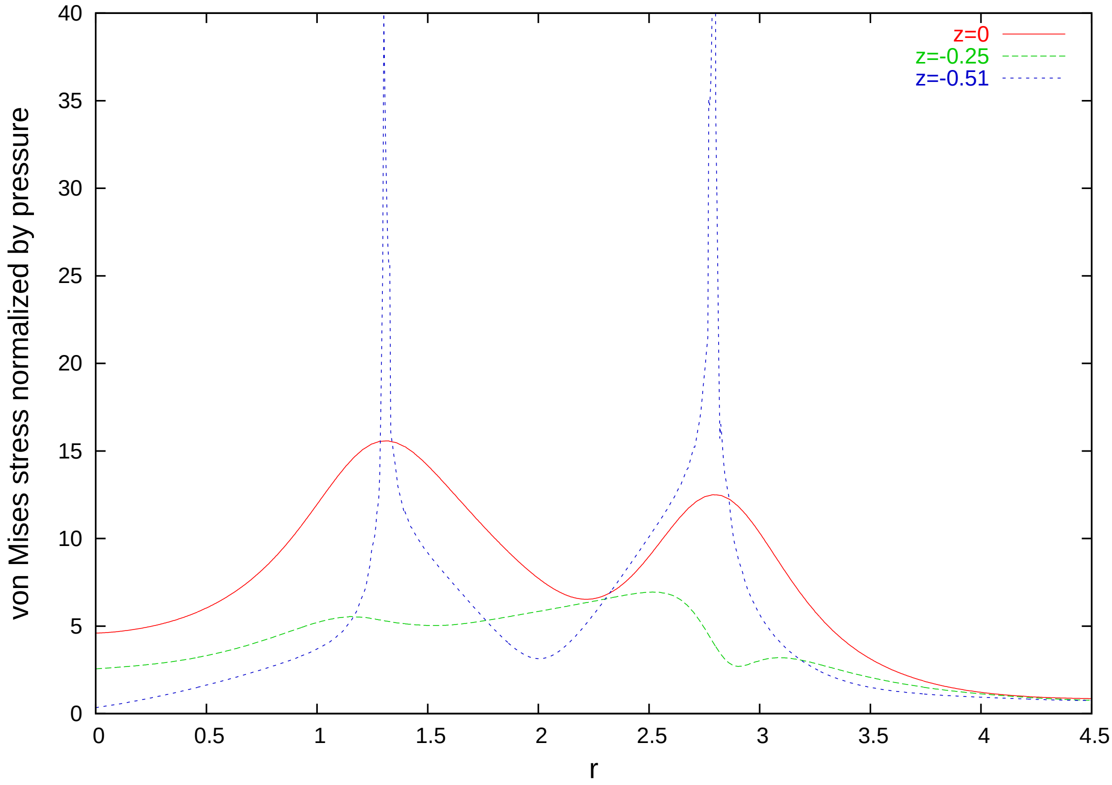

Figure 35: Refer to Figure 10 for explanation of parameters used. Units are in millimeters: $D = 9.2$, $h = 0.51$, $C = 2.8$, $R = 2.9$, $c = 1.49$, $H = 4.0$. von-Mises stress at the surface, and at the plate center and the bottom of plate ($z = 0$ corresponds to the upper surface, while $z = -0.51$ to the plate bottom). Pressure applied is $1MPa$, and material parameters are these as used for Titanium: $E = 106MPa$ and $\nu = 0.34$. The graphs are normalized by applied pressure.

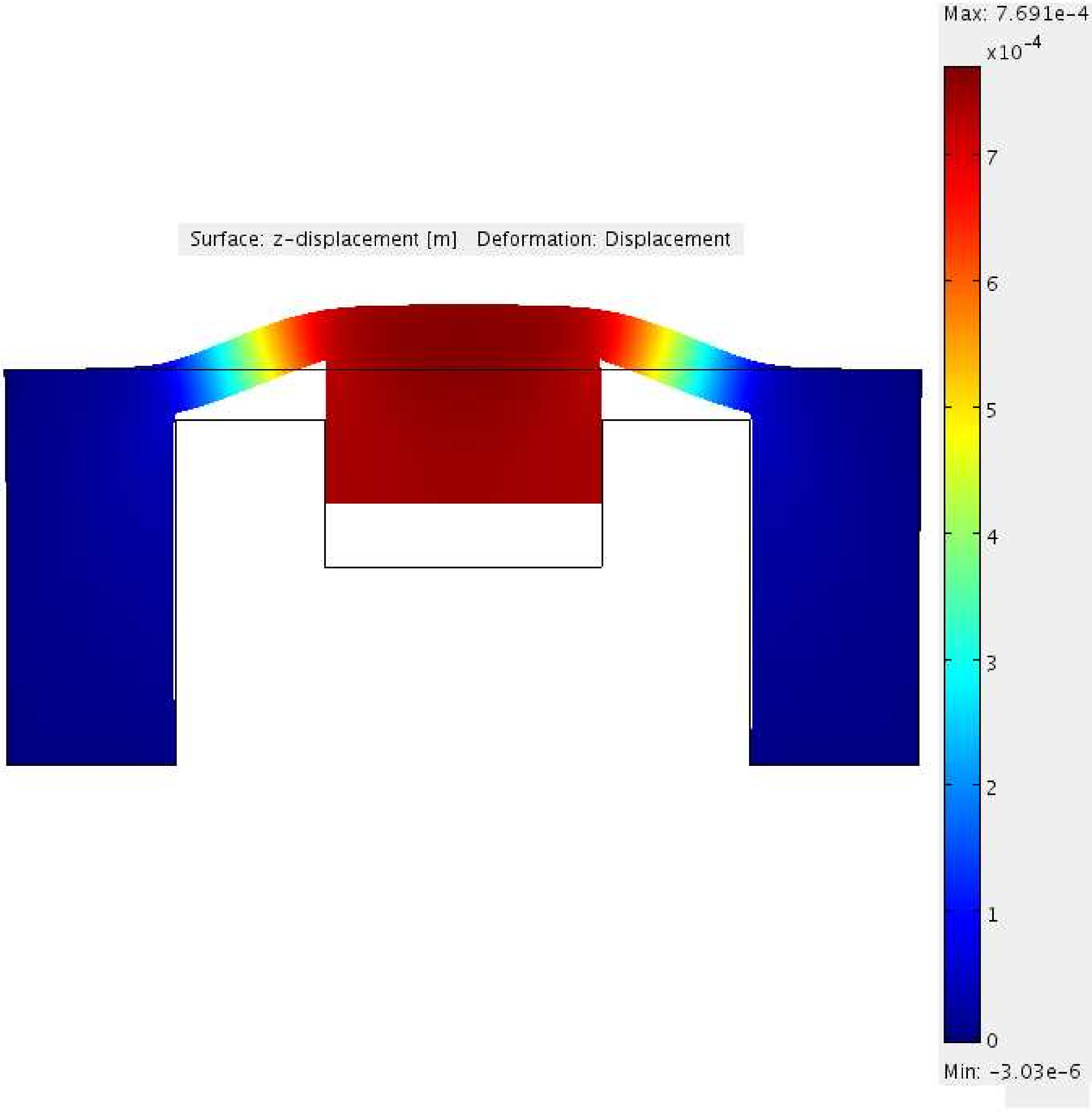

Figure 36: A typical deformation cross-section for parameters as described in Figure 35. The deformation is not to scale, and much exagerated in magnitude, for a better illustration. The right color map describes the absolute magnitude of deformation. The applied pressure is $1MPa$.

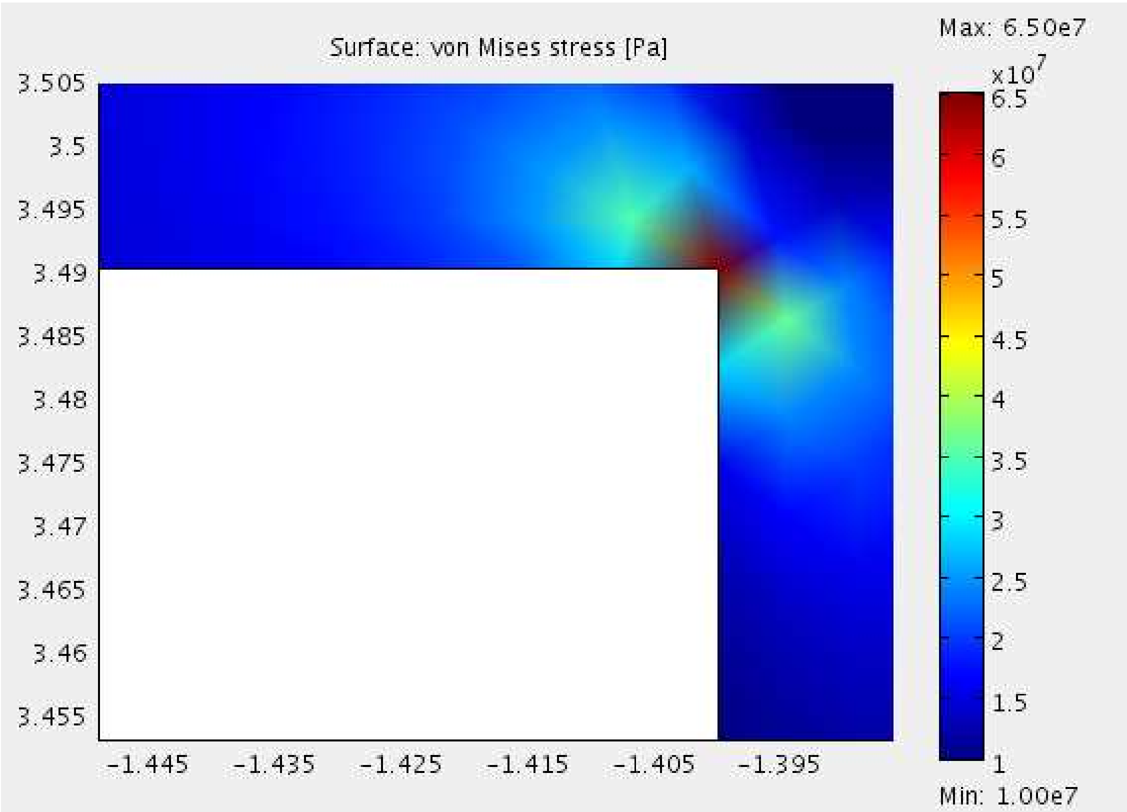

Figure 37: Von Mises stress near the corner formed by plate and hard core ($x = -1.4$ and $y = 3.49$, in mm), for parameters as described in Figure 35 and the applied pressure of $1MPa$.

8.11 Plate with solder on the surface

Solder thickness on real device is around $0.04mm$. We do not know it's Young modulus and Poison ratio, and, for modeling purpose, we assume arbitrarily, $E = 30\ GPa$, and $\nu = 0.34$. We assume cell dimentions as in Figure 10, with the following values of parameters (in mm): $D = 9.2$, $h = 0.51$, $C = 2.8$, $R = 2.9$, $c = 1.49$, $H = 4.0$. Solder layer is assumed to have radius of 4.6.

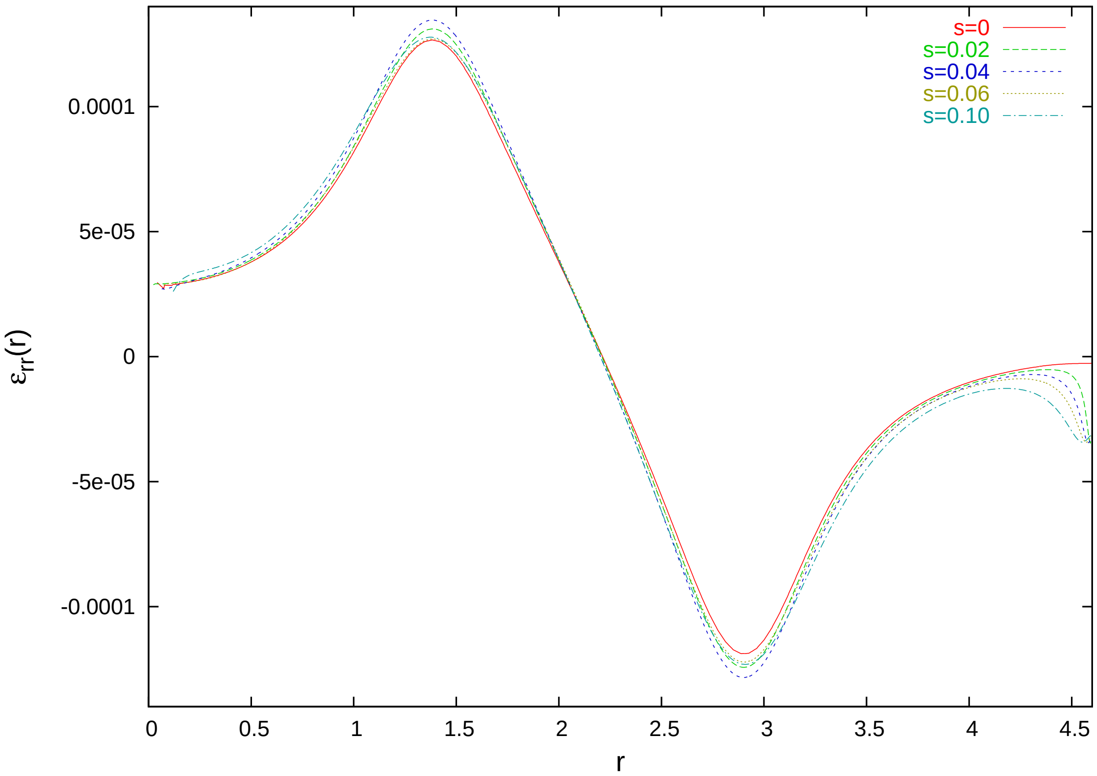

Figure 38: The strain tensor component, $\varepsilon_{rr}(r)$, when solder layer is present, for several values of solder layer thickness s, as shown in the figure. Parameters used are as these described in the text.

8.12 Contribution of Residual Thermal Stress

Residual Thermal Stress (and residual thermal strain) occur when a structure of two or more materials that were tightly joined together at one temperature and after that the temperature has changed, while their thermal expansion coefficients are different.

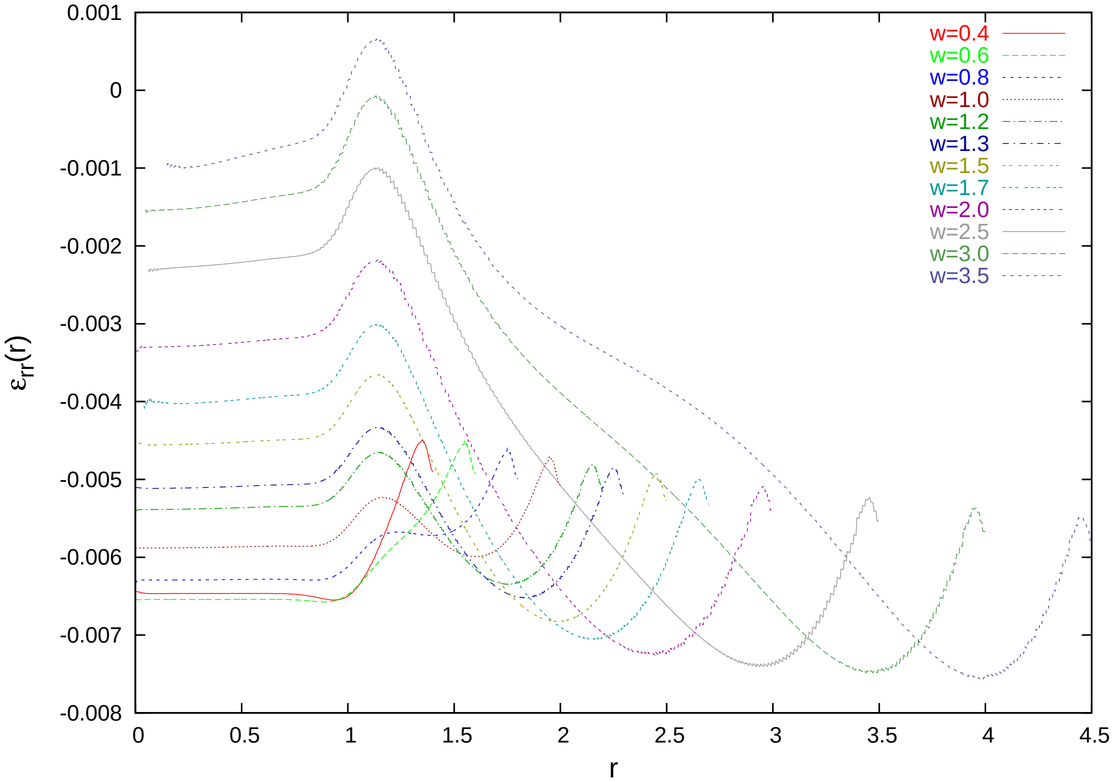

Figure 39: The residual strain tensor component, $\varepsilon_{rr}(r)$ is modeled at the surface after cooling from temperature of melting point of solder to room temperature (e.i. from $972K$ to $300K$). The upper layer has a higher Young modulus ($E = 42800Pa$, $\nu = 0.33$, thickness 0.05), and it is fixed to the entire surface of a cell shown in Figure 10 (with no core). Cell internal radius is 1, thickness is $h = 0.2$, material Young modulus is 4 times lower than that of the upper layer, with $E = 10693Pa$ and $\nu = 0.33$. Thermal expansion of the upper layer is $7.77^{-6}/K$ and of the lower one is $10.41^{-6}/K$ (which corresponds, respectively, to approximate effective thermal expansion coefficients of Sapphire and Titanium, respectively). The upper layer contracts less during cooling than cell material. The effect of wall thickness w (with values of w as shown in the figure) is studied.

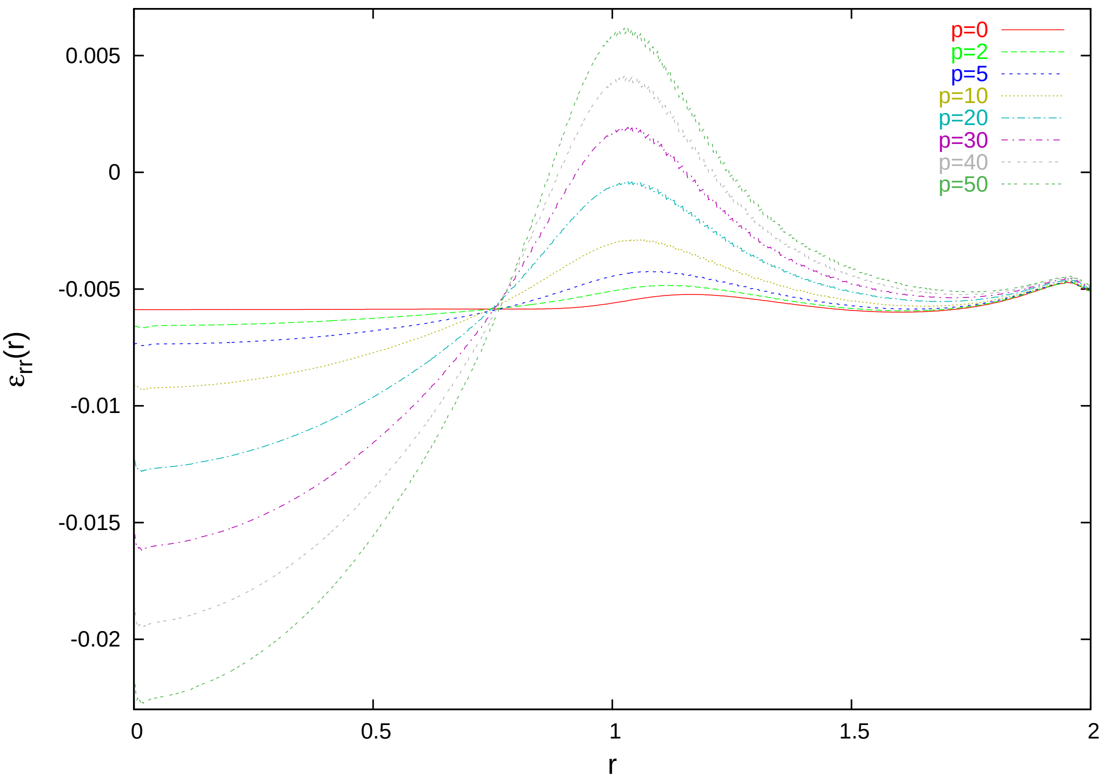

Figure 40: The strain tensor component, $\varepsilon_{rr}(r)$ as modeled at the surface, including residual strain due to cooling from temperature of melting point of solder to room temperature (e.i. from $972K$ to $300K$), after pressure p of several values (as described in the Figure) is applied. The geometrical model is identical to that one described in Figure 39. Wall thickness $w = 1.0$. The $z-$displacement maximum for the case when $p = 0$ is around of 2% of the inner cell radius $r = 1$. At around these or larger deformations one should expect the presense of the onset of nonlinear effects, however, as shown in the next figure, nonlinearities do not play yet a significant role.

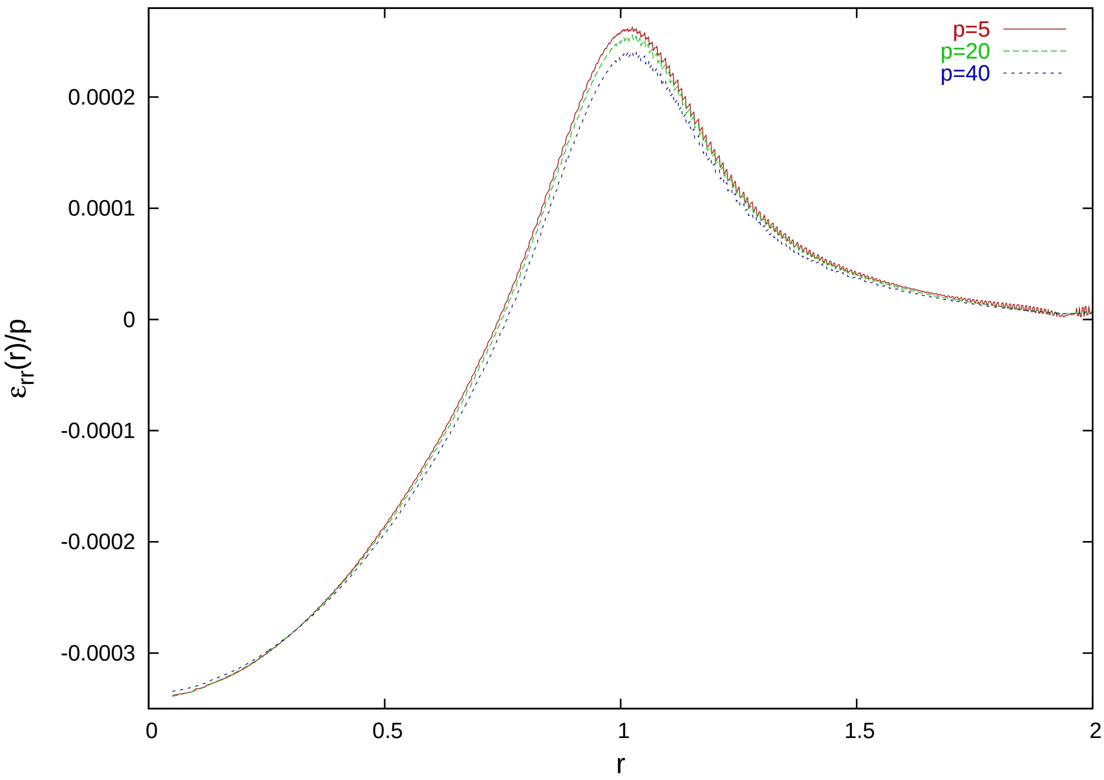

Figure 41: The strain tensor component, $\varepsilon_{rr}(r)$ after the residual thermal strain is subtracted and normalization is done by the applied pressure p, for pressure values as shown in the figure. The data are the same as these in Figure 40. Small nonlinearities are visible already at these pressures, however, the results demonstrate clearly that the strain observed is a direct sum of contribution due to thermal effects and the one due to applied external pressure.

Список литературы

[1] Shackelford, James F. et al, *"Frontmatter Materials Science and Engineering Handbook*, Ed. James F. Shackelford & W. Alexander; Boca Raton: CRC Press LLC, 2001

[2] www.kayelaby.npl.co.uk

[3] ts.nist.gov

[4] S. Timoshenko and S. Woinowsky-Krieger, *Theory of Plates and Shells.* McGraw Hill, 1959.

[5] Allan F. Bower *Applied Mechanics of Solids*

[6] *Марочник стали и сплавов*, www.splav.kharkov.com

[7] *David R. Lide, ed.*, CRC Handbook of Chemistry and Physics, 89th Edition (Internet Version 2009), CRC Press/Taylor and Francis, Boca Raton, FL.

[8] *Wachtman Jr., J.B., et. al.* J.Res. Nat. Bur. Stand. - A. Physics and Chemistry 64A, 213 (1960).

[9] *Donald C. Stouffer, L. Thomas Dame*, Inelastic deformation of metals: models, mechanical properties, and metallurgy, Wiley, 1996

[10] eqworld.ipmnet.ru

[11] *Sadd M.H.*, Elasticity: theory, applications, and numerics

[12] *Riley K., Hobson M.*, Mathematical Methods for Physics and Engineering.

8.13 Appendix A

8.13.1 Particular solutions of the biharmonic equation [10]

$$w(x,y) = (A \cdot cosh(\beta x) + B \cdot sinh(\beta x) + Cx \cdot cosh(\beta x) + Dx \cdot sinh(\beta x))\,(a \cdot cos(\beta y) + b \cdot sin(\beta y)) \quad (8.1)$$

$$w(x,y) = (A \cdot cos(\beta x) + B \cdot sin(\beta x) + Cx \cdot cos(\beta x) + Dx \cdot sin(\beta x))\,(a \cdot cosh(\beta y) + b \cdot sinh(\beta y)) \quad (8.2)$$

$$w(x,y) = A \cdot r^2 \cdot lnr + B \cdot r^2 + C \cdot lnr + D, \quad r = \sqrt{(x-a)^2 + (y-b)^2} \quad (8.3)$$

8.13.2 Boundary value problems for the upper half-plane

Domain: $-\infty < x < +\infty$, $0 \le y < +\infty$. The desired function and its derivative along the normal are prescribed at the boundary:

$w = 0$ at $y = 0$, $\partial w/\partial y = f(x)$ at $y = 0$

Solution:

$$w(x,y) = \int_{-\infty}^{+\infty} f(\zeta) \cdot G(x-\zeta, y) d\zeta, \quad G(x,y) = \frac{1}{\pi} \frac{y^2}{x^2 + y^2} \quad (8.4)$$

Domain: $-\infty < x < +\infty$, $0 \le y < +\infty$. The derivatives of the desired function are prescribed at the boundary:

$\partial w/\partial x = f(x)$ at $y = 0$, $\partial w/\partial y = g(x)$ at $y = 0$.

Solution:

$$w(x,y) = \frac{1}{\pi} \int_{-\infty}^{+\infty} f(\zeta) \cdot \left[arctan\left(\frac{x-\zeta}{y}\right) + \frac{y(x-\zeta)}{(x-\zeta)^2 + y^2} \right] d\zeta + \frac{y^2}{\pi} \int_{-\infty}^{+\infty} \frac{g(\zeta) d\zeta}{(x-\zeta)^2 + y^2} + C \quad (8.5)$$

where C is an arbitrary constant.

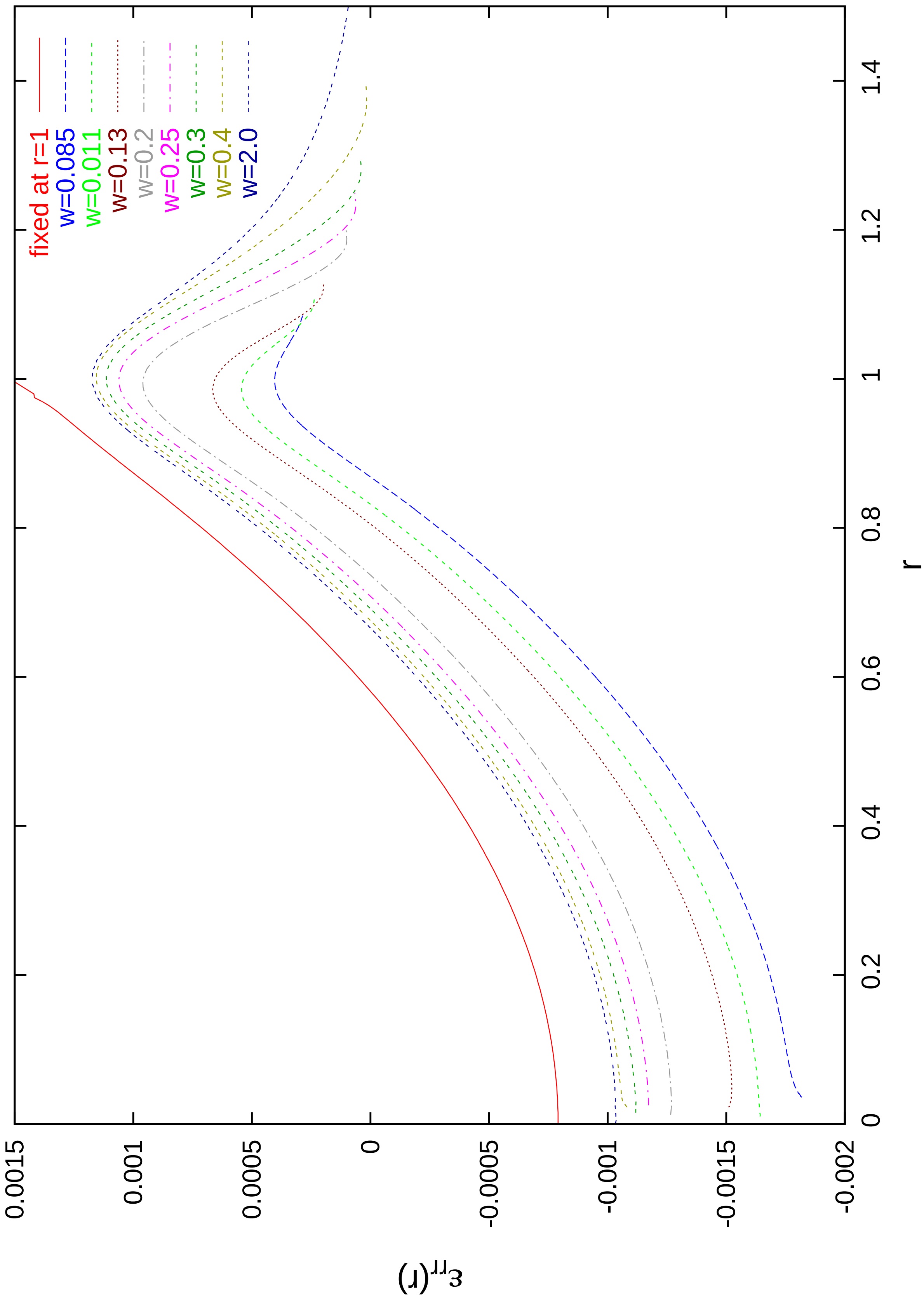

fixed at r=1
w=0.085
w=0.011
w=0.13
w=0.2
w=0.25
w=0.3
w=0.4
w=2.0
r
ε_rr(r)

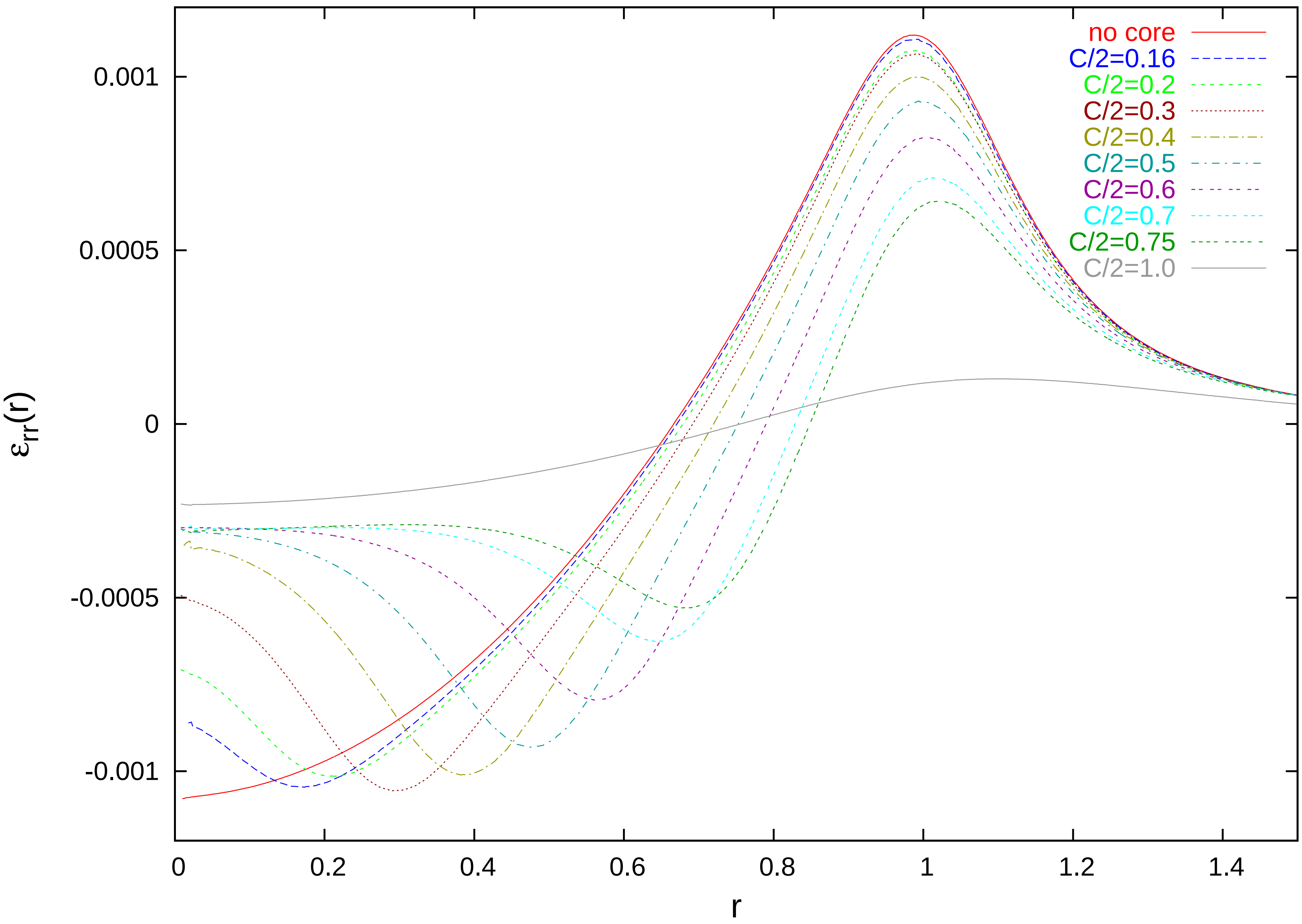

no core
C/2=0.16
C/2=0.2
C/2=0.3
C/2=0.4
C/2=0.5
C/2=0.6
C/2=0.7
C/2=0.75
C/2=1.0
0.001
0.0005
0
-0.0005
-0.001
ε_rr(r)
0
0.2
0.4
0.6
0.8
1
1.2
1.4
r

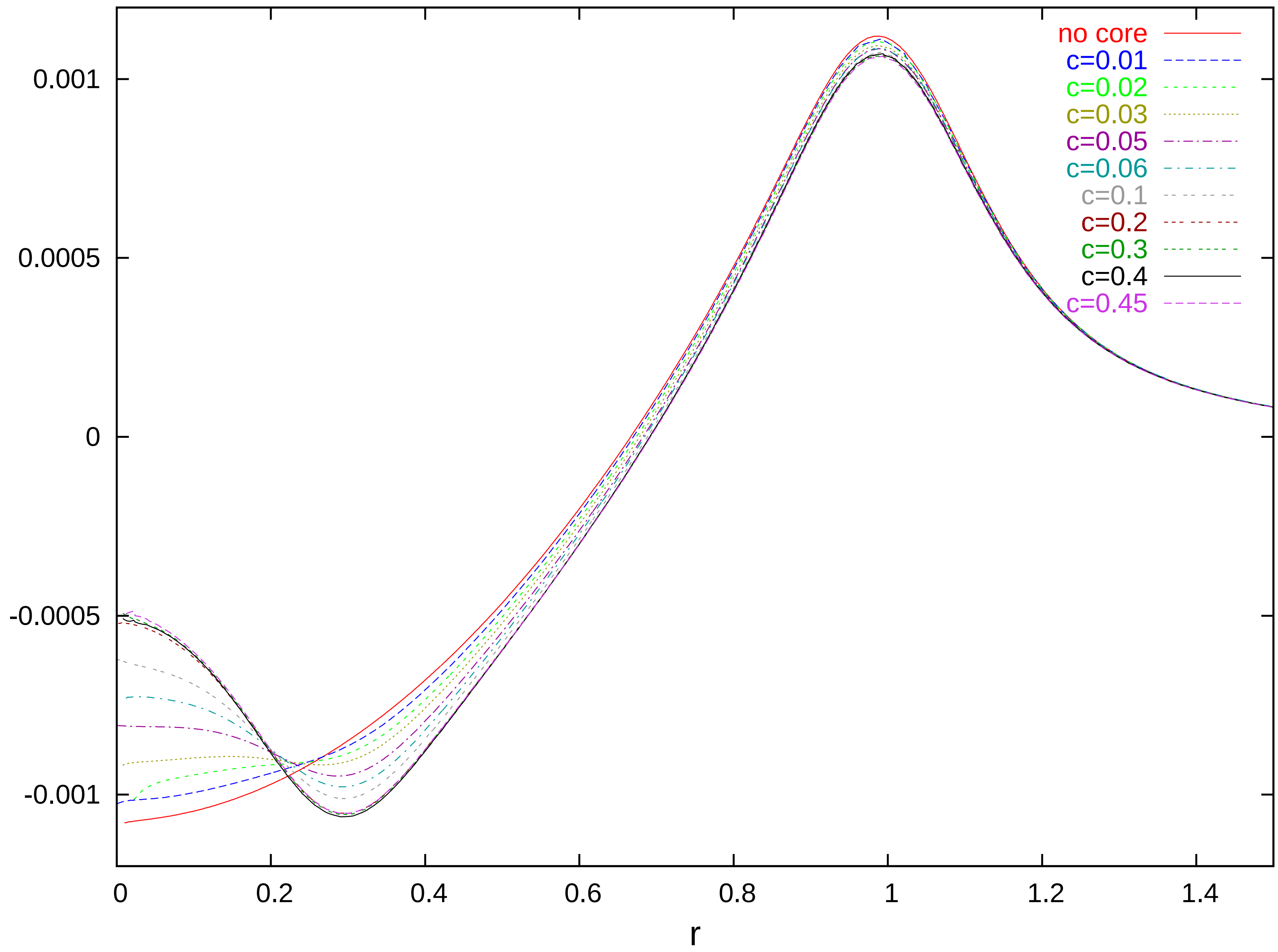
no core
c=0.01
c=0.02
c=0.03
c=0.05
c=0.06
c=0.1
c=0.2
c=0.3
c=0.4
c=0.45
0.001
0.0005
0
-0.0005
-0.001
$\varepsilon_{rr}(r)$
0
0.2
0.4
0.6
0.8
1
1.2
1.4
r

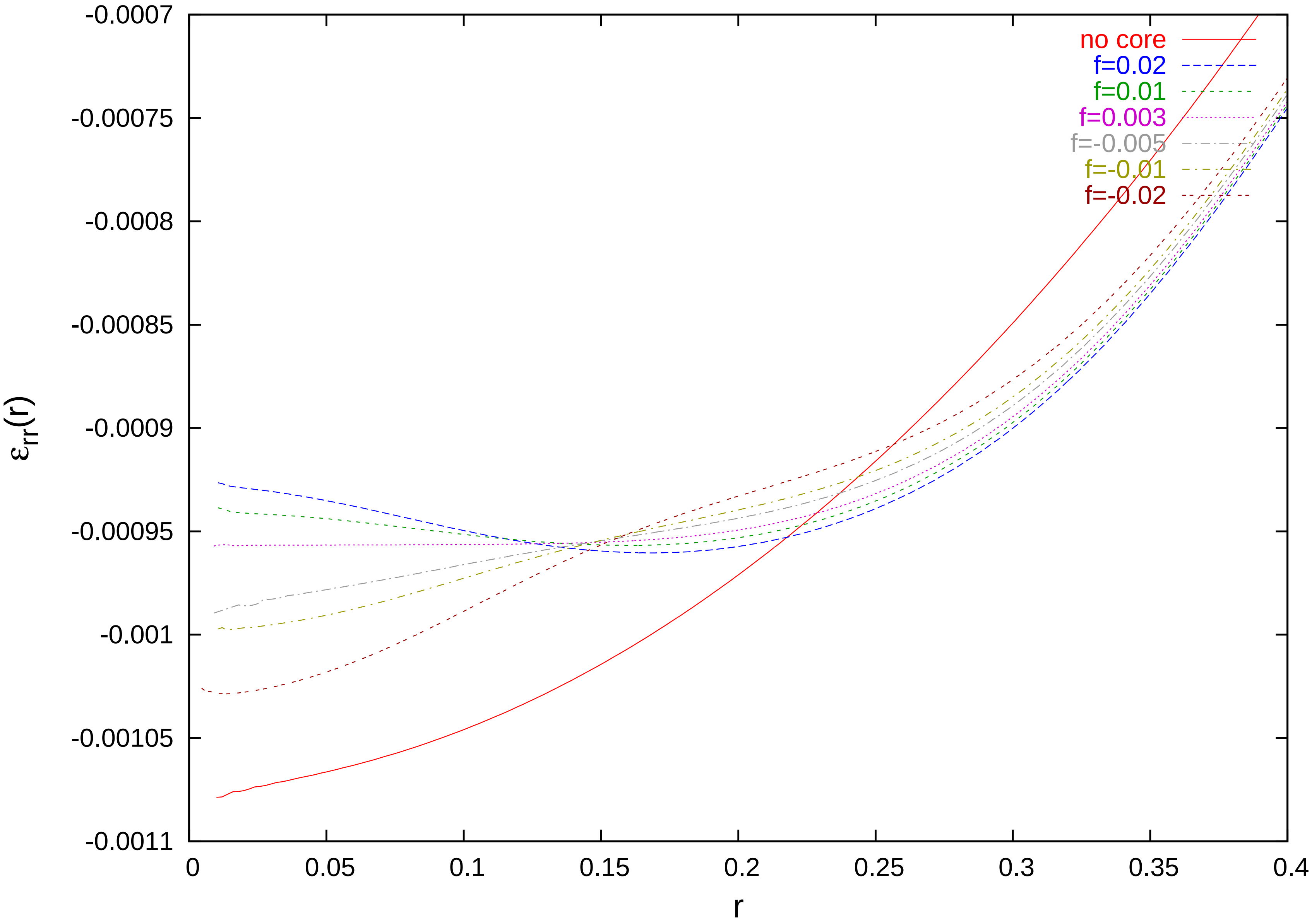

no core
f=0.02
f=0.01
f=0.003
f=-0.005
f=-0.01
f=-0.02
-0.0007
-0.00075
-0.0008
-0.00085
-0.0009
-0.00095
-0.001
-0.00105
-0.0011
0
0.05
0.1
0.15
0.2
0.25
0.3
0.35
0.4
r
$\varepsilon_{rr}(r)$

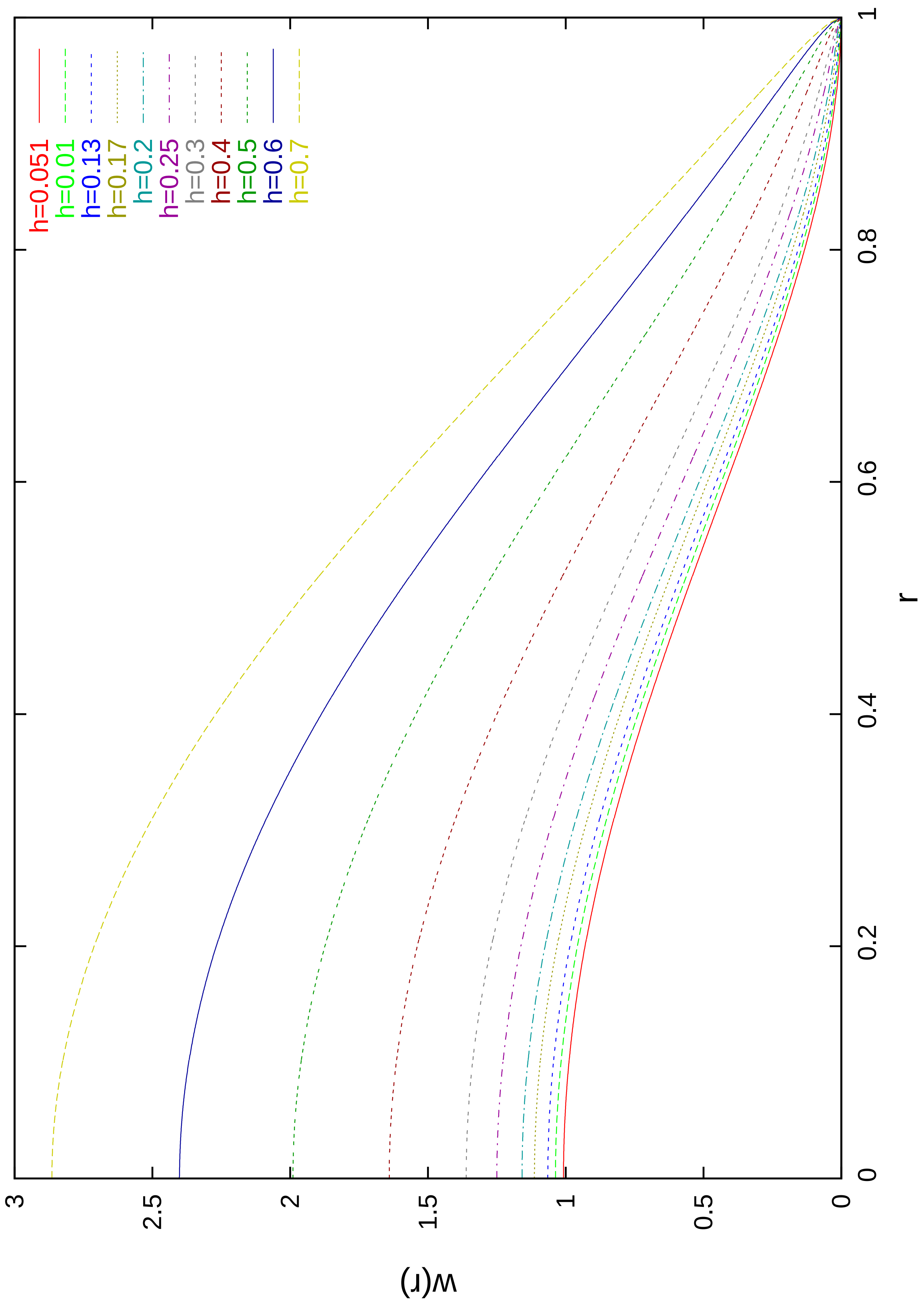
h=0.051
h=0.01
h=0.13
h=0.17
h=0.2
h=0.25
h=0.3
h=0.4
h=0.5
h=0.6
h=0.7
r
w(r)
0
0.2
0.4
0.6
0.8
1
0
0.5
1
1.5
2
2.5
3

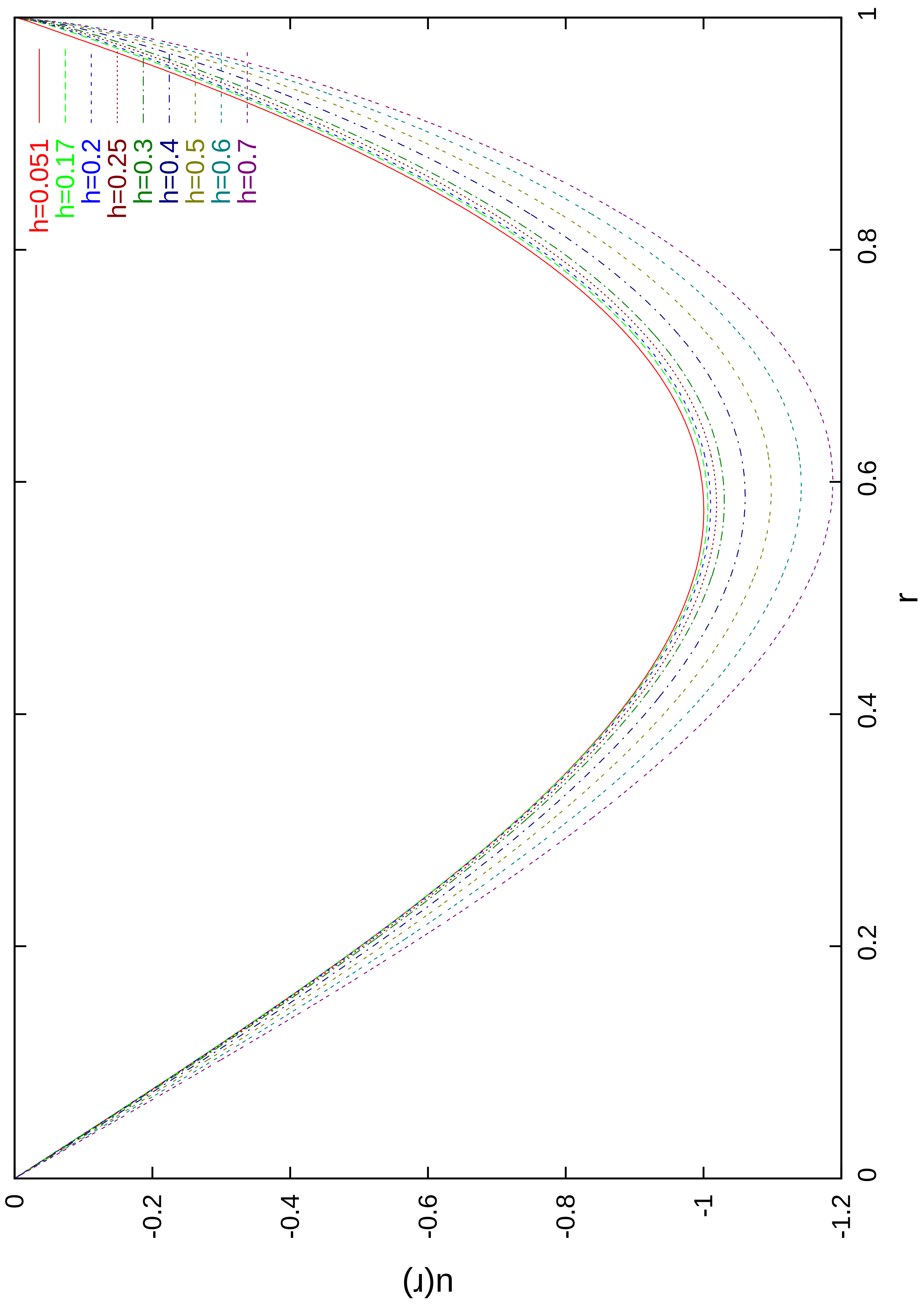

h=0.051
h=0.17
h=0.2
h=0.25
h=0.3
h=0.4
h=0.5
h=0.6
h=0.7
u(r)
r
0
-0.2
-0.4
-0.6
-0.8
-1
-1.2
0
0.2
0.4
0.6
0.8
1

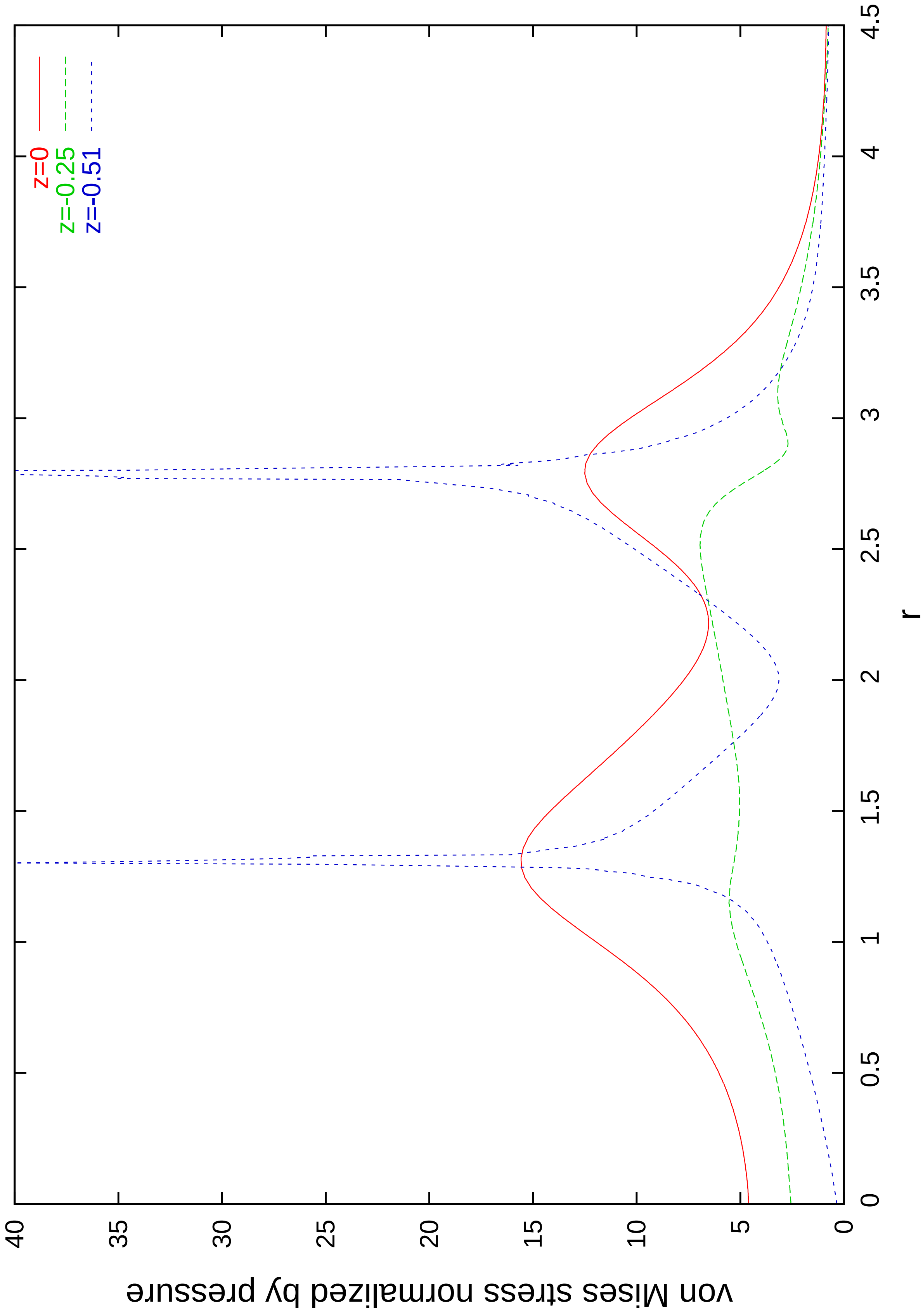

z=0
z=-0.25
z=-0.51
von Mises stress normalized by pressure
r
0
5
10
15
20
25
30
35
40
0
0.5
1
1.5
2
2.5
3
3.5
4
4.5

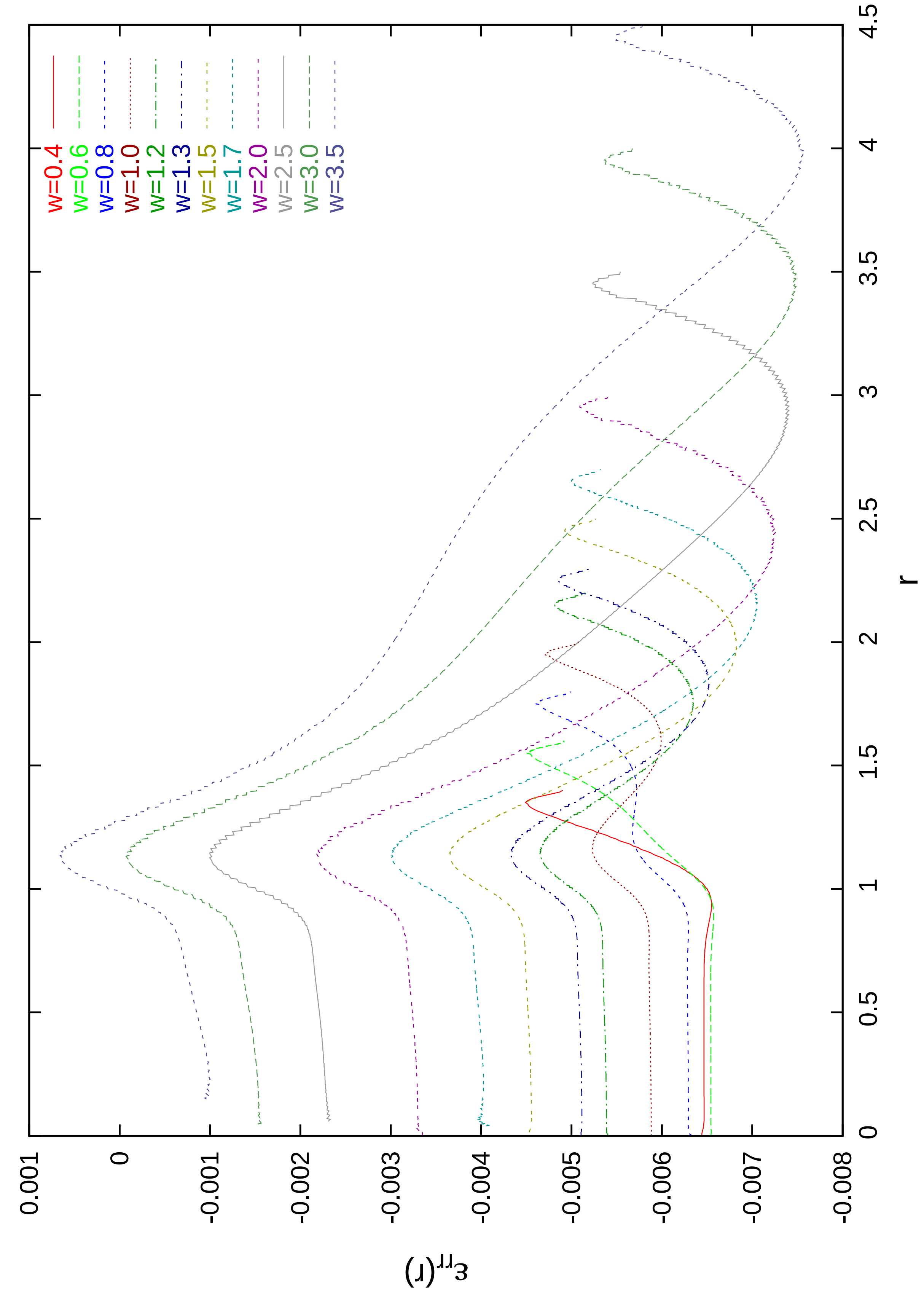
w=0.4
w=0.6
w=0.8
w=1.0
w=1.2
w=1.3
w=1.5
w=1.7
w=2.0
w=2.5
w=3.0
w=3.5
r
ε_rr(r)
0
0.5
1
1.5
2
2.5
3
3.5
4
4.5
0.001
0
-0.001
-0.002
-0.003
-0.004
-0.005
-0.006
-0.007
-0.008

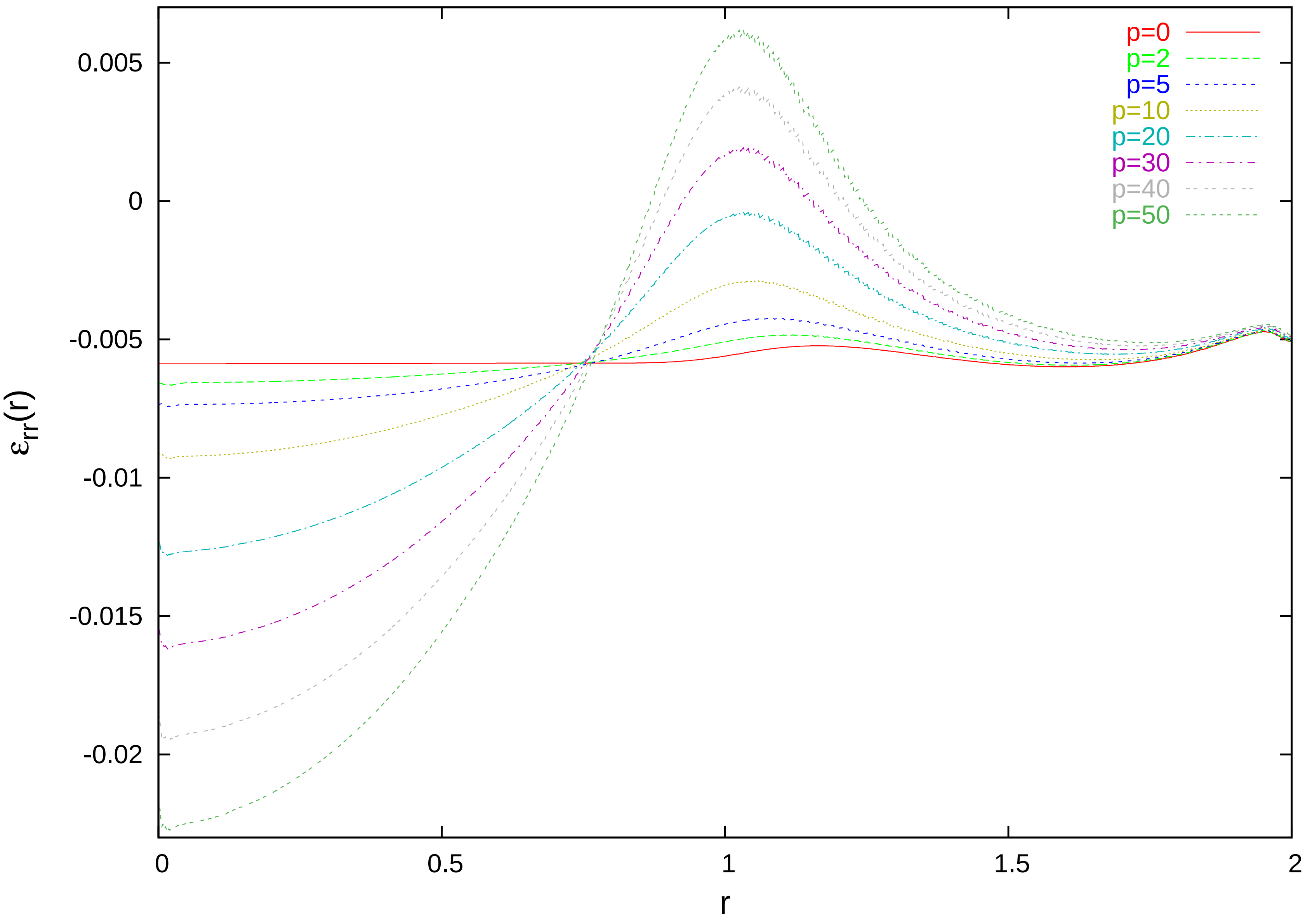
p=0
p=2
p=5
p=10
p=20
p=30
p=40
p=50
0.005
0
-0.005
-0.01
-0.015
-0.02
$\varepsilon_{rr}(r)$
0
0.5
1
1.5
2
r

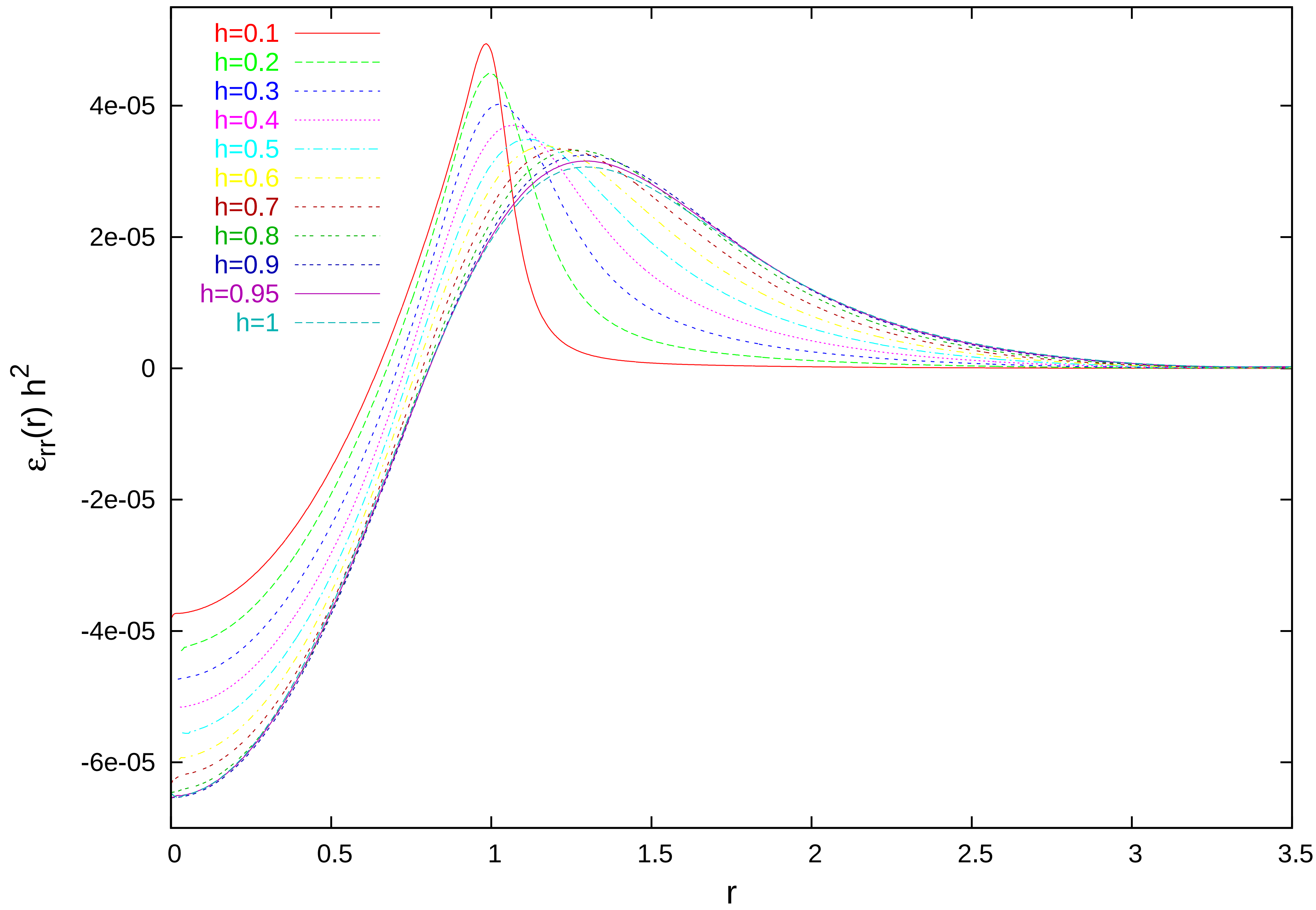

h=0.1
h=0.2
h=0.3
h=0.4
h=0.5
h=0.6
h=0.7
h=0.8
h=0.9
h=0.95
h=1
4e-05
2e-05
0
-2e-05
-4e-05
-6e-05
$\varepsilon_{rr}(r)\,h^2$
0
0.5
1
1.5
2
2.5
3
3.5
r

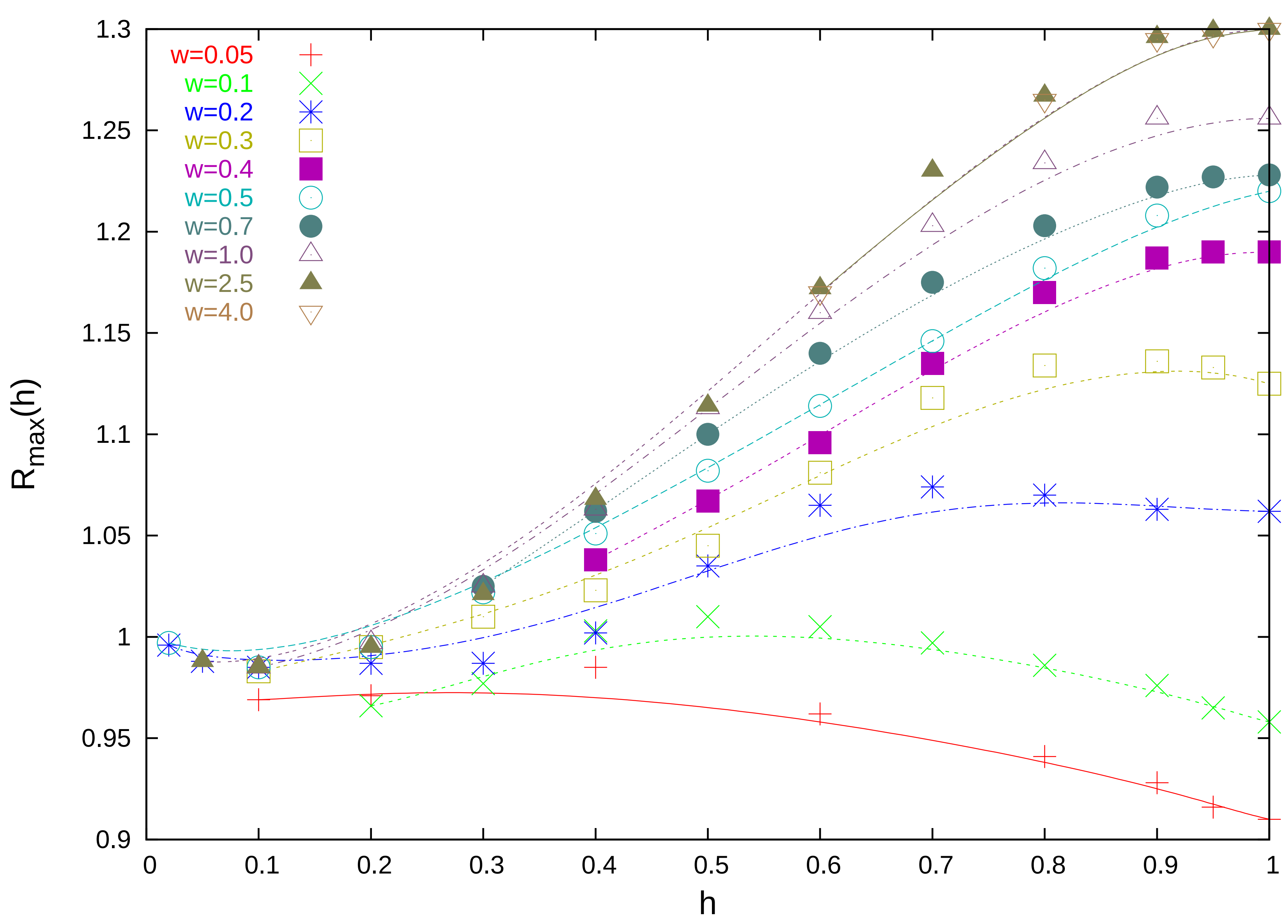

w=0.05
w=0.1
w=0.2
w=0.3
w=0.4
w=0.5
w=0.7
w=1.0
w=2.5
w=4.0
$R_{max}(h)$
h
1.3
1.25
1.2
1.15
1.1
1.05
1
0.95
0.9
0
0.1
0.2
0.3
0.4
0.5
0.6
0.7
0.8
0.9
1

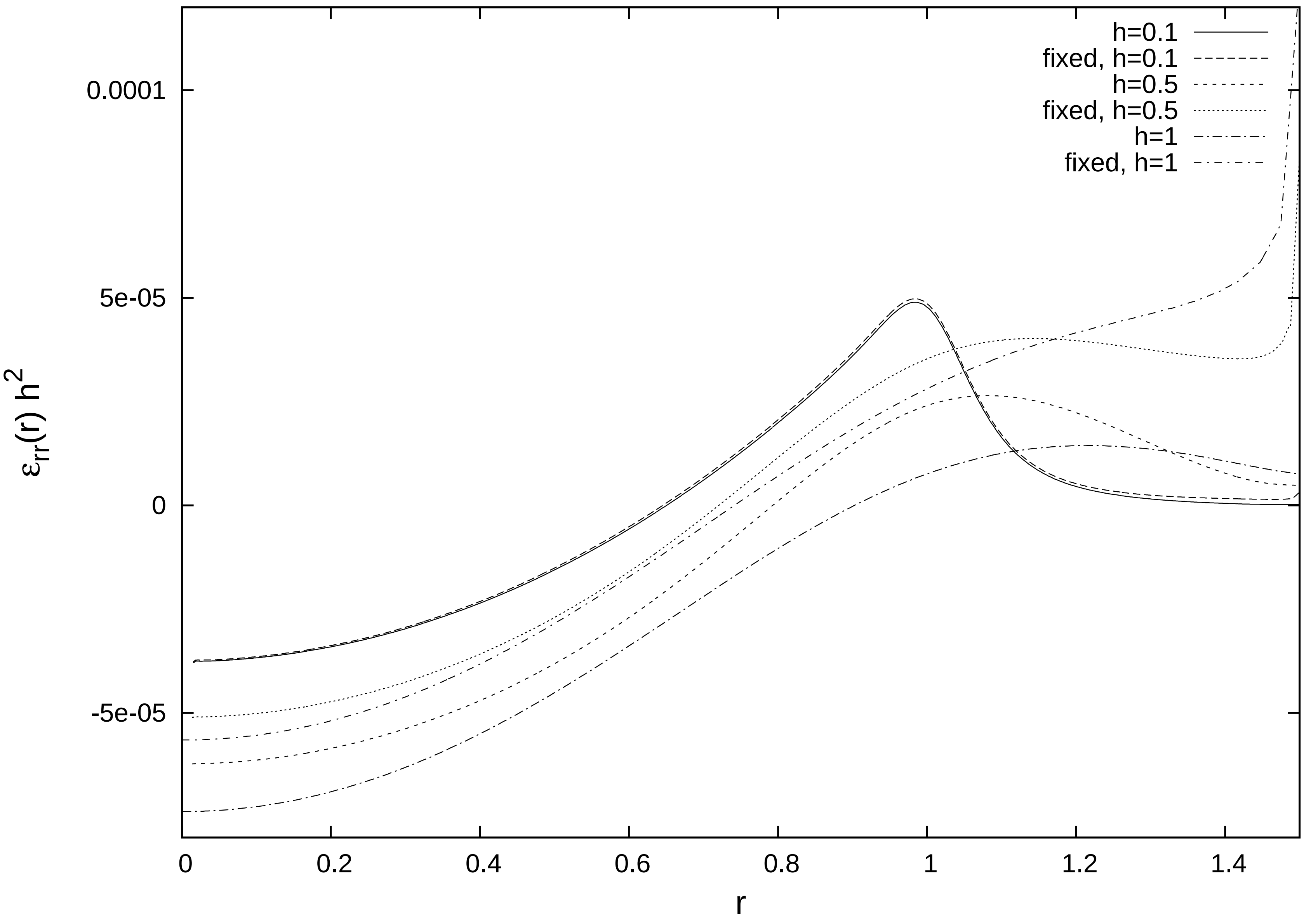

h=0.1
fixed, h=0.1
h=0.5
fixed, h=0.5
h=1
fixed, h=1
0.0001
5e-05
0
-5e-05
0
0.2
0.4
0.6
0.8
1
1.2
1.4
r
$\varepsilon_{rr}(r)\,h^2$

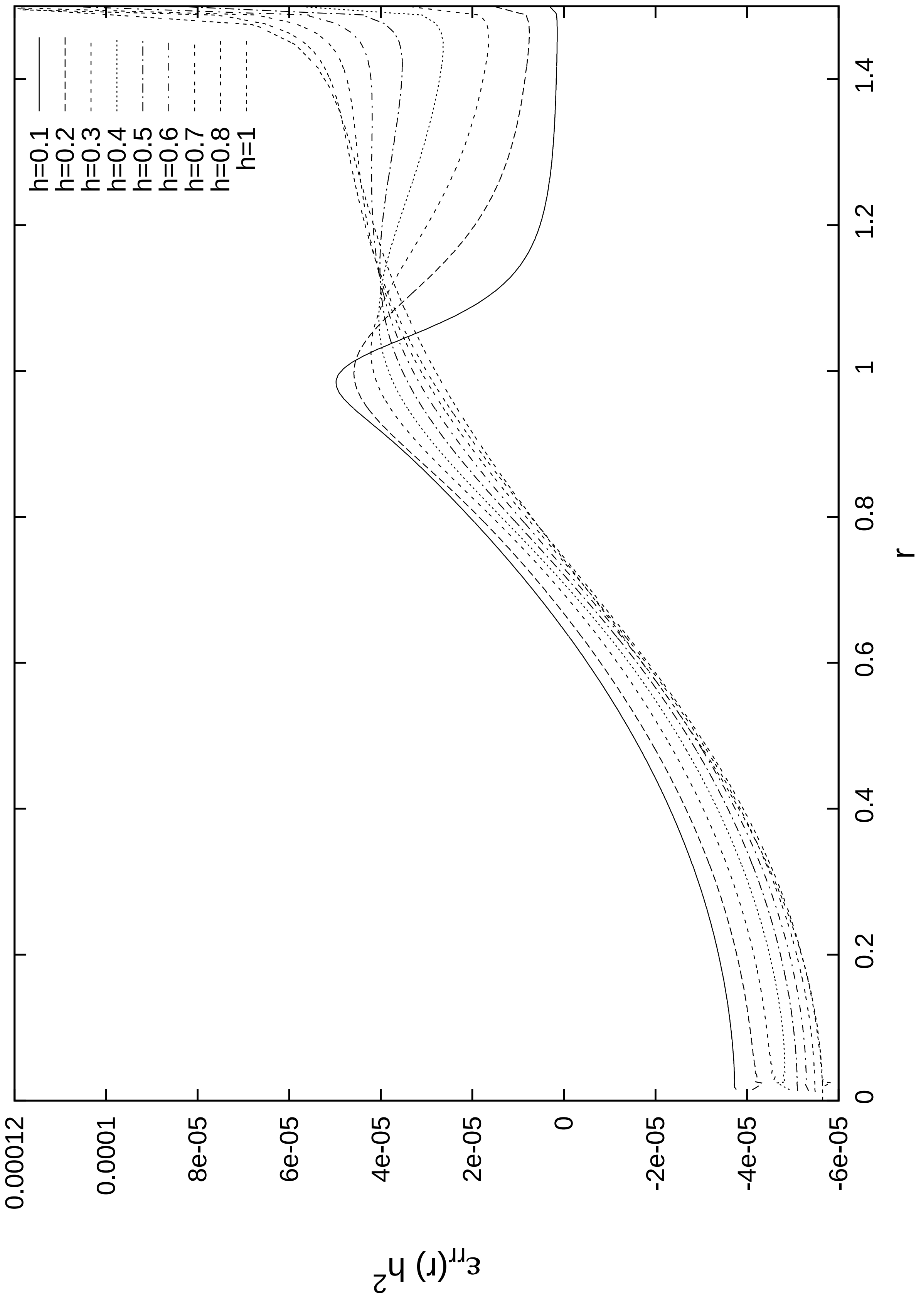
h=0.1
h=0.2
h=0.3
h=0.4
h=0.5
h=0.6
h=0.7
h=0.8
h=1
r
$\varepsilon_{rr}(r)\,h^2$
0
0.2
0.4
0.6
0.8
1
1.2
1.4
0.00012
0.0001
8e-05
6e-05
4e-05
2e-05
0
-2e-05
-4e-05
-6e-05

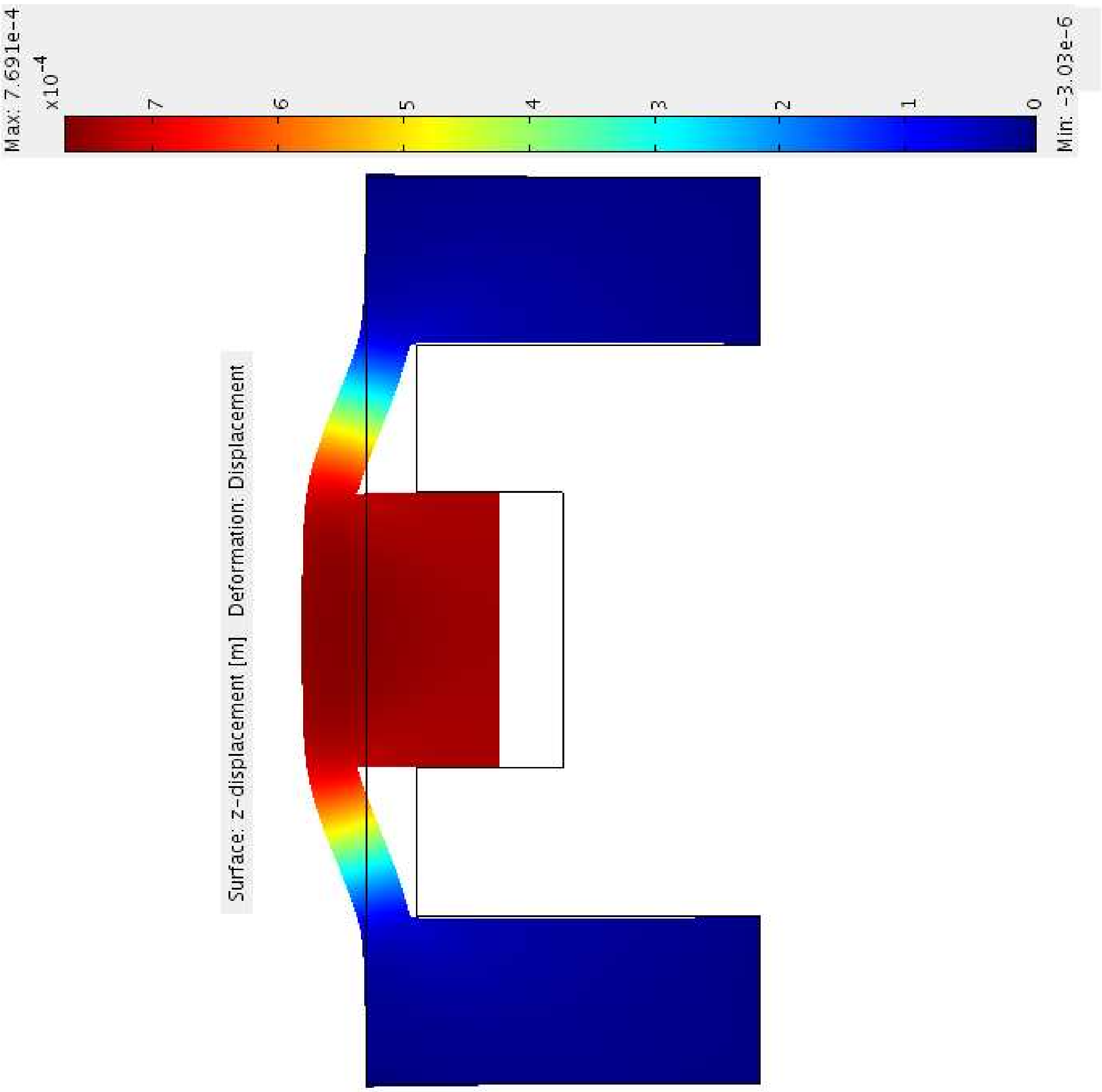
Surface: z-displacement [m] Deformation: Displacement
Max: 7.691e-4
x10^-4
7
6
5
4
3
2
1
0
Min: -3.03e-6

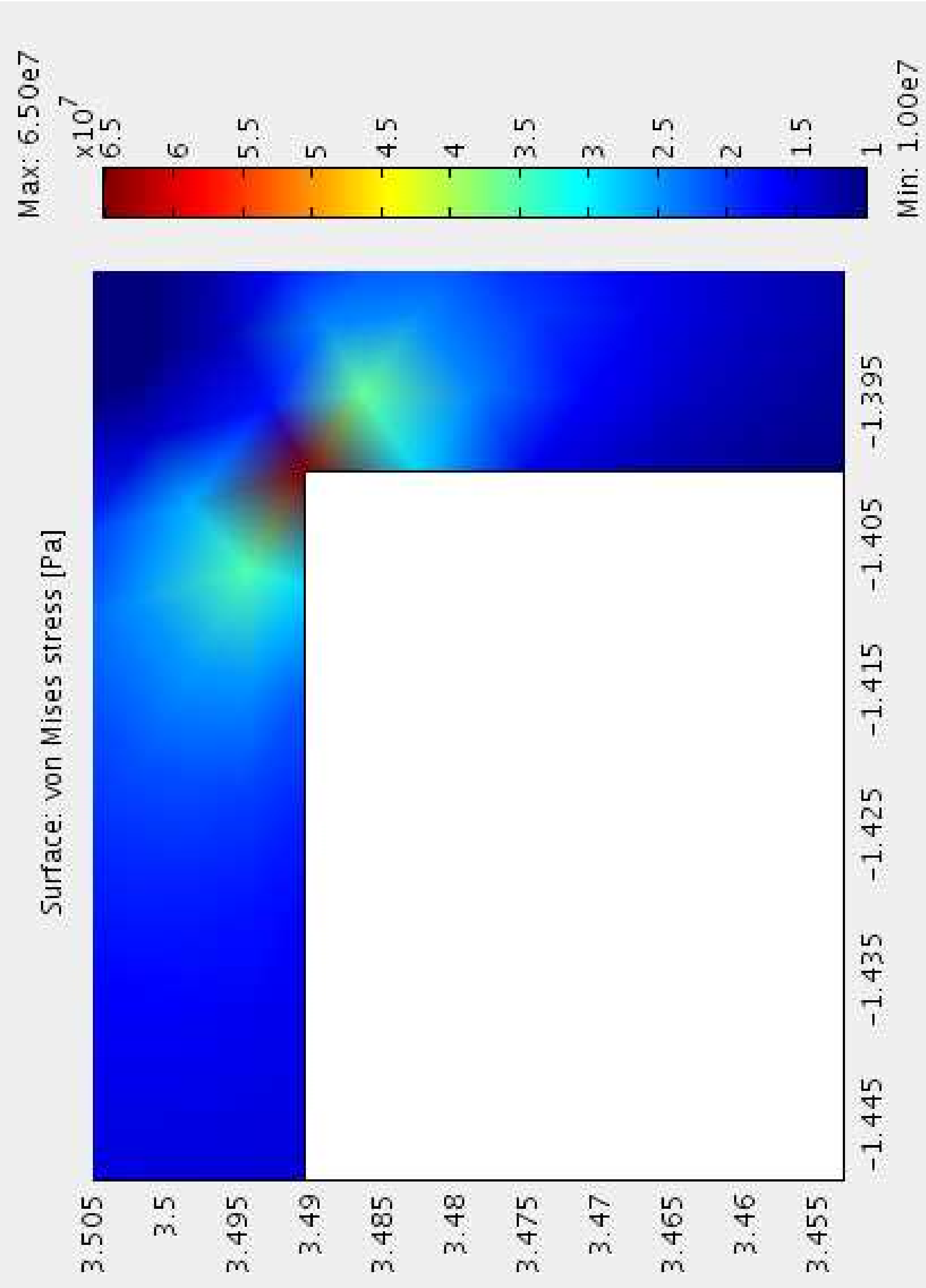
Surface: von Mises stress [Pa]
Max: 6.50e7
Min: 1.00e7
x10^7
6.5
6
5.5
5
4.5
4
3.5
3
2.5
2
1.5
1
3.505
3.5
3.495
3.49
3.485
3.48
3.475
3.47
3.465
3.46
3.455
-1.445
-1.435
-1.425
-1.415
-1.405
-1.395

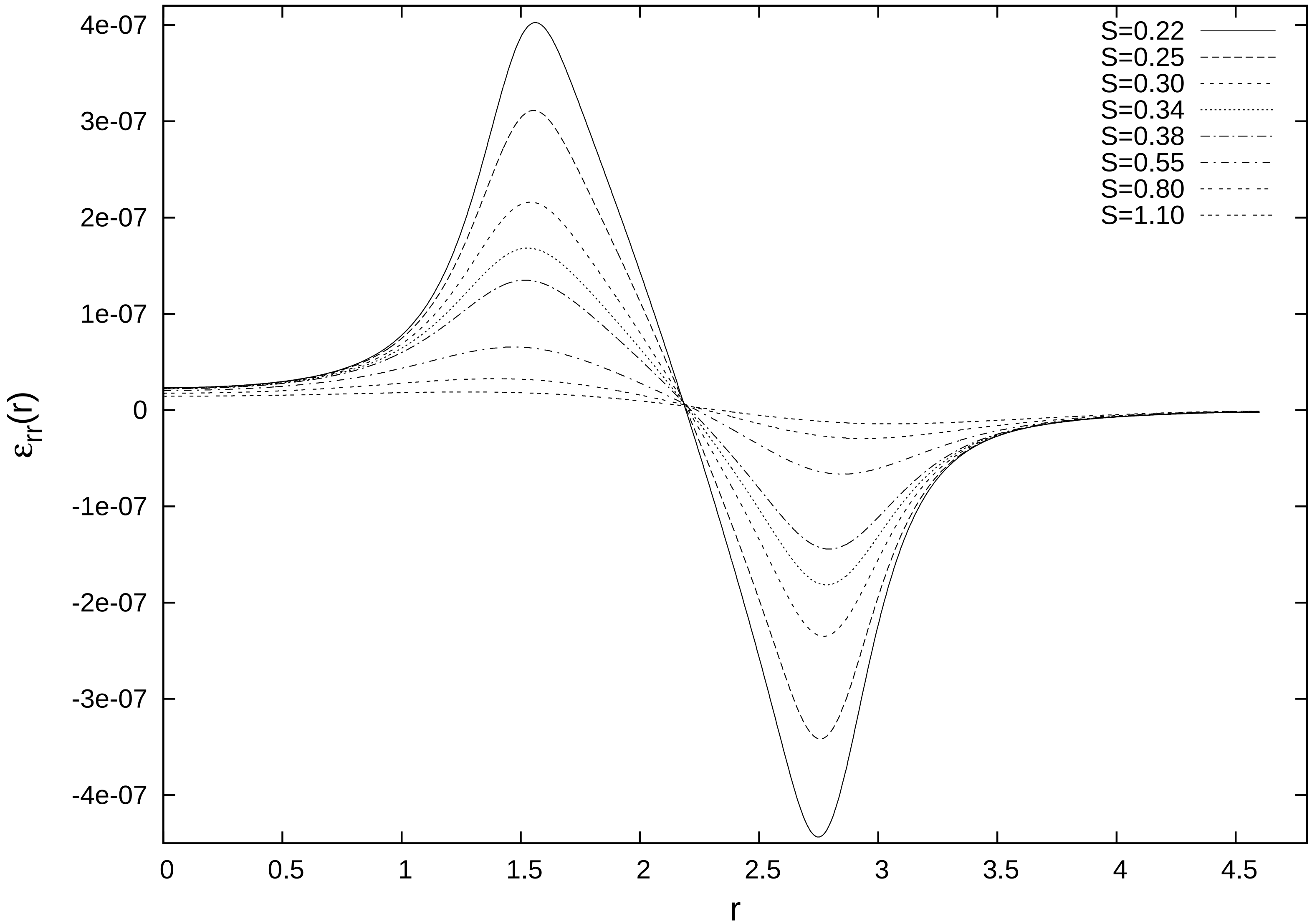

S=0.22
S=0.25
S=0.30
S=0.34
S=0.38
S=0.55
S=0.80
S=1.10
4e-07
3e-07
2e-07
1e-07
0
-1e-07
-2e-07
-3e-07
-4e-07
0
0.5
1
1.5
2
2.5
3
3.5
4
4.5
r
$\varepsilon_{rr}(r)$

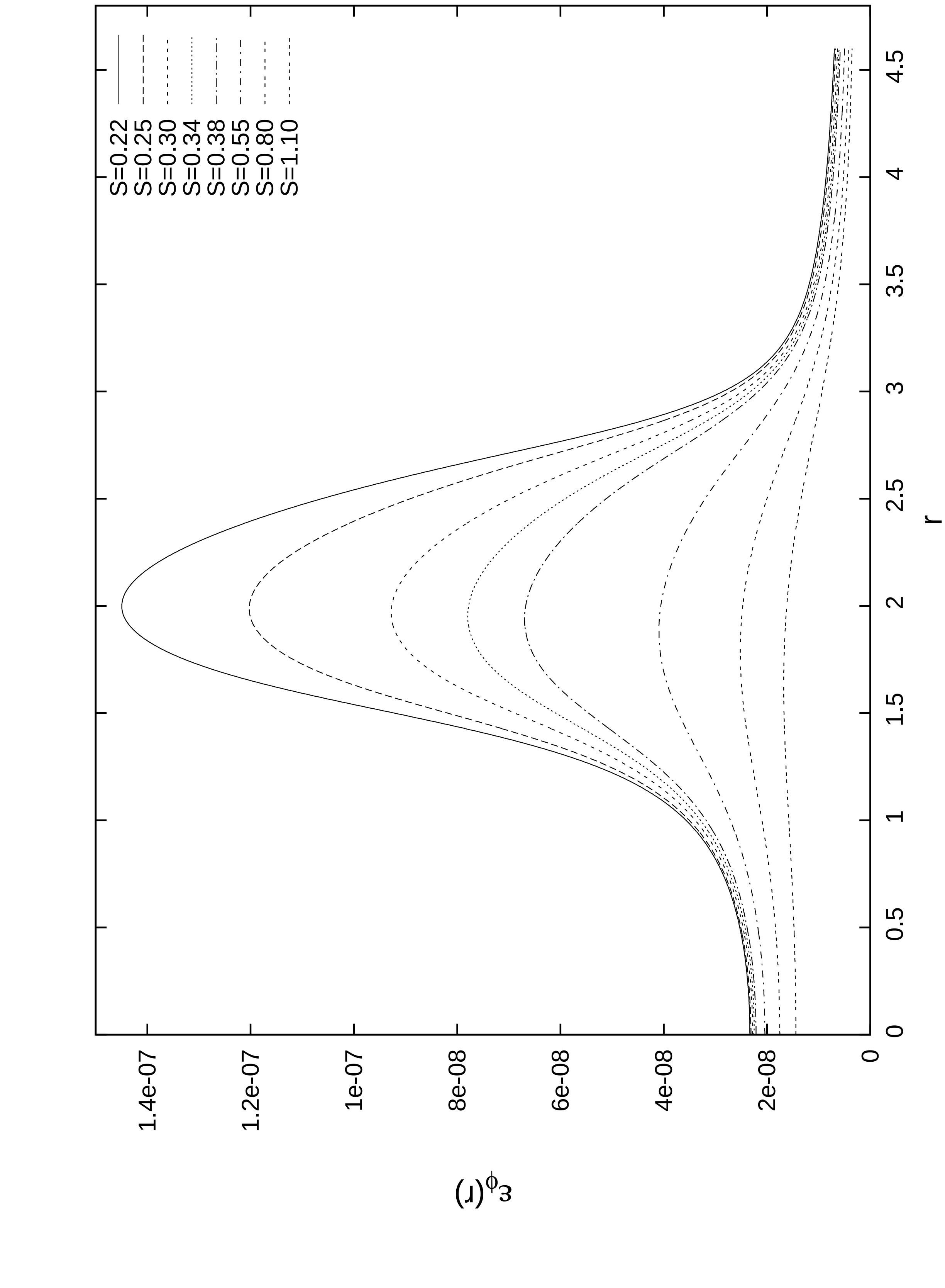
S=0.22
S=0.25
S=0.30
S=0.34
S=0.38
S=0.55
S=0.80
S=1.10
r
ε_φ(r)
0
0.5
1
1.5
2
2.5
3
3.5
4
4.5
0
2e-08
4e-08
6e-08
8e-08
1e-07
1.2e-07
1.4e-07

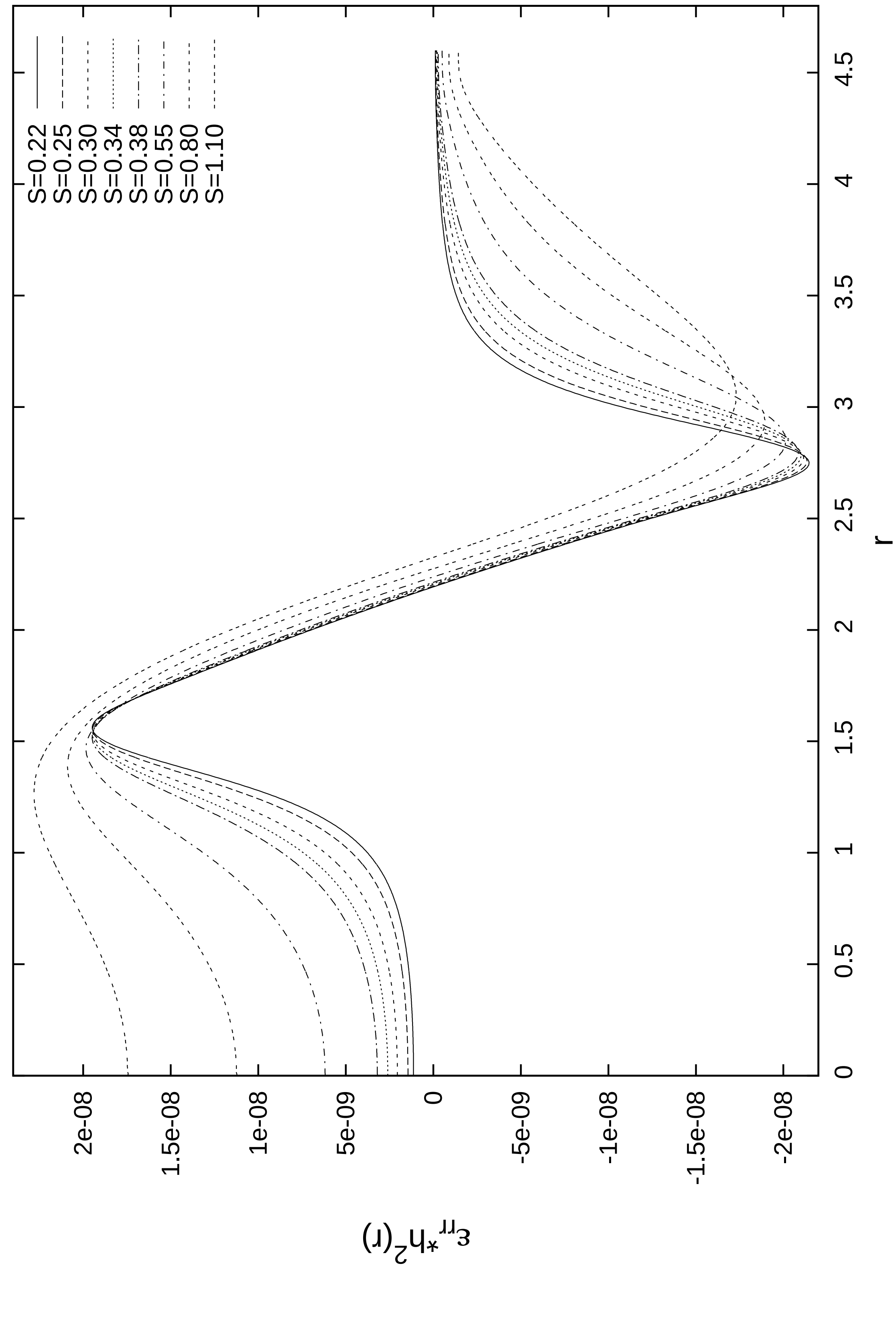
S=0.22
S=0.25
S=0.30
S=0.34
S=0.38
S=0.55
S=0.80
S=1.10
r
$\varepsilon_{rr}*h^2(r)$
0
0.5
1
1.5
2
2.5
3
3.5
4
4.5
2e-08
1.5e-08
1e-08
5e-09
0
-5e-09
-1e-08
-1.5e-08
-2e-08

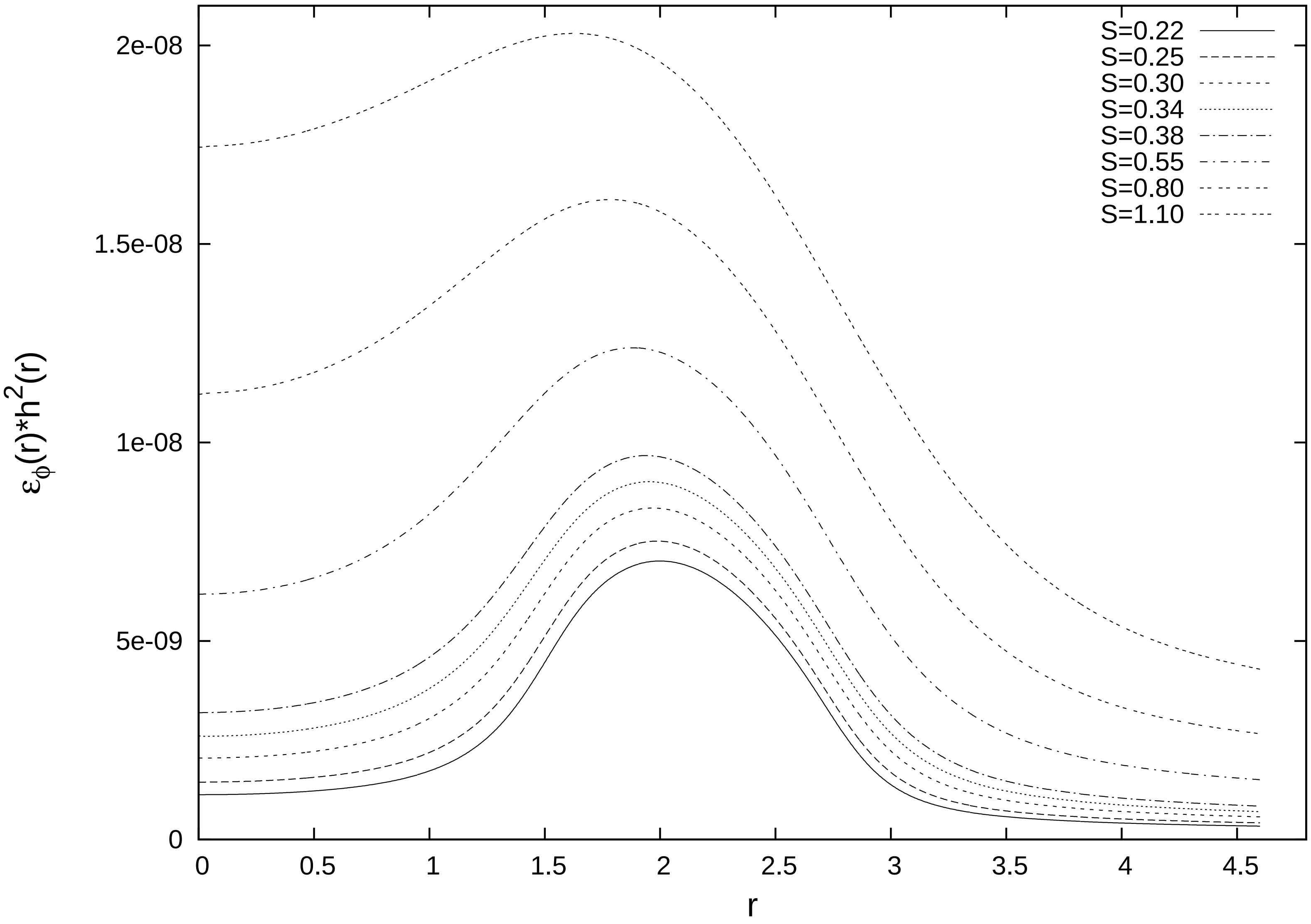

S=0.22
S=0.25
S=0.30
S=0.34
S=0.38
S=0.55
S=0.80
S=1.10
2e-08
1.5e-08
1e-08
5e-09
0
0.5
1
1.5
2
2.5
3
3.5
4
4.5
r
$\varepsilon_\phi(r)*h^2(r)$

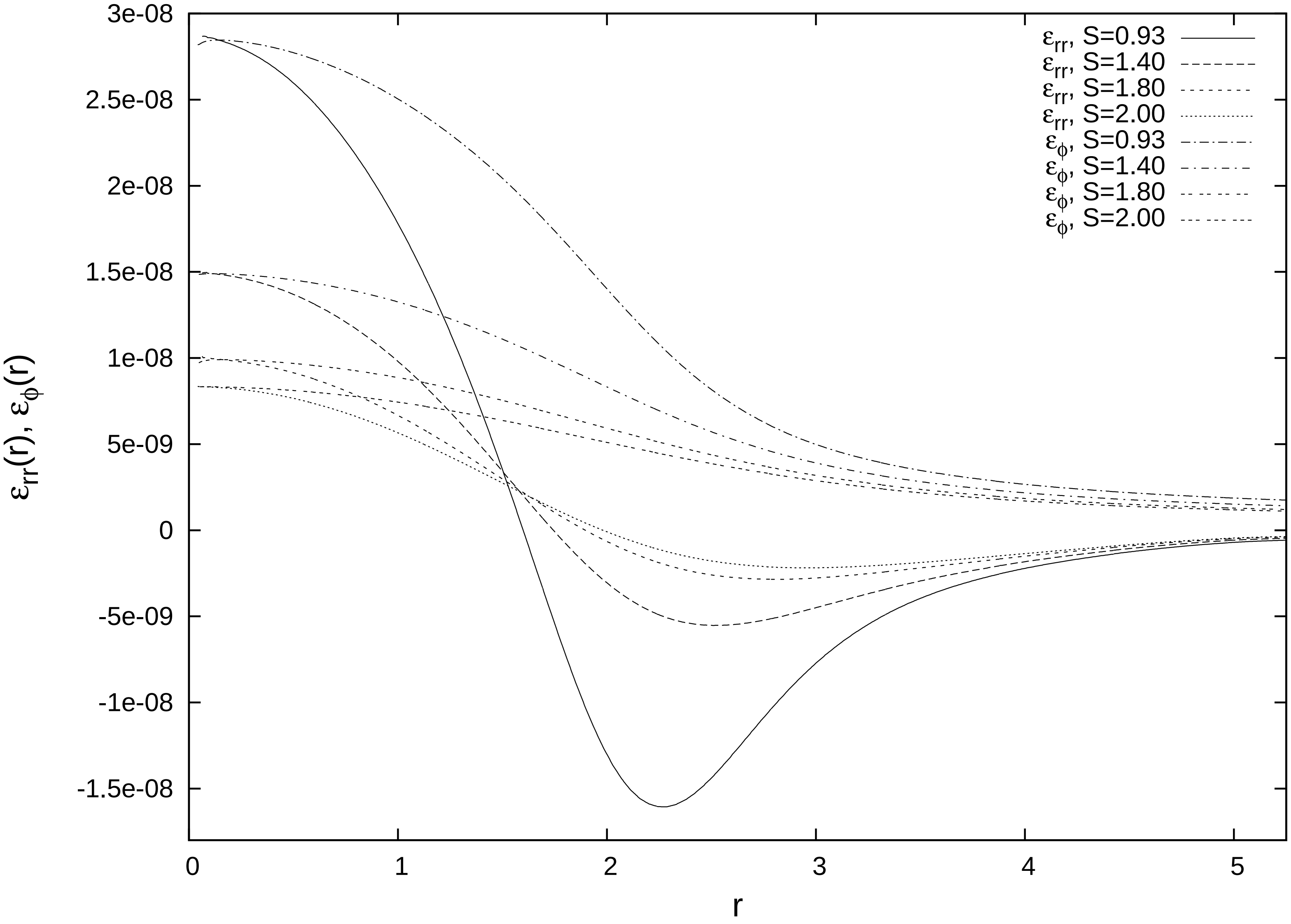

3e-08
2.5e-08
2e-08
1.5e-08
1e-08
5e-09
0
-5e-09
-1e-08
-1.5e-08
0
1
2
3
4
5
r
$\varepsilon_{rr}(r)$, $\varepsilon_{\phi}(r)$
ε_{rr}, S=0.93
ε_{rr}, S=1.40
ε_{rr}, S=1.80
ε_{rr}, S=2.00
ε_{ϕ}, S=0.93
ε_{ϕ}, S=1.40
ε_{ϕ}, S=1.80
ε_{ϕ}, S=2.00

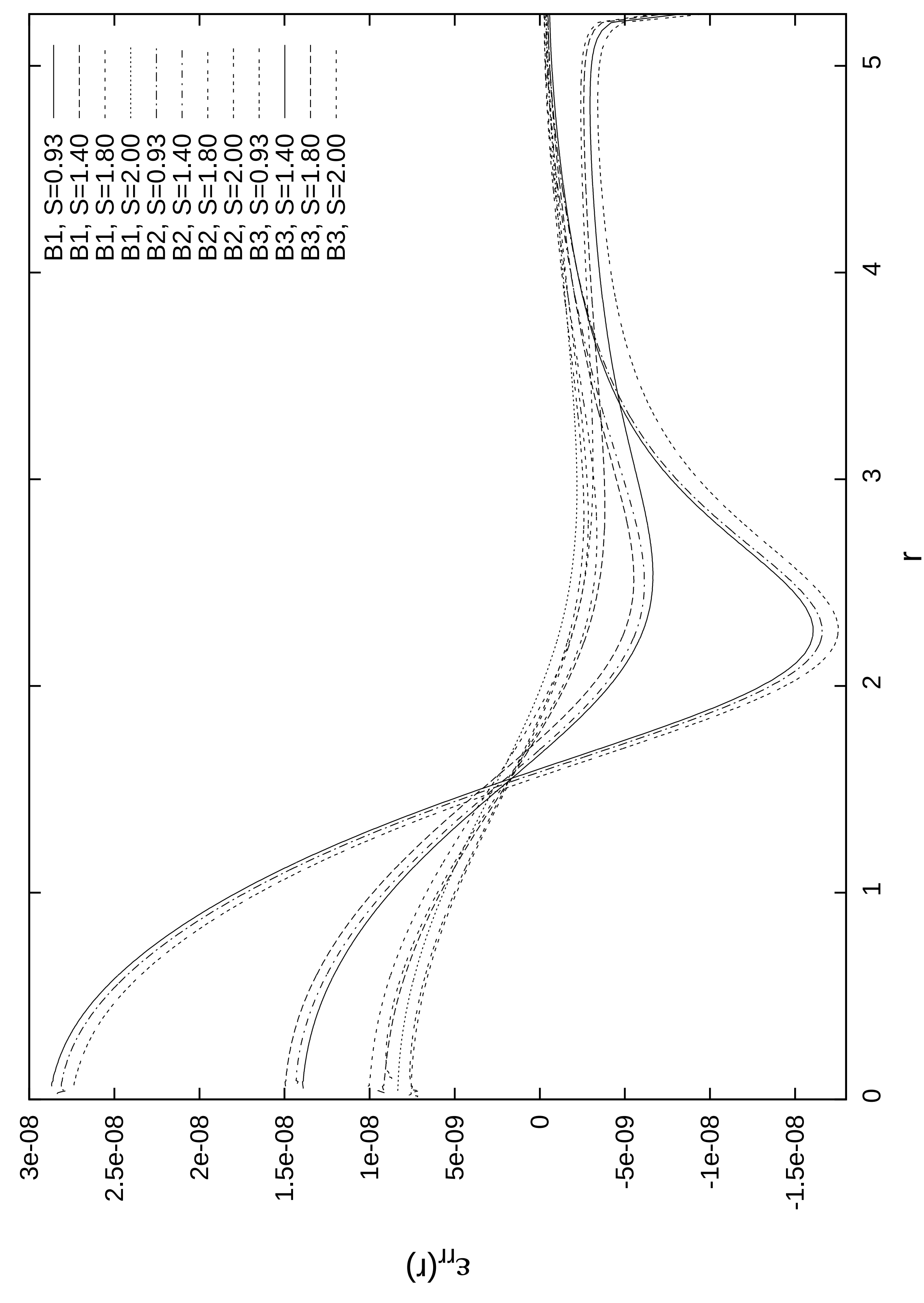

$\epsilon_{rr}(r)$
r
3e-08
2.5e-08
2e-08
1.5e-08
1e-08
5e-09
0
-5e-09
-1e-08
-1.5e-08
0
1
2
3
4
5
B1, S=0.93
B1, S=1.40
B1, S=1.80
B1, S=2.00
B2, S=0.93
B2, S=1.40
B2, S=1.80
B2, S=2.00
B3, S=0.93
B3, S=1.40
B3, S=1.80
B3, S=2.00

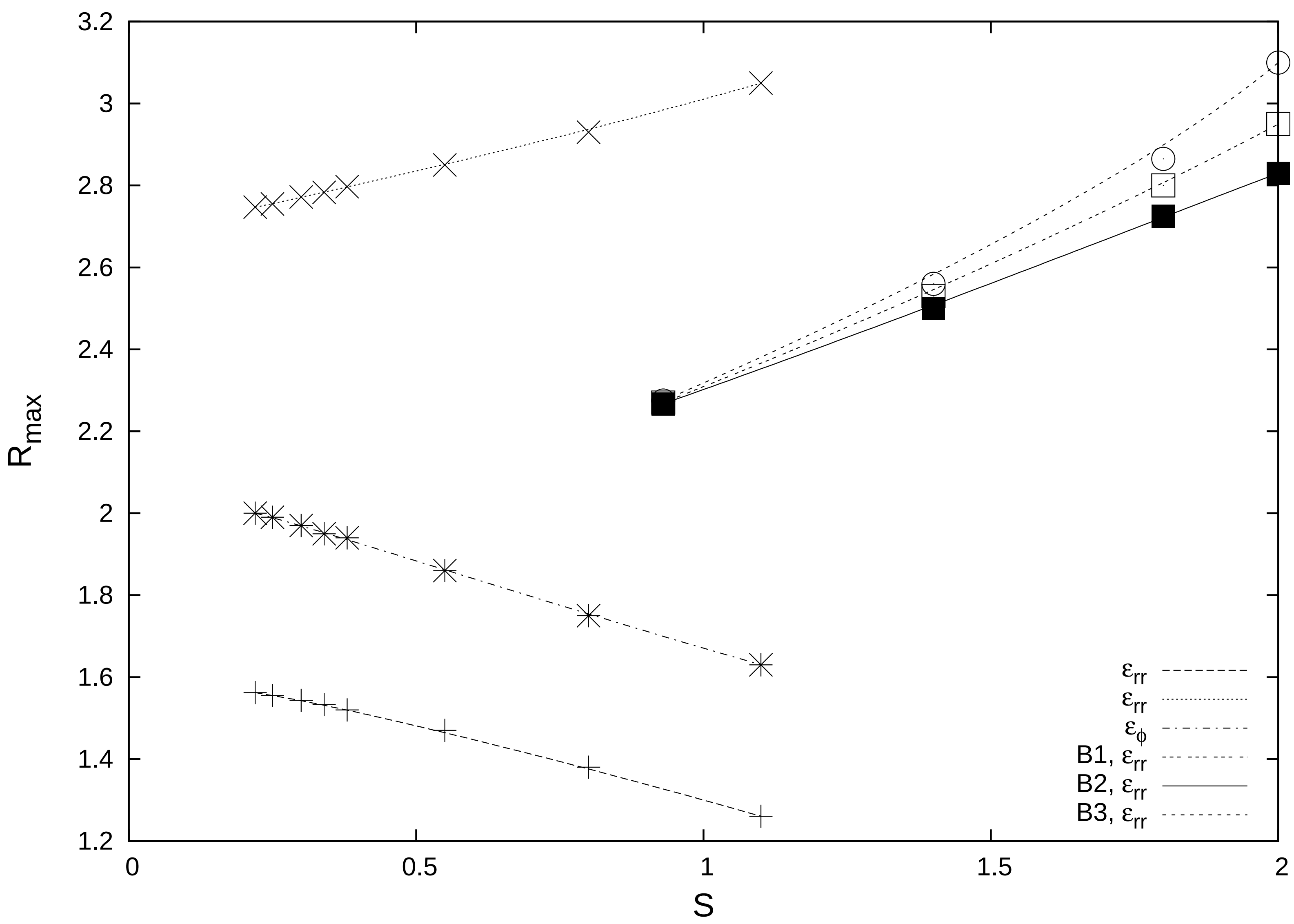

R_{max}
S
ε_{rr}
ε_{rr}
ε_{ϕ}
B1, ε_{rr}
B2, ε_{rr}
B3, ε_{rr}